広島大学学位請求論文

Unified Study of Kinetics and Dynamics on the Elementary Processes in Collisions of Vibrationally Excited Molecules

(振動励起分子の衝突素過程に関する速度論と動力学の融合研究)

2014 年

広島大学大学院理学研究科

化学専攻

河野 七瀬

目　次

1. 主論文

Unified Study of Kinetics and Dynamics on the Elementary Processes in Collisions of Vibrationally Excited Molecules

（振動励起分子の衝突素過程に関する速度論と動力学の融合研究）

河野 七瀬

2. 公表論文

(1) Acceleration of the Reaction OH + CO → H + CO_2 by Vibrational Excitation of OH.

Nanase Kohno, Mari Izumi, Hiroshi Kohguchi, and Katsuyoshi Yamasaki

‥‥‥‥*J. Phys. Chem. A*，**115**，19，4867–4873，**2011.**

(2) Rate Coefficients for Vibrational Relaxation of OH($X^2\Pi$, v = 1–4) by He.

Nanase Kohno, Jun Yamashita, Chihiro Kadochiku, Hiroshi Kohguchi, and Katsuyoshi Yamasaki

‥‥‥‥‥‥ *J. Phys. Chem. A*，**117**，16，3253–3259，**2012.**

主論文

Unified Study of Kinetics and Dynamics on the Elementary Processes in Collisions of Vibrationally Excited Molecules
(振動励起分子の衝突素過程に関する速度論と動力学の融合研究)

河野 七瀬

Preface and Acknowledgments

This dissertation is described on the basis of my study in the Physical Chemistry of Kinetics group at Hiroshima University from 2011 through 2014. I have studied the elementary processes of vibrationally excited molecules in gas phase and treated following reactions with laser-based technique: OH(v) + He, OH(v) + CO, and NH_2(v) + NO.

I wish to express my sincere thanks to Professor Katsuyoshi Yamasaki for his kind guidance and encouragement for these years. I am deeply grateful to Professor Hiroshi Kohguchi and Professor Osamu Takahashi for their significant suggestions in the seminar. I am deeply indebted to Professor Takayuki Ebata and Professor Misako Aida for their intensive reading of this dissertation and valuable comments.

Special thanks go to the members of the Physical Chemistry of Kinetics group and friends of mine: Ms. Mari Ishibe(Izumi), Mr. Kenichi Orimi and Mr. Junya Uchida for their technical assistance, many discussions, friendship and making these years quite enjoyable and memorable. Many thanks are also extended to my family for moral and economic support to my graduate study.

Finally, this work was supported by a Grant-in-Aid for JSPS Fellows (Grant Number 24•5470), the Sasakawa Scientific Research Grant from The Japan Science Society, the Strategic Fostering Program for Young Researchers Engaged in Natural Sciences of Hiroshima University, and the Graduate student overseas presentation support expense from Graduate School of Science of Hiroshima University.

CONTENTS

CHAPTER 1 GENERAL INTRODUCTION ····· 1

References ····· 5

CHAPTER 2 RATE COEFFICIENTS FOR VIBRATIONAL RELAXATION OF OH($X^2\Pi$, v = 1–4) BY He ····· 8

2.1 INTRODUCTION ····· 8

2.2 EXPERIMENT ····· 9

2.2.1 Apparatus ····· 9

2.2.2 Generation of Vibrationally Excited OH(v) ····· 10

2.2.3 Detection of OH(v) by LIF Technique ····· 11

2.2.4 Time Profiles of OH(v) ····· 13

2.2.5 Samples ····· 14

2.3 RESULTS AND DISCUSSION ····· 14

2.3.1 Analysis of the Time Profiles by the Integrated Profiles Method ··· 14

2.3.2 Evaluation of the Rate of Diffusion1 ····· 8

2.3.3 Evaluation of the Effect of Impurities ····· 20

2.3.4 Rate Coefficients for Vibrational Relaxation of OH(v) by He ····· 22

2.4 SUMMARY ····· 23

References ····· 25

CHAPTER 3 ACCELERATION OF THE REACTION OH + CO → H + CO_2 BY VIBRATIONAL EXCITATION OF OH ····· 49

3.1 INTRODUCTION ····· 49

3.2 EXPERIMENT ····· 51

3.2.1 Apparatus ····· 51

3.2.2 Generation of Vibrationally Excited OH(v) ····· 52

3.2.3 Detection of Vibrationally Excited OH(v) by LIF Technique ····· 52
3.2.4 Detection of H Atoms by Two-photon LIF Technique ····· 53
3.2.5 Time Profiles of OH(v) and H Atoms ····· 53
3.2.6 Removal of Impurity ····· 54
3.2.7 Samples ····· 55
3.3 RESULTS AND DISCUSSION ····· 55
3.3.1 Analysis of the Time Profiles of OH(v) and H Atoms ····· 55
3.3.2 Chemical Reaction and Intramolecular Vibrational Relaxation of HOCO ····· 60
3.4 SUMMARY ····· 63
References ····· 64

CHAPTER 4 ENHANCEMENT OF THE $NH_2 + NO \rightarrow OH + H + N_2$ REACTION BY VIBRATIONAL EXCITATION OF NH_2 ····· 87
4.1 INTRODUCTION ····· 87
4.2 EXPERIMENT ····· 89
4.2.1 Apparatus ····· 89
4.2.2 Generation of Vibrationally Excited NH_2(v) ····· 89
4.2.3 Detection of Vibrationally Excited NH_2(v) ····· 90
4.2.4 Detection of Vibrationally Excited OH(v) ····· 90
4.2.5 Detection of H Atoms ····· 91
4.2.6 Samples ····· 92
4.3 RESULTS AND DISCUSSION ····· 92
4.3.1 Vibrational Relaxation of NH_2(v) by Collisions with CF_4 ····· 92
4.3.2 The Effect of Vibrational Excitation of NH_2 on the Production of OH ····· 93
4.3.3 Branching Ratio of Reaction Channel 1a ····· 94
References ····· 97

CHAPTER 1 GENERAL INTRODUCTION

Atomic and molecular collisions are elastic, inelastic, or reactive. Elastic collision is defined as one in which there is no loss of total kinetic energy in the collision. Inelastic collision is the one in which some kinetic energy is changed into their internal degrees of freedom, and the total kinetic energy is not conserved. Chemical reaction takes place in reactive collision in which kinetic energy is needed to break the bond or form new one. Inelastic and reactive collisions, in particular, have been studied in a variety of fields for a long time and attracting the researchers concerned with atomic and molecular collisions as an elementary process. There have been two types of approach for studying molecular collisions. One is *kinetics* giving information on the rates of reaction; the other is *dynamics* elucidating the energy deposition and differential cross sections of collisions. The body of theory about chemical reaction has been developed since the mid-nineteenth century. The first study on chemical kinetics was performed in 1850. Wilhelmy[1] studied the rate for inversion of sucrose (hydrolysis of D-(+)-glucose and D-(−)-fructose in the presence of acid) and found the rate to be in proportion to the concentrations of both the sugar and the acid. Theory of chemical kinetics showed drastic progress with the development of chemical industry in the industrial revolution era. van't Hoff[2] published *Études de Dynamique chimique* (*Studies in Chemical Dynamics*), in which he generalized and further developed the work by Wilhelmy. He analyzed the temperature dependence of the equilibrium constant and of the forward and backward reaction rates.

Modern chemical kinetics is based on the concept of "activation of molecules", and rate coefficient is expressed by the following expression:

$$k = A \exp(-E / RT) \tag{1}$$

called Arrhenius equation, where A is the frequency factor, E is the activation energy of reaction, R is the gas constant, and T is the thermodynamic temperature. Arrhenius had presented the equation in 1889[3] and the equation is still employed in the analysis of kinetic studies. In 1935, Eyring[4] developed a statistical treatment called the "theory of absolute reaction rates" or "transition state theory".

Theoretical study on inelastic collisions has been developed since the 1930s. Landau and Teller[5] published their article on the mechanism of energy transfer in molecular collisions. They elucidated the low rate of the vibration-to-translation (V−T) energy exchange in diatomic gases in detail. And furthermore, in 1954, Schwartz, Slawsky and Herzfeld[6,7] introduced the three-dimensional collision model, which was a cornerstone of the interpretation of various vibrational non-equiblium phenomena in gases for the next decade.

The invention of lasers in 1960s had brought a revolution in the study on chemical reactions. Lasers offer high resolutions of time and energy and allow the preparation of vibrationally excited molecules. The development of spectroscopic technique such as laser-induced fluorescence (LIF,8) and multiple-photon ionization (MPI,9,10) have allowed us to detect a single quantum state, to unravel vibrational energy transfer by collisions, and to control chemical reactions by vibrational excitation of reactant molecules.

Cashion and Polanyi[11] measured the vibrational state distribution of HCl formed in the reaction of atomic hydrogen with Cl_2 in 1960, which is the first systematic study on the reactions of vibrationally excited molecules. From the late 1980s until now, some groups reported the effect of vibrational excitation of reactants on bimolecular reaction. In their pioneeting studies, Crim's group[12,13] reported that excited the third overtone ($4\nu_{OH}$) of O–H stretching vibration of HOD accelerates the chemical reaction

with H atoms producing OD at least two orders of magnitude larger than that producing OH. Zare's group[14-16] investigated the vibrational mode dependence on reaction, and elucidated the umbrella mode of NH_3^+ accelerates the proton transfer in collisions with ND_3, while the mode depletes the charge transfer and D-atom abstraction. Anderson's group[17-20] reported that bending mode of $C_2H_2^+$ enhances the reaction with CH_4 more efficiently than C-C stretching mode. Liu's group[21-25] demonstrated that C-H stretching excitation is not more effective than translational energy in chemical reaction Cl + CHD_3 and hinders the reaction F + CHD_3. In addition, they referred vibrationally excitation of reactants does not necessarily accelerate chemical reaction and that the effects of vibrational excitation of reactants on chemical reactions have not elucidated yet. The study of chemical reaction of vibrationally excited molecules, therefore, is important; however, there have been few reports on the absolute rate coefficients of the elementary processes in collisions of vibrationally excited molecules.[26]

The goal of the present study is to elucidate the effect of vibrational excitation of reactants on vibrational relaxations and chemical reactions. Studies on kinetics of vibrational excited molecules extract the information on the dynamics. New findings will contribute to unraveling complex chemical processes in combustion and atmosphere and to controlling of chemical reactions.

Temperature dependence of rate coefficients has been measured and activation energy has been obtained by equation 1. Activation energy, however, gives no direct information on how the vibrational motion of reacting molecules contributes to overcome the potential energy barrier of the reaction. In this study, the effects of vibrational energy on vibrational relaxation and chemical reaction have been studied. Vibrationally excited molecules were prepared with pulse lasers, and the state specific rate coefficients and the production yields under the control of vibrational energy of

reactants have been determined.

This dissertation consists of four chapters. Contents of each chapter are described below briefly:

(1) General introduction (this chapter)

(2) Vibrational relaxation of OH(v) by collisions with He: Vibrationally excited hydroxyl, OH($v \leq 4$) were generated by the reaction of molecular hydrogen with O(^{1}D) produced by the photolysis of O_3 at 266 nm and detected by LIF technique. The time-resolved LIF intensities of OH($v \leq 4$) were recorded at different He buffer pressures and analyzed by the originally developed integrated profiles method (IPM).[27,28] The rate coefficients for extremely slow vibrational relaxation of OH($v \leq 4$) by collisions with He have been determined. The mechanism of relaxation and correlation with the previously reported high vibrational levels (v = 10–12) has been discussed.

(3) Chemical reaction of vibrationally excited OH(v) with CO: Vibrationally excited hydroxyl, OH($v \leq 4$) were generated by the reaction of molecular hydrogen with O(^{1}D) produced by the photolysis of O_3 at 266 nm and detected by LIF technique. H atoms were detected by the two-photon excited LIF technique. The time profiles of LIF of OH(v) and H atoms were analyzed by the numerical integration of the rate equations. The absolute rate coefficients for reaction and relaxation have been determined at each vibrational level of OH(v).

(4) Chemical reaction of vibrationally excited NH_2(v) with NO: Vibrationally excited amino radical, NH_2(v) were produced in the UV photolysis of NH_3 at 193 nm. NH_2(v), OH and H atoms were detected by single-photon and two-photon excited LIF techniques. Control of the vibrational energy of NH_2(v) by addition of CF_4, which is an efficient relaxation partner of NH_2, has given the yields of OH.

References

(1) Wilhelmy, L. Ueber das Gesetz, nach welchem die Einwirkung der Säuren auf den Rohrzucker stattfindet (The law by which the action of acid on cane sugar occurs). *Ann. Physik. Chemie* (Poggendorf) **1850**, *81*, 413–433, 499–526.

(2) Hoff, J. H. van't *Études de Dynamique chimique* (*Studies of Chemical Dynamics*); Amsterdam : Frederik Muller, 1884.

(3) Arrhenius, Z. Über die Reaktionsgeschwindigkeit bei der Inversion von Rohrzucker durch Säuren. *Z. Phys. Chem.* **1889**, *4*, 226–248.

(4) Eyring, H. The Activated Complex in Chemical Reactions. *J. Chem. Phys.* **1935**, *3*, 107–115.

(5) Landau, L.; Teller, E. Zur Theorie der Schalldispersion (Theory of sound dispersion). *Phys. Z. Sow.* **1936**, *10*, 34–43.

(6) Schwartz, R. N.; Slawsky, Z. I.; Herzfeld, K. F. Calculation of Vibrational Relaxation Times in Gases. *J. Chem. Phys.* **1952**, *20*, 1591–1599.

(7) Schwartz, R. N.; Herzfeld, K. F. Vibrational Relaxation Times in Gases (ThreeDimensional Treatment). *J. Chem. Phys.* **1954**, *22*, 767–773.

(8) Zare, R. N.; Dagdigian, P. J. Tunable Laser Fluorescence Method for Product State Analysis. *Science* **1974**, *185*, 739–747.

(9) Demtröder, W. *Laser Spectroscopy*, 2nd ed.; Springer-Verlag, Berlin, 1995.

(10) Lin, S. H.; Fujimura, Y.; Neusser, H. J.; Schlag, E. W. *Mutiphoton Spectroscopy of Molecules*; New York: Academic Press, 1984.

(11) Cashion, J. K.; Polanyi, J. C. Infra-Red Chemiluminescence. I. Infra-Red Emission from Hydrogen Chloride Formed in the Systems Atomic Hydrogen Plus Chlorine, Atomic Hydrogen Plus Hydrogen Chloride, Atomic Hydrogen Plus Deuterium Chloride, and Atomic Deuterium Plus Hydrogen Chloride. *Proc. R. Soc.*

London **1960**, *258*, 529–563.

(12) Sinha, A.; Hsiao, M. C.; Crim, F. F. Bond-selected bimolecular chemistry: H + HOD($4\nu_{OH}$) → OD + H_2. *J. Chem. Phys.* **1990**, *92*, 6333–6335.

(13) Metz, R. B.; Thoemke, J. D.; Pfeiffer, J. M.; Crim, F. F. Selectively breaking either bond in the bimolecular reaction of HOD with hydrogen atoms. *J. Chem. Phys.* **1993**, *99*, 1744–1751.

(14) Conaway, W. E.; Ebata, T.; Zare, R. N. Vibrationally state-selected reaction of ammonia ions. III. $NH_3^+(v)$ + ND_3 and $ND_3^+(v)$ + NH_3. *J. Chem. Phys.* **1987**, *87*, 3453–3460.

(15) Guettler, R. D.; Jones, G. C., Jr.; Posey, L. A.; Zare, R. N. Partial Control of an Ion-Molecule Reaction by Selection of the Internal Motion of the Polyatomic Reagent Ion. *Science* **1994**, *266*, 259–261.

(16) Poutsma, J. C.; Everest, M. A.; Flad, J. E.; Zare, R. N. Mode selectivity in ion-molecular reaction of NH_3^+. *Appl. Phys. B* **2000**, *71*, 623–625.

(17) Orlando, T. M. The effects of bending and stretching vibration on the reaction of acetylene cations with methane. *J. Chem. Phys.* **1989**, *90*, 1577–1586.

(18) Chiu, Y.-h.; Fu, H.; Huang, J.-t.; Anderson, S. L. Large, mode-selective vibrational effect on the reaction of $C_2H_2^+$ with methane. *J. Chem. Phys.* **1994**, *101*, 5410–5412.

(19) Chiu, Y.-h.; Fu, H.; Huang, J.-t.; Anderson, S. L. Vibrational mode effects, scattering dynamics, and energy disposal in reaction of $C_2H_2^+$ with methane. *J. Chem. Phys.* **1995**, *102*, 1199–1216.

(20) Liu, J.; Anderson, S. L. The origin of the large bending enhancement of the reaction of $C_2H_2^+$ with methane: the effects of bending momentum, ruling out the precursor mechanism, and steps toward “Polanyi rules” for polyatomic reactions. *Phys.*

Chem. Chem. Phys. **2009**, *11*, 8721–8732.

(21) Yan, S. (S.), Wu, Y.-T.; Liu, K. Disentangling mode-specific reaction dynamics from overlapped images. *Phys. Chem. Chem. Phys.* **2007**, *9*, 250–254.

(22) Yan, S.; Wu, Y.-T.; Zhang, B.; Yue, X.-F.; Liu, K. Do Vibrational Excitations of CHD_3 Preferentially Promote Reactivity Toward the Chlorine Atom?. *Science* **2007**, *316*, 1723–1726.

(23) Zhang, W.; Kawamata, H.; Liu, K. CH Stretching Excitation in the Early Barrier F + CHD_3 Reaction Inhibits CH Bond Cleavage. *Science* **2009**, *325*, 303-306.

(24) Wang, F.; Lin, J.-S.; Liu, K. Steric Control of the Reaction of CH Stretch-Excited CHD_3 with Chlorine Atom. *Science* **2011**, *331*, 900-903.

(25) Wang, F.; Lin, J.-S.; Cheng, Y.; Liu, K. Vibrational Enhancement Factor of the Cl + CHD_3(v_1 = 1) Reaction: Rotational-Probe Effects. *J. Phys. Chem. Lett.* **2013**, *4*, 323–327.

(26) Barnes, P. W.; Sims, I. R.; Smith, I. W. M.; Lendvay, G.; Schatz, G. C. The branching ratio between reaction and relaxation in the removal of H_2O from its $|04\rangle^-$ vibrational state in collisions with H atoms. *J. Chem. Phys.* **2001**, *115*, 4586–4592.

(27) Yamasaki, K.; Watanabe, A. A New Method of Determining the Rate Constants for State-to-State Vibrational Relaxation: An Integrated Profiles Method. *Bull. Chem. Soc. Jpn.* **1997**, *70*, 89–95.

(28) Yamasaki, K.; Watanabe, A.; Kakuda, T.; Tokue, I. Application of a New Method to the Determination of Rate Constants: Examination of the Effect of Noise on the Data. *Int. J. Chem. Kinet.* **1998**, *30*, 47–54.

CHAPTER 2 RATE COEFFICIENTS FOR VIBRATIONAL RELAXATION OF OH($X^2\Pi$, v = 1–4) BY He

2.1 INTRODUCTION

The hydroxyl radical (OH) is one of the most important species in the atmospheric chemistry, because OH is involved in a number of reactions, such as the oxidation of hydrocarbons in the troposphere and the HO_x cycle of ozone depletion in the stratosphere.[1] In the upper mesosphere, vibrationally excited OH generated by the reaction of hydrogen atom with ozone emits infrared fluorescence called nightglow.[2] There have been many experimental and theoretical studies on the rate coefficients for vibrational relaxation of a wide range of vibrational levels of $OH(X^2\Pi)$, $v = 1-12$, mainly by collisions with major constituents of the atmosphere to construct the models of atmospheric chemistry.

The relaxation partners are classified into three groups based on the magnitudes of the rate coefficients for relaxation. Polar molecules with X–H bonds (X = O, N, S) are efficient relaxants: for example H_2O,[3,4] NH_3,[3-7] and CH_3SH.[4] Less- or non-polar molecules have intermediate efficiency: O_2,[5,8-12] CO_2,[3,5,8-12] N_2O,[5] and CH_4.[3-5] Relaxation by monatomic and nonpolar molecules, He,[5] Ar,[3,5] H_2,[5] and N_2,[3,5] is very slow. Some of the reported rate coefficients of the third group are upper limits, for example, the rate coefficients of He in units of cm^3 $molecule^{-1}$ s^{-1} are $< 1\times10^{-14}$,[5] $< 2\times10^{-12}$,[10] $(3\pm1)\times10^{-13}$,[12] and $\sim 6\times10^{-13}$,[12] $(3.6\pm0.6)\times10^{-12}$ [8] for v = 2, 9, 10, 11, and 12, respectively. Rate coefficients for vibrational relaxation of $OH(X^2\Pi, v = 1-12)$ by various collision partners are listed in Table 2.1. The inert gases with small rate coefficients are frequently used as buffer gases in the laboratory experiments, and accurate rate coefficients for relaxation are necessary to estimate the effect of

background relaxation; for example, in the measurements of the total pressure dependence of kinetics on chemical reactions or energy transfer processes. At 100 Torr of He, the upper limit of the pseudofirst-order relaxation rate of $v = 2$ is estimated to be $< 3.2 \times 10^4$ s^{-1} which is not negligibly small in discussing the kinetics of vibrationally excited levels of OH. The authors, therefore, are motivated to determine the rate coefficients for very slow relaxation of the relatively low vibrational levels $v = 1 - 4$ of $OH(X^2\Pi)$ by collisions with He. The originally developed linear kinetic analysis (integrated profiles method (IPM)),[13-15] which is useful to determine the rate coefficients of consecutive processes, has been applied in the present study. There are two keys to be note in the present measurements: diffusion and impurities. Diffusion in a buffer gas always depends on the total pressures, and the rate of diffusion must be measured at a given buffer gas pressure. Impurities frequently have larger rate coefficients for vibrational relaxation of OH than the inert buffer gases. It is usually difficult, however, to identify the species of impurities and to measure their concentrations precisely. In the present study, analyses for evaluating the rate of diffusion and for bypassing the quantitative evaluation of impurities have been devised, determining the rate coefficients for vibrational relaxation of $OH(X^2\Pi, v = 1 - 4)$ by He.

2.2 EXPERIMENT

2.2.1 Apparatus

The experimental setup is shown in Figure 2.1. Apparatus consists of four sections: lasers, flow systems, photodetectors and data acquisition systems. A reaction cell made of Pyrex has quartz Brewster windows and four baffles were set to reduce stray light and the fluorescence from the Pyrex cell itself. Gases in the reaction cell were evacuated with an oil-less pump (Alcatel Vacuum Technology ACP28G). The beam of

Nd^{3+}:YAG laser (Spectra Physics GCR-130) for photolysis was reflected with a dichroic mirror and went through the Pellin-Broca prism. The UV light was directed to the reaction cell with a dichroic mirror through an aperture, which was set on both sides of reaction cell for trimming and aligning the laser beams. The fluence of the YAG laser beam was measured with a joule meter (Gentec ED-100A) by reflection from the quartz Brewster window. The tunable light of Nd^{3+}:YAG laser (Spectra Physics GCR-130) pumped dye laser (Lambda Physik LPD3002) for detection went through the Pellin-Broca prism, and a separated frequency-doubled beam was reflected to the reaction cell with two 90° quartz prisms. The probe beam counter-propagated with the photolysis beam. The fluence of the dye laser beam was monitored with a joule meter (Gentec ED-100A) by reflection from the quartz plate. The lasers were operated at 10.1 Hz instead of 10.0 Hz to avoid the interference with the frequency (60 Hz) of the power supply line.

2.2.2 Generation of Vibrationally Excited OH(v)

A gaseous mixture of O_3/H_2/He (partial pressures: $p_{O_3} = 0.01 - 0.1$ mTorr, $p_{H_2} =$ 180 mTorr, and $p_{total}(He) = 70 - 130$ Torr) at 298 ± 2 K in a flow cell was irradiated with a 266 nm beam from a Nd^{3+}:YAG laser. Vibrationally excited OH is generated by the reaction:

$$O(^1D) + H_2 \rightarrow OH(X^2\Pi) + H \qquad (1)$$

The initial number density of $O(^1D)$ generated in the photolysis of O_3 is estimated by the following equation:

$$[O(^1D)]_0 = \phi [O_3](1 - e^{-\sigma\rho}) \qquad (I)$$

where ϕ is the quantum yield of the production of $O(^1D)$ in the photolysis; σ the

photoabsorption cross section of O_3; and ρ the area density of photon. ρ is defined by the fluence of laser light, *E*, and the energy of a single photon ε:

$$\rho = \frac{E}{\varepsilon} \qquad \text{(II)}$$

ρ is estimated to be 3.3×10^{15} cm^{-2} from the typical values: E = 2.5 mJ cm^{-2} and ε = 7.49×10^{-19} J at 266 nm. The initial number density of O(^{1}D) is then estimated to be $(0.9-9.1)\times10^{10}$ atoms cm^{-3} from the photon area density ρ, the photoabsorption cross section of O_3 at 266 nm, σ = 9.68×10^{-18} cm^2,[16] the quantum yields of photolysis, ϕ = 0.9 ± 0.1,[16] and the number density of O_3 (p_{O_3} = 0.01 – 0.1 mTorr). The wide range of $[O(^1D)]_0$ was necessary to detect vibrational levels with much different detection sensitivities. The rate coefficient for translational relaxation of O(^{1}D) by He was measured by Matsumi et al.[17] to be 9.9×10^{-11} cm^3 molecule^{-1} s^{-1}. Thermalization of the translational motion of O(^{1}D) is completed within 5 ns in the present experiments. Reaction 1, the rate coefficient of which is 1.3×10^{-10} cm^3 molecule^{-1} s^{-1} at 298 K,[16] generates OH with 1.3 μs of a time constant at 180 mTorr of H_2. The highest vibrational level of OH generated by reaction 1 is expected to be v = 4 based on the standard reaction enthalpy: $\Delta_r H^\circ_{298}$ = 183 kJ mol^{-1} (15271 cm^{-1}).

2.2.3 Detection of OH(v) by LIF Technique

The vibrational levels $v = 0-4$ of OH were excited via the $A^2\Sigma^+ - X^2\Pi$ transition with a Nd^{3+}:YAG laser pumped dye laser and the laser-induced fluorescence (LIF) was detected with a photomultiplier tube (PMT; Hamamatsu R1104). The signals from PMTs were amplified (×10) with the operational amplifier LF356 made in house and averaged with gated integrators (Stanford Research SR-250). The signals from integrators were digitized with A/D converter (Stanforf Research SR-245) for

processing with a computer and the data was stored on a disk. The typical pulse energies of the probe laser were 200 and 800 μJ pulse^{-1} for $v = 0 - 2$ and $v = 3$ and 4, respectively. The vibrational sequence of $\Delta v = 0$ was excited for probing the levels $v = 0 - 2$ and $\Delta v = -2$ for $v = 3$ and 4, because the fluorescence quantum yields of the vibrational levels $v' \geq 3$ of the $A^2\Sigma^+$ state are small due to predissociation. A frequency-doubled light from DCM dye (doubled with BBO III crystal manufactured by Lambda Physik) was used for detecting $v = 0 - 2$, and a fundamental beam prepared by Exalite398 dye for $v = 3$ and 4. The $\Delta v = 0$ sequence is readily saturated at about 10 μJ pulse^{-1}. The present method of analysis, however, is not affected by saturation as long as signal intensities are proportion to the concentration, and high signal-to-noise (S/N) ratios is achieved under the saturation conditions. Figure 2.2 shows the laser pulse energy dependence of the LIF intensity of OH(v = 0). The linear regression line of the logarithmic plot gives the relation $y = x^{0.4}$, where y corresponds to the LIF intensity and x is the laser pulse energy, indicating that the LIF intensity was partially saturated.

The LIF was observed with optical filters to block the stray lights of the photolysis and probe lasers. Transmittance curves of filters in the lab are shown in Figure 2.3 measured with a spectrophotometer (U-3010, HITACHI). Table 2.2 shows the transmittance of the optical filters at the wavelength of the photolysis of O_3 and probe of OH. WG295 (Newport), UV-D36B (Toshiba), UV-D35 (2) (Toshiba) and UV-D35 $\times$ 2 (Toshiba) efficiently block the stray light of the photolysis laser. In this study, UV-D35 (2) was used for detecting $v = 0 - 2$ because of the highest transmittance at the wavelength of $\Delta v = 0$. However, the stray light of probe laser is also transmitted at the high efficiency. In order to block the stray light and increase S/N ratios, the delay time of the sampling gate from the probe laser was optimized. The optimal delay was 0.9 μs.

In the detection of $v = 3$ and 4, the applied voltage to the PMT was high compared to that of $v = 0-2$, and UV - D35$\times$2 instead of UV - D35(2) was suitable to reduce the undesirable signal of the stray light. The typical ratio of number densities, $[He]/[OH]_0 \approx [He]/[O(^1D)]_0$, was at least 3×10^7, satisfying the pseudo first-order reaction conditions. Observed LIF excitation spectra of OH($A^2\Sigma^+ - X^2\Pi$) are shown in Figure 2.4 and 2.5. All the peaks are assigned to rotational lines of the vibrational levels.

2.2.4 Time Profiles of OH(v)

The time-resolved LIF intensities of all the vibrational levels are necessary to obtain the kinetic information on relaxation. To record the time profiles of the LIF intensities, the wavelength of the probe laser was tuned to a rotational line of each vibrational level, and the time delays between the photolysis and the probe laser were scanned with a pulse delay controller made in house. The rotational lines excited were $P_1(N=2)$, $P_1(2)$, $P_1(2)$, $Q_1(2)$, and $Q_1(2)$ of $0-0$, $1-1$, $2-2$, $1-3$, and $2-4$ bands, respectively (peaks colored with red in Figure 2.4 and 2.5), where N denotes the quantum number of total angular momentum without electronic spin. The time constant of the rotational relaxation of OH at the lowest pressure of He in the present experiments (70 Torr) is estimated to be less than 10 ns from the rate coefficients of rotational relaxation of OH by He, $(1.6-8.3)\times10^{-10}$ cm^3 molecule^{-1} s^{-1} for $v = 1-3$ [18] and $(0.5-2.4)\times10^{-10}$ cm^3 molecule^{-1} s^{-1} for $v = 1$.[19] Rotational motion is, therefore, thermalized before vibration relaxation occurs, and the time profile of a single rotational line represents that of the vibrational level of interest. In fact, the time profiles recorded with different rotational lines, $P_1(1)$, $Q_1(1)$, and $Q_1(3)$, were identical with those observed at $N = 2$. The typical number of data points in a time profiles was 1000, and $3-9$ time profiles were averaged to reach sufficient signal-to-noise ratios.

2.2.5 Samples

The total pressure of sample gas was monitored with a capacitance monometer (Baratron 122A). The total pressure measurement together with the mole fractions as measure with calibrated flow controllers (Tylan FC-260KZ and STEC-410) gave the partial pressures of the reagents. O_3 was prepared by an electric discharge in high-grade O_2 (Japan Fine Products, $> 99.99995\%$) with a synthesizer made in house and stored in a 3 dm^3 glass bulb with He ($0.1 - 7.8\%$ dilution). High-grade H_2 ($> 99.99999\%$) and He ($> 99.99995\%$), delivered by Japan Fine Products, were used without further purification.

2.3 RESULTS AND DISCUSSION

2.3.1 Analysis of the Time Profiles by the Integrated Profiles Method

The black dots in Figure 2.6a, b, and c show the recorded time profiles of LIF intensities of the vibrational levels of $OH(X^2\Pi, v = 0 - 4)$ at 70, 100, and 130 Torr of total pressures (He buffer). There are a few significant features in Figure 2.6. All the levels show prompt generation (< 2 μs) subsequent to the irradiation of the photolysis light, which is consistent with the time constant 1.3 μs estimated in the previous section. The distinct growth in the profiles of the levels $v = 0$ and 1 at high He pressures indicates the relaxation from the higher vibrational levels, and corresponds to the faster decay of $v = 2 - 4$ at high total pressures. The slow decay of $v = 0$ is due to diffusion loss from the volume observed with the probe laser whose beam diameter is about 2 mm.

There are several possible side reactions including OH:

$$H + O_3 \rightarrow OH + O_2 \quad (2)$$

$$OH + O_3 \rightarrow HO_2 + O_2 \quad (3)$$

$$OH + H_2 \rightarrow H_2O + H \quad (4)$$

$$O(^3P) + OH \rightarrow O_2 + H \quad (5)$$

$$OH + OH \rightarrow H_2O + O \quad (6)$$

$$OH + OH + M \rightarrow H_2O_2 + M \quad (7)$$

The rate coefficients for bimolecular reactions $2-6$ and termolecular reaction 7 are $k_2 = 2.9\times10^{-11}$; $k_3 = 7.3\times10^{-14}$; $k_4 = 6.7\times10^{-15}$; $k_5 = 3.3\times10^{-11}$; $k_6 = 1.8\times10^{-12}$ cm^3 $molecule^{-1}$ s^{-1}; and $k_7 = 6.9\times10^{-31}$ cm^6 $molecule^{-2}$ s^{-1}.[16] Under the present experimental conditions, the effective first-order rates are estimated to be less than 94, 0.2, 39, 2.9, 0.2, and 0.3 s^{-1} for reactions $2-7$, respectively. Reaction 2 generates vibrationally excited levels mainly $v = 6-9$ of OH,[20-22] and consequently, it might be suggested that the time profiles of the high vibrational levels are disturbed by relaxation from $v = 6-9$. The time profile of the highest level $v = 4$, however, shows simple single-exponential decay, indicating that the effect of reaction 2 is negligibly small under the present experimental conditions ($p_{O_3} < 0.1$ mTorr).

The effects of vibrational relaxation by the ambient gases, H_2 and O_3, have to be examined. Reported rate coefficient for relaxation of $OH(v = 2)$ by H_2 is an upper limit, $<1\times10^{-14}$ cm^3 $molecule^{-1}$ s^{-1}, and 180 mTorr of H_2 give the first-order rate less than 58 s^{-1}.[5] Unfortunately, there is no report on the rate coefficient for relaxation of $OH(v \le 4)$ by O_3 but that for $OH(v = 9)$ by O_3 was determined to be 1.37×10^{-10} cm^3 $molecule^{-1}$ s^{-1} by Nizkorodov et al.[7] The estimated first-order decay rate of $OH(v = 9)$ at 0.1 mTorr of O_3, 440 s^{-1}, is sufficiently smaller than 4400 s^{-1} actually observed decay rate of $v = 4$ (Figure 2.6a), suggesting little effect of relaxation by O_3. In fact, observed time profiles of $OH(v = 0-4)$ little depended on the pressures of O_3 ($p_{O_3} = 0.01-0.1$ mTorr). Accordingly, relaxation of $OH(v)$ is governed mainly by collisions with He under the present experimental conditions.

The effect of impurity on vibrational relaxation must be taken into account, because relaxation of OH(v) by He is very slow due to small interaction between OH and He. The details of evaluation of impurity are discussed in Section 2.3.3. Relaxation by He proceeds via a V–T mechanism with a single-quantum change $v+1 \rightarrow v$ based on the simple selection rule of relaxation.[23] The rate equation of a vibrational level v is written to be:

$$\frac{\mathrm{d}[v]}{\mathrm{d}t} = -(k_v^{\mathrm{He}}[\mathrm{He}] + k_v^{\mathrm{M}}[\mathrm{M}] + k_{v,\mathrm{d}})[v] + (k_{v+1}^{\mathrm{He}}[\mathrm{He}] + k_{v+1}^{\mathrm{M}}[\mathrm{M}])[v+1] \qquad \text{(III)}$$

where k_v^{X} is the rate coefficient for vibrational relaxation from the level v to $v-1$ of OH by collisions with a species X (X = M denotes impurities) and $k_{v,\mathrm{d}}$ rate coefficient for diffusion loss of OH(v) from the observed volume. The second term of eq III is not necessary for $v = 4$, and $k_v^{\mathrm{X}} = 0$ for $v = 0$. The observed LIF intensity of a level v at time t, $I_v(t)$, is in proportion to the population of the vibrational level v at t, [v], $I_v(t) = \alpha_v[v]$, where α_v is the detectability of the level v. Integration of eq III from t_0 to an arbitrary time t gives:

$$\begin{aligned} & I_v(t) - I_v(t_0) \\ &= -(k_v^{\mathrm{He}}[\mathrm{He}] + k_v^{\mathrm{M}}[\mathrm{M}] + k_{v,\mathrm{d}}) \int_{t_0}^{t} I_v(t')\mathrm{d}t' \\ &\quad + (k_{v+1}^{\mathrm{He}}[\mathrm{He}] + k_{v+1}^{\mathrm{M}}[\mathrm{M}]) \frac{\alpha_v}{\alpha_{v+1}} \int_{t_0}^{t} I_{v+1}(t')\mathrm{d}t' \end{aligned} \qquad \text{(IV)}$$

where t_0 is the time when generation (reaction 1) and rotational relaxation of the nascent OH(v) are completed, and typically set to 50 μs. Eq IV can be arranged to be the following form:

$$y_v(t) = -a_v x_v(t) + b_{v+1} \qquad \text{(V)}$$

where

$$y_v(t) = \left[I_v(t) - I_v(t_0)\right] \Big/ \int_{t_0}^{t} I_{v+1}(t')\mathrm{d}t' \qquad \text{(VI)}$$

$$x_v(t) = \int_{t_0}^{t} I_v(t')\mathrm{d}t' \Big/ \int_{t_0}^{t} I_{v+1}(t')\mathrm{d}t' \qquad \text{(VII)}$$

$$a_v = k_v^{\mathrm{He}}[\mathrm{He}] + k_v^{\mathrm{M}}[\mathrm{M}] + k_{v,\mathrm{d}} \equiv k_v + k_{v,\mathrm{d}} \qquad \text{(VIII)}$$

$$b_{v+1} = (k_{v+1}^{\mathrm{He}}[\mathrm{He}] + k_{v+1}^{\mathrm{M}}[\mathrm{M}])\frac{\alpha_v}{\alpha_{v+1}} \equiv k_{v+1}\frac{\alpha_v}{\alpha_{v+1}} \qquad \text{(IX)}$$

A linear regression analysis of the plot $y_v(t)$ versus $x_v(t)$, called an IPM plot, gives a_v and b_{v+1} from the slope and intercept, respectively. Figure 2.7a, 2.8a, and 2.9a show the IPM plots for the vibrational levels $v = 1-3$ at 70, 100, and 130 Torr, respectively. Figure 2.7b, 2.8b, and 2.9b depict the IPM plot of $v = 4$, and its ordinate and abscissa correspond to $I_4(t) - I_4(t_0)$ and $\int I_4(t')\mathrm{d}t'$, respectively. All the plots show linear correlation, indicating that relaxation proceeds via the single-quantum relaxation $v \rightarrow v-1$ as expected.

Another type of IPM analysis including relaxation with both single- and double-quantum relaxation ($\Delta v = 1$ and 2) also was made to evaluate the contribution of double-quantum relaxation. The equation of analysis is given as follows:

$$\begin{aligned} & I_v(t) - I_v(t_0) \\ = & -(k_v^{\mathrm{He}}[\mathrm{He}] + k_v^{\mathrm{M}}[\mathrm{M}] + k_{v,\mathrm{d}}) \int_{t_0}^{t} I_v(t')\mathrm{d}t' \\ & + (k_{v+1\rightarrow v}^{\mathrm{He}}[\mathrm{He}] + k_{v+1\rightarrow v}^{\mathrm{M}}[\mathrm{M}])\frac{\alpha_v}{\alpha_{v+1}} \int_{t_0}^{t} I_{v+1}(t')\mathrm{d}t' \\ & + (k_{v+2\rightarrow v}^{\mathrm{He}}[\mathrm{He}] + k_{v+2\rightarrow v}^{\mathrm{M}}[\mathrm{M}])\frac{\alpha_v}{\alpha_{v+2}} \int_{t_0}^{t} I_{v+2}(t')\mathrm{d}t' \end{aligned} \qquad \text{(X)}$$

where $k_{v+1\rightarrow v}^{\mathrm{X}}$ and $k_{v+2\rightarrow v}^{\mathrm{X}}$ are the rate coefficients for vibrational relaxation from the levels $v+1$ and $v+2$ to v, respectively, by collisions with a species X. This equation can be dealt with a simple linear multivalued regression analysis. The coefficient of the

last term on the right side, $(k^{\mathrm{He}}_{v+2\to v}[\mathrm{He}]+k^{\mathrm{M}}_{v+2\to v}[\mathrm{M}])(\alpha_v/\alpha_{v+2})$, directly relates to the double-quantum relaxation. The values of the coefficient, however, have very large confidence limits ($>\pm 100\%$) and do not depend on [He], and consequently, the contribution of the double-quantum relaxation of OH(v) by He cannot be evaluated in the present study.

The time profile of a vibrational level v can be calculated using the convolution integral:

$$I_v(t) = I_v(t_0)\mathrm{e}^{-a_v t} + b_{v+1}\int_{t_0}^{t} I_{v+1}(t')\mathrm{e}^{-a_v(t-t')}\,\mathrm{d}t' \qquad \text{(XI)}$$

where a_v and b_{v+1} are determined from the IPM plot by eq V. Calculated $I_v(t)$, shown with the red lines in Figure 2.6, well-reproduces all the observed time profiles of OH(v). In common kinetic analyses, a bimolecular rate constant of interest, k_v^{He}, is determined from the slope of the straight line fit from regression analysis of a plot a_v versus [He]. In the present study, however, $k_{v,\mathrm{d}}$ may depend on [He], and consequently, the values of $k_{v,\mathrm{d}}$ at different He pressures must first be determined.

2.3.2 Evaluation of the Rate of Diffusion

The frequency of collisions between OH and He at 100 Torr is about 2×10^9 s^{-1}, whose time constant is 0.5 ns, and the translational motion of all the vibrational levels $v=0-4$ are thermalized immediately, and consequently, the rates of diffusion of $v=0-4$ are nearly identical: $k_{v,\mathrm{d}} \approx k_{0,\mathrm{d}} \equiv a_0$. In principle, the IPM analysis using the time profiles of $v=0$ and 1 gives a_0; however, the confidence limits of a_0 obtained from IPM plots were too large to give a decisive value to a_0. Another analysis using all the time profiles of $v=0-4$ was made for determining the rate coefficients of diffusion. The sum of eq III over $v=0-4$ gives:

$$\sum_{v=0}^{4}[v] = \left(\sum_{v=0}^{4}[v]_0\right)\mathrm{e}^{-a_0 t} \qquad \text{(XII)}$$

suggesting that the sum of the populations of $v = 0-4$ shows the single-exponential decay with a_0 as an apparent first-order rate coefficient. Unfortunately, recorded time profiles are LIF intensities $I_v(t)$ instead of (relative) populations $[v]$, and the time dependence of the sum $\Sigma I_v(t)$ does not represent that of the sum $\Sigma[v]$. If the relative detectabilities α_v/α_{v+1} are obtained in the IPM analysis, relative populations can be calculated. The rate coefficients of diffusion $k_{v,\mathrm{d}}$, however, are unknown, and neither relative detectabilities nor relative populations can be derived from the present data. We have, therefore, used reported nascent vibrational distributions to make a plot of the sum of populations versus time.

Several groups [24-32] have reported the nascent vibrational energy distributions of OH generated in the $O(^1D) + H_2 \rightarrow OH(v) + H$ reaction. Their sources of $O(^1D)$ were photolysis of O_3 at 248,[25,27,29] 266,[24,26,30], and $200-300$ nm,[28] and O_2 at 157 nm.[31,32] The collision energies at the center of mass of $O(^1D)$ and H_2 are 661, 597, and 452 cm^{-1} for O_3/248, O_3/266, and O_2/157 nm photolysis, respectively. Translational motion of $O(^1D)$ is thermalized within 5 ns at 70 Torr of He, and the thermal collision energy between $O(^1D)$ and H_2 is $(3/2)RT$ = 311 cm^{-1} at 298 K and closest to the conditions of Yang's group.[31,32] The sum of the populations, therefore, were calculated using the nascent vibrational distributions reported by Yang's group: $v = 0/v = 1/v = 2/v = 3/v = 4$ = 0.29/0.25/0.23/0.15/0.08

Figure 2.10 shows the time profiles of the total populations ($\Sigma[v]$), indicating that the rates of diffusion are slower at higher total pressure. A single-exponential analysis gives a_0 to be 300 ± 60, 240 ± 30, and 190 ± 40 s^{-1} at 70, 100, and 130 Torr, respectively. The diffusion coefficient D is estimated to be 7.2×10^{-5} m^2 s^{-1} by

$D = (1/3)\bar{v}\lambda_m$ from gas kinetic theory,[33] where $\bar{v}$ is the average velocity of OH and λ_m is the mean free path of OH in a He buffer gas. The time constants for diffusion loss are calculated to be about 3.4, 4.8, and 6.3 ms at 70, 100, and 130 Torr, respectively. Corresponding first-order diffusion rate coefficients, $k_{v,d} \approx 300$, 210, and 160 s^{-1}, at 70, 100, and 130 Torr, respectively, are in good agreement with those actually measured.

2.3.3 Evaluation of the Effect of Impurities

The rate coefficients of very slow processes are, in general, difficult to measure, because a large amount of reactant must be introduced to the system, and impurities with large rate coefficients disturb the observation of elementary process of interest. In the present experiments, H_2O might be the most problematic impurity, because H_2O is an efficient relaxation partner with a rate coefficient $(2.58 - 3.66)\times10^{-11}$ cm^3 $molecule^{-1}$ s^{-1} for $v = 2$ [3,4] and at least 2500 times faster than He. The whole gas line including the pressure regulator of gas cylinders was evacuated for a day or more with an oil-less pump to lower the effect of impurity. The relative concentration of impurity (probably H_2O) was measured by observing the time profiles of OH without H_2. Weak signal of the LIF of OH was observed without H_2. This unexpected OH might be generated by a reaction:

$$O(^1D) + H_2O \rightarrow 2OH(X^2\Pi) \quad (8)$$

because thorough removal of a small amount of H_2O desorbed from the inner wall of the gas supply line was difficult even by long evacuation. The highest vibrational level of $OH(X^2\Pi)$ in reaction 8 is expected to be $v = 2$ from the exothermicity of the reaction $\Delta_r H^\circ_{298} = -122$ kJ mol^{-1} (10160 cm^{-3}). Vibrational levels $v \leq 2$ were actually detected and no signal due to $v \geq 3$ was observed. Figure 2.11a shows the time profile

of OH(v = 1) recorded without H_2 after long evacuation. On the other hand, Figure 2.11b shows the time profile of OH(v = 1) recorded in the absence of H_2 after the whole gas line including the pressure regulator of a cylinder was filled with He at 1000 Torr for a week without evacuation. Both growth and decay rates of the profile b in Figure 2.11 are extremely fast because of the fast processes of reaction 8 and vibrational relaxation by impurities, respectively. The fast growth and decay rates of the profile of OH(v) in the absence of H_2 indicate that the concentrations of impurities are high. The time profiles of OH(v = 1) generated in the reaction 1 were actually quite different depending on the amount of impurities, as shown in Figure 2.12.

Figure 2.13 shows the time profiles of $OH(v = 0)$ recorded without H_2 at different He pressures. The rates of the exponential growth are nearly identical irrespective of the He pressure: 1990 ± 340, 1780 ± 300, and 1790 ± 240 s^{-1} at 70, 100, and 130 Torr, respectively (the stated confidence limits are 2σ), indicating that the impurities (probably H_2O) do not come out of the He cylinder but mix at the flowing line. The concentration of a component in the flow cell is related to a flow rate and flow velocity as $C = F/(V \times A)$, where C is the concentration of a component (in units of molecules m^{-3}), V is the flow velocity ($m\ s^{-1}$) of the gas in the cell, A is the cross section of the cell (m^2), and F is the flow rate ($molecules\ s^{-1}$) of the component. There are two ways to change the total pressure: (a) change the flow velocity of the gas in the cell with a constant He flow rate; (b) change the flow rate of He with a constant flow velocity. Method (a) changes both the total pressure and the concentrations of impurities, whether or not the impurities originate from He cylinder. Method (b), on the other hand, changes only the He pressure and keeps the concentrations of impurities constant, if the impurities does not originate from He cylinder but from the gas supply line. Method (b), therefore, was employed to change the total pressure in this study. All

time profiles were recorded at the constant flow velocity, $V = 0.1$ m s^{-1}.

The findings show that He pressure dependence of the time profiles can be measured without changing the concentration of the impurities, and that the plots of k_v versus [He] can be made (k_v is defined in eq VIII). Figure 2.14 shows the plots of k_v versus [He] for $v = 1 - 4$, and the slopes of the straight line fit from regression analysis give the bimolecular rate coefficients for relaxation by He k_v^{He}. The total pressure range, $70 - 130$ Torr, which is not wide, is a compromise between the total pressure and flow velocity. At total pressure lower than 70 Torr, relaxation is too slow to observe with a good signal-to-noise ratio; at higher than 130 Torr, flow velocity has to be too low due to a limited pumping speed.

2.3.4 Rate Coefficients for Vibrational Relaxation of OH(v) by He

k_v^{He} for $v = 1 - 4$ determined from Figure 2.14 are listed in Table 2.3. The stated confidence limits are 2σ. The rate coefficients for vibrational relaxation of OH(v) by He have been reported for $v = 2$, 9, 10, 11, and 12. Of these the rate coefficients for $v = 2$ and 9 are upper limits. The simple model of vibrational relaxation between diatomic molecules and atoms, based on Landau–Teller (LT) model and Schwartz–Slawsky–Herzfeld (SSH) theory, shows a relation $k_v^{\mathrm{He}} \mu v$, i.e., $k_v^{\mathrm{He}} / v \approx$ constant.[23,34] According to the results of the present study, $k_v^{\mathrm{He}} / v = 2.9$, 6.8, 17, and 41 for $v = 1 - 4$ and 3000, 5450, and 30000 for $v = 10 - 12$ from the previous reports in units of 10^{-17} cm^3 molecule^{-1} s^{-1}. The strong dependence of k_v^{He} / v on v is due mainly to the anharmonicity of the vibration of OH. The efficiency of energy-transfer process is evaluated by the adiabaticity parameter.[35]

$$\zeta = \frac{a \Delta E}{h\nu} \qquad \text{(XIII)}$$

where a is an action length; h is the Planck's constant; v is a relative velocity between OH and He; and ΔE is an energy converted from vibration to translation. In the single-quantum relaxation, ΔE is identical with the vibrational energy spacing between the adjacent vibrational levels $\Delta G_{v-1/2} \equiv G(v) - G(v-1)$. The change in $\Delta G_{v-1/2}$ with v is due to the anharmonicity of vibrational levels. Under the typical conditions of OH and He at 298 K, $a \approx 0.2$ nm,[35] $\mathrm{v} = 1400$ m s^{-1}, and $\Delta E = \Delta G_{v-1/2} = 3570$ and 1670 cm^{-1}, giving $\zeta \approx 15.3$ and 7.0 for $v = 1$ and 11, respectively. $\zeta > 1$ indicates that the present V–T energy-transfer process is in the adiabatic regime, and consequently, the efficiency of vibrational relaxation of OH(v) by He is governed by the exponential gap law.

$$\frac{k_v^{\mathrm{He}}}{v} \propto \exp(-\zeta) = \exp\left(-\frac{a\Delta E}{h\mathrm{v}}\right) \propto \exp(-\Delta E) = \exp(-\Delta G_{v-1/2}) \qquad \text{(XIV)}$$

The plot between $\ln(k_v^{\mathrm{He}}/v)$ and $\Delta G_{v-1/2}$ depicted in Figure 2.15 shows that relaxation of OH of low $(v = 1-4)$ and high $(v = 10-12)$ vibrational levels can be connected based on the relation given by eq XIV. The linear regression line gives the following eq:

$$\ln\left(\frac{k_v^{\mathrm{He}}}{v}\right) = A - B \times \Delta G_{v-1/2} \qquad \text{(XV)}$$

where $A = -21.6$ and $B = 0.00459\ \mathrm{cm}^{-1}$, and the rate coefficients of vibrational relaxation of OH($v = 1-12$) by He can be calculated by eq XV.

2.4 SUMMARY

The rate coefficients for vibrational relaxation of the vibrational levels $v = 1-4$ of OH($\mathrm{X}^2\Pi$) by collisions with He have been measured for the first time in the present study. The kinetic analysis (IPM) made it possible to determine the very small rate

coefficients without the correction for the observed LIF intensities by photochemical parameters. The rate coefficient for $OH(v=2)$ has been found to be about 70 times smaller than the reported upper limit. The efficiencies of vibrational relaxation of $OH(v=1-4)$ by He increase with the vibrational energies of OH and nicely correlate to those of $OH(v=10-12)$ reported by other groups according to the harmonic effect based on LT model and SSH theory and anharmonic effect in the adiabatic regime of *V–T* mechanism.

References

(1) Warneck, P. *Chemistry of the Natural Atmosphere,* 2nd ed.; Academic Press: London, 2000.

(2) Bates, D. R.; Nicolet, M. The Photochemistry of Atmospheric Water Vapor. *J. Geophys. Res.* **1950**, *55*, 301–327.

(3) Raiche, G. A.; Jeffries, J. B.; Rensberger, K. J.; Crosley, D. R. Vibrational Energy Transfer in OH $X^2\Pi_i$, $v = 2$ and 1. *J. Chem. Phys.* **1990**, *92*, 7258–7263.

(4) Silvente, E.; Richter, R. C.; Hynes, A. Kinetics of the Vibrational Deactivation of OH $X^2\Pi$ ($v = 3, 2, 1$) with Hydrides and Reduced Sulfides. *J. Chem. Soc., Faraday Trans.* **1997**, *93*, 2821–2830.

(5) Rensberger, K. J.; Jeffries, J. B.; Crosley, D. R. Vibrational Relaxation of OH ($X^2\Pi_i$, $v = 2$). *J. Chem. Phys.* **1989**, *90*, 2174–2181.

(6) Cheskis, S. G.; Iogansen, A. A.; Kulakov, P. V.; Sarkisov. O. M.; Titov, A. A. Laser Photolysis of Ozone in the Presence of Ammonia: Vibrationally Excited OH Radicals. *Chem. Phys. Lett.* **1988**, *143*, 348–352.

(7) Nizkorodov, S. A.; Harper, W. W.; Nesbitt, D. J. Fast Vibrational Relaxation of OH($v = 9$) by Ammonia and Ozone. *Chem. Phys. Lett.* **2001**, *341*, 107-114.

(8) Sappey, A. D.; Copeland, R. A. Collision Dynamics of OH($X^2\Pi_i$, $v = 12$). *J. Chem. Phys.* **1990**, *93*, 5741–5746.

(9) Dodd, J. A.; Lipson, S. J.; Blumberg, W. A. M. Formation and Vibrational Relaxation of OH ($X^2\Pi_i$, v) by O_2 and CO_2. *J. Chem. Phys.* **1991**, *95*, 5752-5762.

(10) Chalamala, B. R.; Copeland, R. A. Collision Dynamics of OH($X^2\Pi$, $v = 9$). *J. Chem. Phys.* **1993**, *99*, 5807–5811.

(11) Knutsen, K.; Dyer, M. J.; Copeland, R. A. Collisional Removal of OH ($X^2\Pi$, $v = 7$) by O_2, N_2, CO_2, and N_2O. *J. Chem. Phys.* **1996**, *104*, 5798–5802.

(12) Dyer, M. J.; Knutsen, K.; Copeland, R. A. Energy Transfer in the Ground State of OH: Measurements of OH(v = 8,10,11) Removal. *J. Chem. Phys.* **1997**, *107*, 7809–7815.

(13) Yamasaki, K.; Watanabe, A. A New Method of Determining the Rate Constants for State-to-State Vibrational Relaxation: An Integrated Profiles Method. *Bull. Chem. Soc. Jpn.* **1997**, *70*, 89–95.

(14) Yamasaki, K.; Watanabe, A.; Kakuda, T.; Tokue, I. Application of a New Method to the Determination of Rate Constants: Examination of the Effect of Noise on the Data. *Int. J. Chem. Kinet.* **1998**, *30*, 47–54.

(15) Watanabe, S.; Usuda, S.-y.; Fujii, H.; Hatano, H.; Tokue, I.; Yamasaki, K. Vibrational Relaxation of $O_2(X^3\Sigma_g^-, v = 9 - 13)$ by Collisions with O_2. *Phys. Chem. Chem. Phys.* **2007**, *9*, 4407–4413.

(16) Friedl, R. R.; Golden, D. M.; Kurylo, M. J.; Moortgat, G. K.; Rudek, K.-H.; Wine, P. H.; Ravishankara, A. R.; Kolb, C. E.; Molina, M. J.; Pitts, F.-B. J.; Huie, R. E.; Orkin, V. L.; F.-Pitts, B. J. *Chemical Kinetics and Photochemical Data for Use in Atmospheric Studies,* Evaluation No. 15; Jet Propulsion Laboratory, California Institute of Technology: Pasadena, CA, 2006.

(17) Matsumi, Y.; Shamsuddin, S. M.; Sato, Y.; Kawasaki, M. Velocity Relaxation of Hot $O(^1D)$ Atoms by Collisions with Rare Gases, N_2, and O_2. *J. Chem. Phys.* **1994**, *101*, 9610–9618.

(18) Holtzclaw, K. W.; Upschulte, B. L.; Caledonia, G. E.; Cronin, J. F.; Green, B. D.; Lipson, S. J.; Blumberg, W. A. M.; Dodd, J. A. Rotational Relaxation of High-N States of OH ($X^2\Pi$, v = 1–3) by O_2. *J. Geophys. Res.* **1997**, *102*, 4521–4528.

(19) Hickson, K. M.; Sadowski, C. M.; Smith, I. W. M. Rate Coefficients for Rotational Energy Transfer from the Levels OH($X^2\Pi_{3/2}$, $v = 1, j_i$ = 1.5, 3.5–8.5) in

Collisions with He, Ar, N_2 and HNO_3. *Phys. Chem. Chem. Phys.* **2002**, *4*, 5613−5621.

(20) Charters, P. E.; MacDonald, R. G.; Polanyi, J. C. Formation of Vibrationally Excited OH by the Reaction H + O3. *Appl. Opt.* **1971**, *10*, 1747−1754.

(21) Ohyama, H.; Kasai, T.; Yoshimura, Y.; Kimura, H.; Kuwata, K. Initial Distribution of Vibration of the OH Radicals Produced in the H + O3 → $OH(X^2\Pi_{3/2,1/2}) + O_2$ Reaction. Chemiluminescence by a Crossed Beam Technique. *Chem. Phys. Lett.* **1985**, *118*, 263−266.

(22) Klenerman, D.; Smith, I. W. M. Infrared Chemiluminescence Studies Using a SISAM Spectrometer. Reactions Producing Vibrationally Excited OH. *J. Chem. Soc., Faraday Trans. 2* **1987**, *83*, 229−241.

(23) Yardley, J. T. *Introduction to Molecular Energy Transfer*; Academic Press: New York, 1980.

(24) Smith, G. K.; Butler, J. E. OH ($X^2\Pi_i$) Product Internal Energy Distribution Formed in the Reaction of $O(^1D_2)$ with H_2. *J. Chem. Phys.* **1980**, *73*, 2243−2253.

(25) Butler, J. E.; MacDonald, R. G.; Donaldson, D. J.; Sloan, J. J. Vibrational Excitation of OH($X^2\Pi$) Produced in the Reaction of $O(^1D)$ with H_2. *Chem. Phys. Lett.* **1983**, *95*, 183−188.

(26) Butler, J. E.; Jursich, G. M.; Watson, I. A.; Wiesenfeld, J. R. Reaction Dynamics of $O(^1D_2) + H_2$, HD, D_2: OH, OD($X^2\Pi_i$) Product Internal Energy Distributions. *J. Chem. Phys.* **1986**, *84*, 5365−5377.

(27) Aker, P. M.; Sloan, J. J. The Initial Product Vibrational Energy Distribution in the Reaction between $O(^1D_2)$ and H_2. *J. Chem. Phys.* **1986**, *85*, 1412−1417.

(28) Huang, Y.; Gu, Y.; Liu, C.; Yang, X.; Tao, Y. The Nascent Product Vibrational Energy Distribution of the Reaction $O(^1D) + H_2$ by the Grating Selection Chemical Laser Technique. *Chem. Phys. Lett.* **1986**, *127*, 432−437.

(29) Cleveland, C. B.; Jursich, G. M.; Trolier, M.; Wiesenfeld, J. R. Dynamics of the Reaction $O(^1D_2) + H_2 \rightarrow OH(X^2\Pi, v'' = 2, 3) + H$: Full Characterization of Product Energetics. *J. Chem. Phys.* **1987**, *86*, 3253−3264.

(30) Mikulecky, K.; Gericke, K.-H. The Influence of Vibrational and Translational Motion on the Reaction Dynamics of $O(^1D) + H_2(^1\Sigma_g^+, v)$. *J. Chem. Phys.* **1992**, *96*, 7490−7499.

(31) Liu, X.; Lin, J. J.; Harich, S.; Schatz, G. C.; Yang, X. A Quantum State-Resolved Insertion Reaction: $O(1D) + H_2(J = 0) \rightarrow OH(^2\Pi, v, N) + H(^2S)$. *Science* **2000**, *289*, 1536−1538.

(32) Aoiz, F. J.; Bañares, L.; Castillo, J. F.; Herrero,V. J.; M.-Haya, B.; Honvault, P.; Launay, J. M.; Liu, X.; Lin, J. J.; Harich, S. A.; Wang, C. C.; Yang, X. The $O(^1D) + H_2$ Reaction at 56 meV Collision Energy: A Comparison between Quantum Mechanical, Quasiclassical Trajectory, and Crossed Beam Results. *J. Chem. Phys.* **2002**, *116*, 10692−10703.

(33) Houston, P. L. *Chemical Kinetics and Reaction Dynamics*; McGraw-Hill: New York, 2001.

(34) Nikitin, E. E.; Troe, J. 70 Years of Landau−Teller Theory for Collisional Energy Transfer. Semiclassical Three-Dimensional Generalizations of the Classical Collinear Model. *Phys. Chem. Chem. Phys.* **2008**, *10*, 1483−1501.

(35) Levine, R. D. *Molecular Reaction Dynamics*; Cambridge University Press: Cambridge, 2005.

Table 2.1. Rate coefficients k_v for vibrational relaxation of OH($X^2\Pi$, $v = 1-12$).

v	1	2	3	4	5	6	7	8	9	10	11	12
H_2O	2.09 ± 0.08 (11)[b]	3.66 ± 0.17 (11)[b]	9.08 ± 1.53 (11)[b]									
NH_3	2.86 ± 0.12 (11)[b]	1.26 ± 0.12 (10)[b]	3.0 ± 1.0 (10)[c]									
CH_3SH	2.51 ± 0.13 (11)[b]	2.60 ± 0.21 (11)[b]										
O_2	1.3 ± 0.4 (13)[d]	2.7 ± 0.8 (13)[d]	5.2 ± 1.5 (13)[d]	8.8 ± 3.0 (13)[d]	1.7 ± 0.7 (12)[d]	3.0 ± 1.5 (12)[d]	7 ± 2 (12)[e]	8.0 ± 1.0 (12)[f]	1.7 ± 1.1 (11)[g]	1.50 ± 0.12 (11)[f]	2.79 ± 0.14 (11)[f]	1.6 ± 0.2 (11)[h]
CO_2	1.8 ± 0.5 (13)[d]	4.8 ± 1.5 (13)[d]	1.4 ± 0.5 (12)[d]	2.8 ± 1.0 (12)[d]			6.7 ± 1.0 (11)[e]	6.4 ± 0.4 (11)[f]	5.7 ± 0.6 (11)[g]	1.86 ± 0.34 (11)[f]	1.9 ± 0.4 (11)[f]	5.6 ± 1.5 (11)[h]
N_2O		4.6 ± 0.6 (13)[i]					3.0 ± 0.6 (11)[e]	6.2 ± 0.7 (11)[f]	6.4 ± 1.0 (11)[g]	3.7 ± 0.3 (11)[f]		
CH_4	5.06 ± 0.40 (13)[b]	2.02 ± 0.20 (12)[b]	4.49 ± 0.20 (12)[b]									
DMS	2.55 ± 0.09 (11)[b]	5.34 ± 0.73 (11)[b]										
CS_2	1.17 ± 0.08 (11)[b]	1.57 ± 0.08 (11)[b]										
CH_3Br	5.05 ± 0.39 (13)[b]	1.80 ± 0.36 (12)[b]										
He		<1 (14)[i]							<2 (12)[g]	3 ± 1 (13)[f]	~6 (13)[f]	3.6 ± 0.6 (12)[h]
Ar		<1 (14)[j]							<2 (13)[g]			2.6 ± 0.5 (12)[h]
H_2		<1 (14)[i]							<3 (12)[g]			3.0 ± 0.8 (12)[h]
N_2		<1 (14)[j]					<6 (13)[e]	7 ± 4 (13)[f]	<5 (13)[g]	1.6 ± 0.6 (12)[f]		2.5 ± 0.7 (12)[h]

Rate coefficients are in units of cm^3 $molecule^{-1}$ s^{-1}. Number between brackets, (x), shows the order of rate coefficients, 10^{-x}.

[a] Collision partners.

[b] ref 4; [c] ref 6; [d] ref 9; [e] ref 11; [f] ref 12; [g] ref 10; [h] ref 8; [i] ref 5; [j] ref 3

Table 2.2. Transmittances of the optical filters at the wavelengths of the photolysis of O_3 and probe of OH.

	BP 3039	BP 3071	Cut On WG295	UV-D33	UV-D36B	UV-D35 (1)	UV-D35 (2)	UV_D35 ×2
266 nm (Photolysis)	1.9	0.1	0	61.3	0	0.6	0	0
309 nm (0-0 band)	26.8	14	48.5	87.1	14.7	66.7	54.3	36.2
314 nm (1-1 band)	25.6	6.3	61.5	87.5	23.1	73.1	63.6	46.5
320 nm (2-2 band)	21.6	1.2	70.8	87.7	33.5	78.3	70.8	55.4
396 nm (1-3 band)	0	0	91.7	29.6	0	1.0	8.9	0.1
400 nm (2-4 band)	0	0	90.9	19.9	0	3.2	2.6	0.1

Transmittances were measured by spectrophotometer (U-3010, HITACHI). Transmittances are in units of %. BP : band-pass filter (Melles Griot), Cut on : Colored Glass Filter (Newport), UV-D×× : UV band-pass filter (Toshiba). Nambers between brackets of UD-D35 show the assigned number for distinction in laboratory. The transmittance of UV-D35 × 2 is that of the case using two UV-D35.

Table 2.3. Rate coefficients k_v^{He} for vibrational relaxation of OH($X^2\Pi$, v = 1–4) by collisions with He determined by IPM.

v	1	2	3	4
k_v^{He}	$(2.9 \pm 1.5)\times10^{-17}$ [a]	$(1.4 \pm 0.4)\times10^{-16}$	$(5.2 \pm 0.5)\times10^{-16}$	$(1.6 \pm 0.2)\times10^{-15}$

[a] Rate coefficients are in units of cm^3 $molecule^{-1}$ s^{-1} and the stated confidence limits are $\pm2\sigma$.

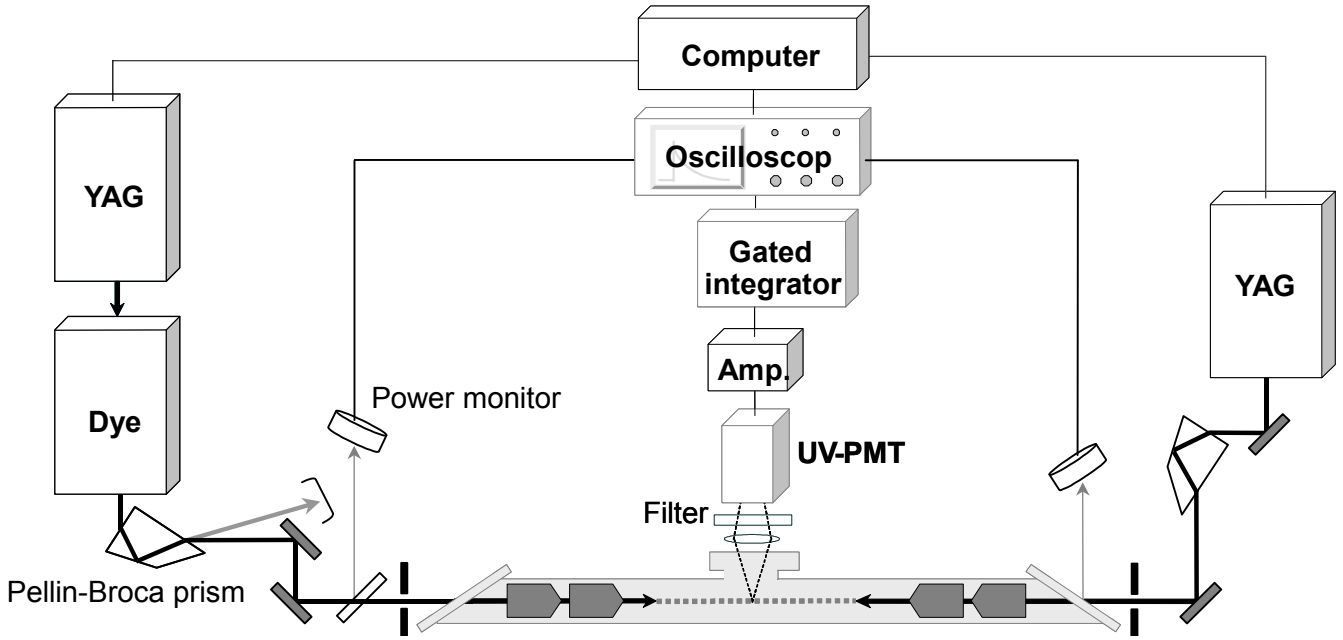

Figure 2.1. A schematic diagram of experimental apparatus. Amp. : preamplifier made in house, PMT : photomultiplier tube.

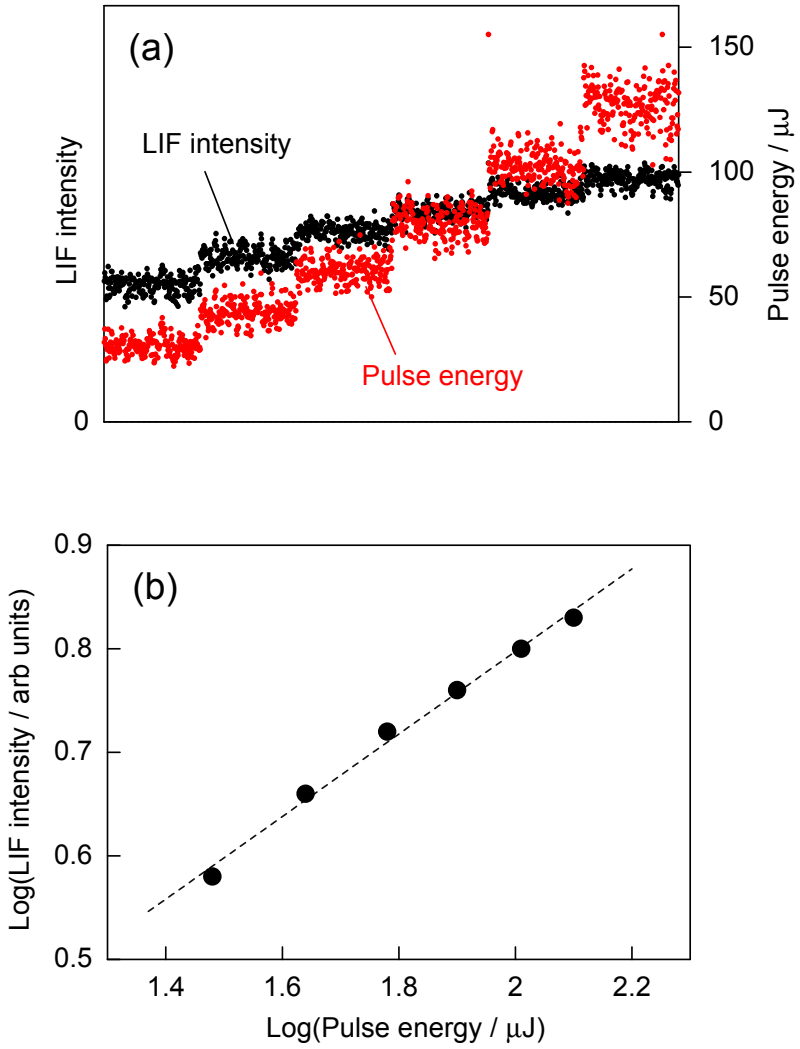

Figure 2.2. The dependence of the LIF intensity of OH($v = 0$) on the pulse energy of the probe laser. Part a shows the LIF intensity at different pulse energies of the probe laser. Part b is the logarithmic plot of the LIF intensity versus the pulse energy. The broken line shows a straight line fit from linear regression analysis.

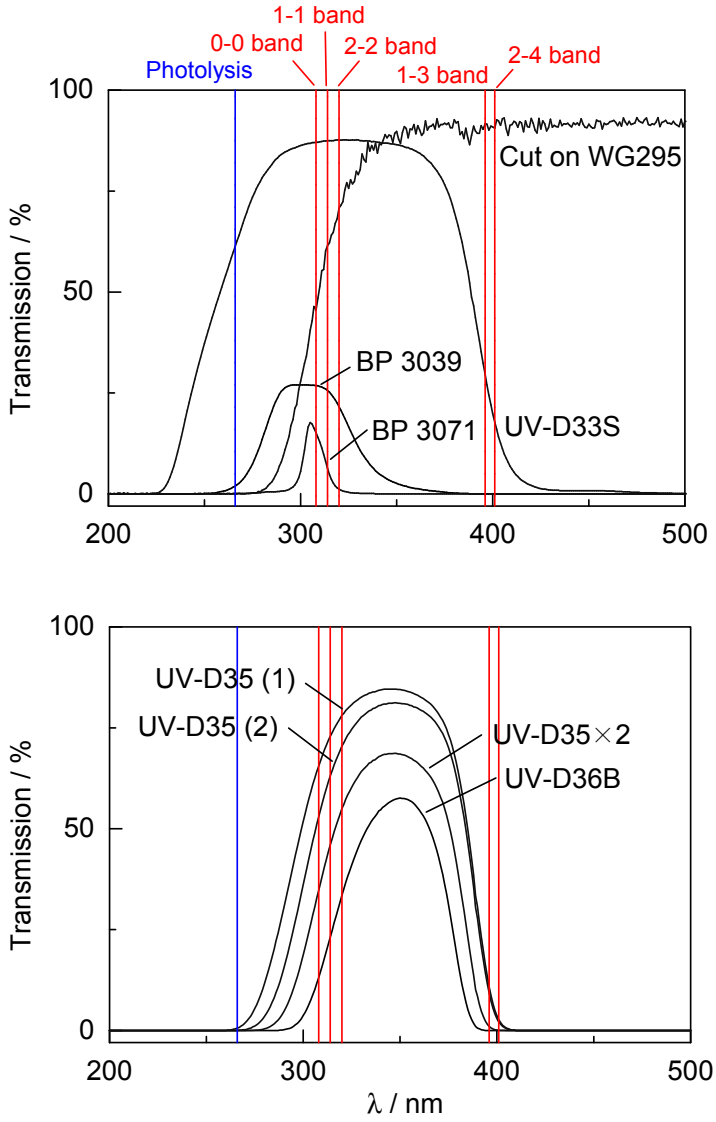

Figure 2.3. Transmittance curves of the optical filters. BP : band-pass filter (Melles Griot), Cut on : Colored Glass Filter (Newport), UV-D×× : UV band-pass filter (Toshiba). In this dissertation, UV-D35 (2) and UV-D35 × 2 were used for detection of $v = 0 - 2$ and $v = 3, 4$, respectively. Nambers between brackets of UD-D35 show the lot numbers. The curve of UV-D35 × 2 is made of a squared transmittance of UV-D35. Lines colored with red shows the wavelengths of the photolysis of O_3 and excited band of OH.

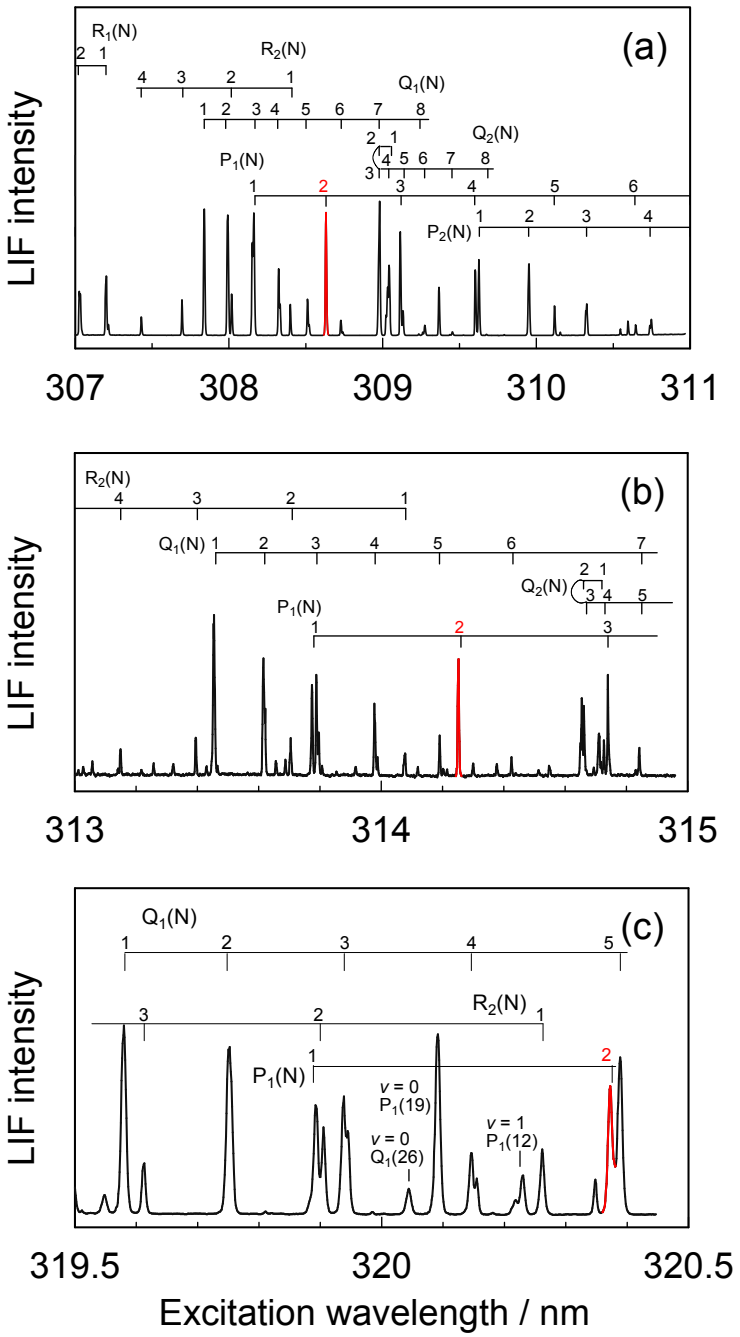

Figure 2.4. Laser-induced fluorescence excitation spectra of OH($X^2\Pi$, $v = 0$, 1, and 2) generated in the O(^{1}D) + H_2 reaction. The fluorescence was excited via the $\Delta v = 0$ sequence: (a) 0–0; (b) 1–1; (c) 2–2. Delay times between the photolysis and probe lasers were (a) 300, (b) 4, and (c) 4 μs.

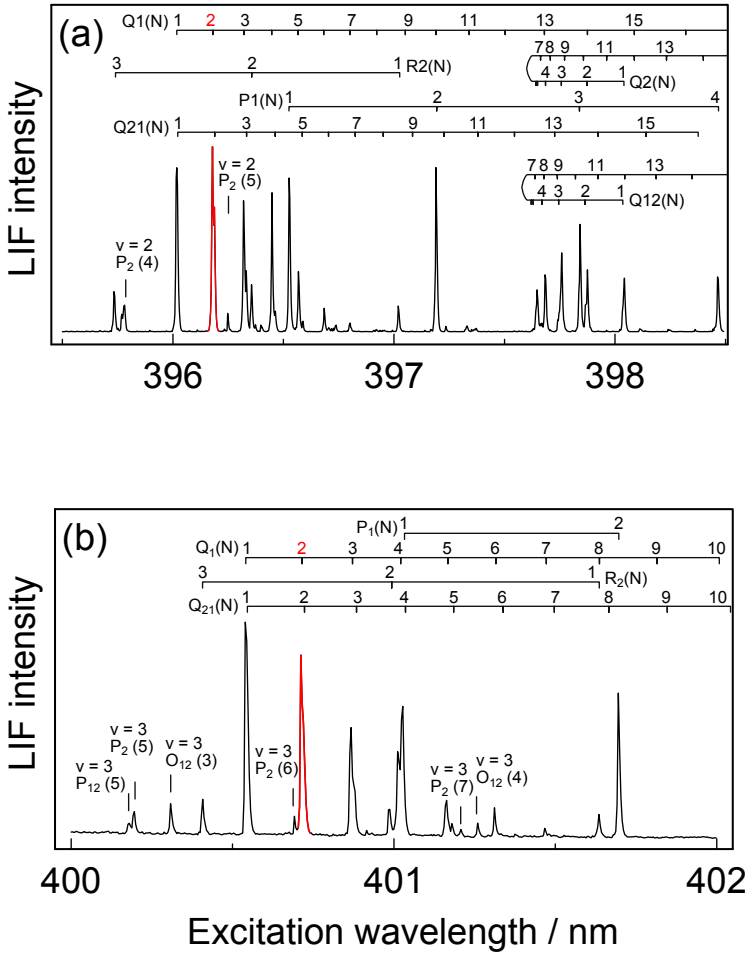

Figure 2.5. Laser-induced fluorescence excitation spectra of OH($X^2\Pi$, $v = 3$ and 4) generated in the $O(^1D) + H_2$ reaction. The fluorescence was excited via the $\Delta v = -2$ sequence: (a) 1–3; (b) 2–4. Delay times between the photolysis and probe lasers were 100 μs in both spectra.

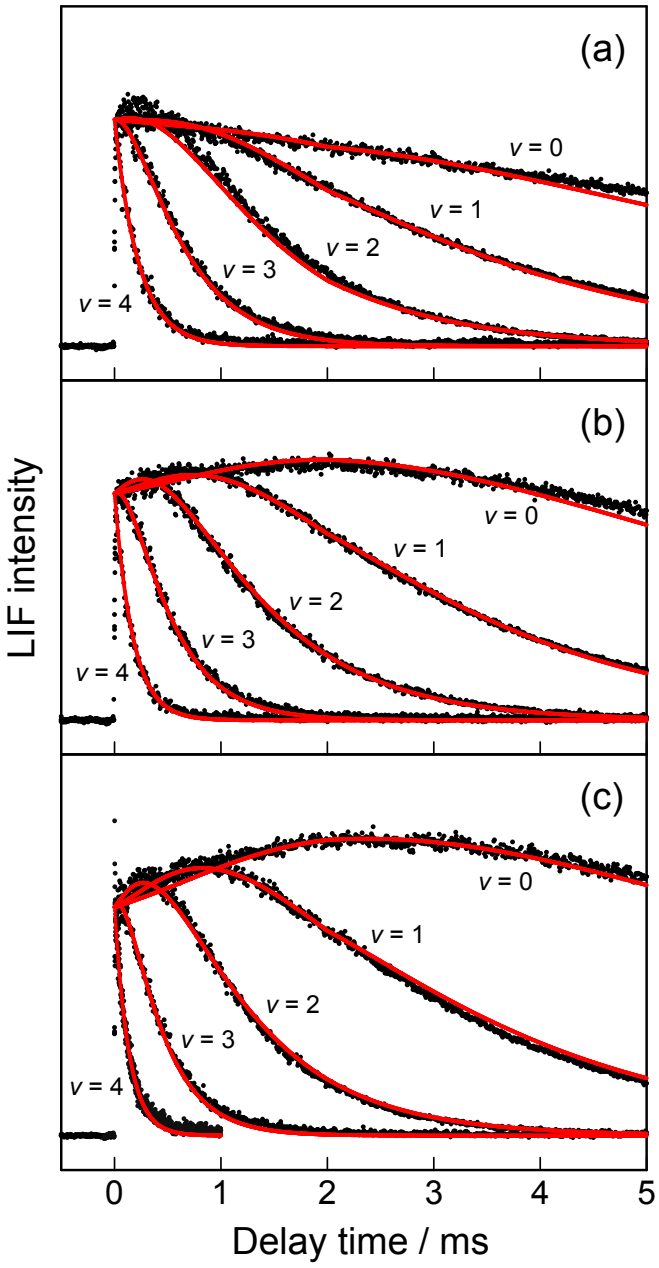
(a)
v = 0
v = 1
v = 2
v = 3
v = 4
(b)
v = 0
v = 1
v = 2
v = 3
v = 4
(c)
v = 0
v = 1
v = 2
v = 3
v = 4
LIF intensity
0
1
2
3
4
5
Delay time / ms

Figure 2.6.

Figure 2.6. Time-resolved LIF intensities of the vibrational levels $v = 0 - 4$ of $OH(X^2\Pi)$ generated in the reaction $O(^1D) + H_2$. The pressures of He buffer are (a) 70, (b) 100, and (c) 130 Torr. The partial pressures of the sample gases: $p(O_3)$ = 0.01 mTorr for $v = 0 - 2$ and 0.1 mTorr for $v = 3$ and 4; and $p(H_2)$ = 180 mTorr. The abscissa is the delay time between the photolysis and probe laser. All the profiles are so scaled as to make their initial intensities the same. The step sizes of the time scans were 5.5 μs, except for that of v = 4 at 130 Torr was 1.1 μs. The black and red dots denote observed data and the results of simulation by eq XI in the text, respectively.

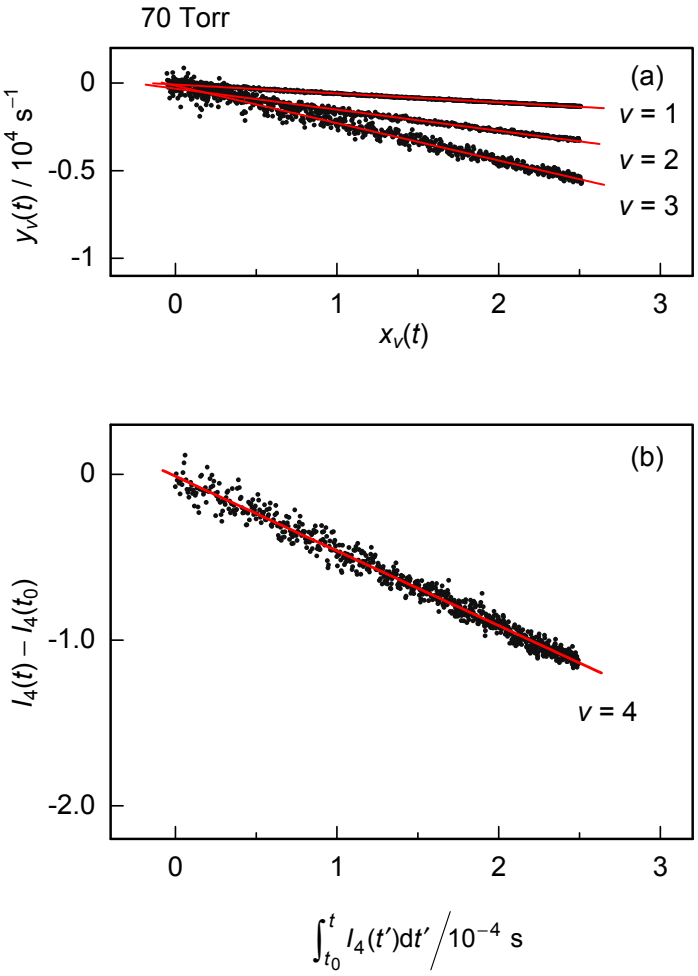

Figure 2.7. IPM plots made from the time profiles shown in Figure 2.6a at 70 Torr of He. $y_v(t)$ and $x_v(t)$ in part a are defined by eqs VI and VII in the text, respectively. The ordinate and abscissa of part b are $I_4(t) - I_4(t_0)$ and $\int I_4(t')dt'$, respectively. The slopes given by a linear regression (red lines) correspond to the apparent pseudofirst-order decay rates, a_v defined by eq VIII, of the vibrational levels.

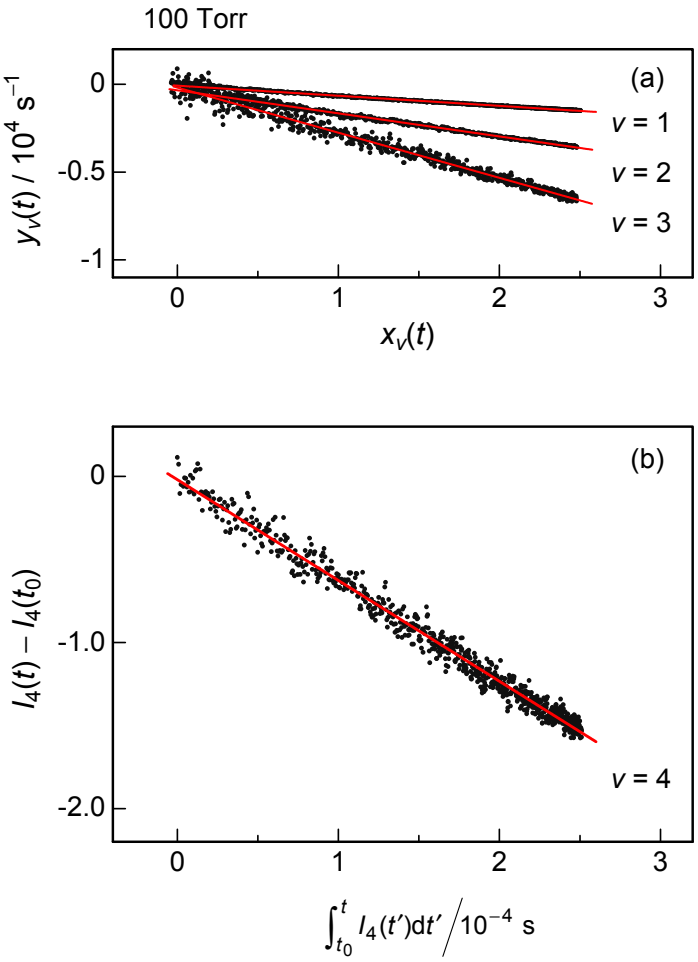

Figure 2.8. IPM plots made from the time profiles shown in Figure 2.6b at 100 Torr of He.

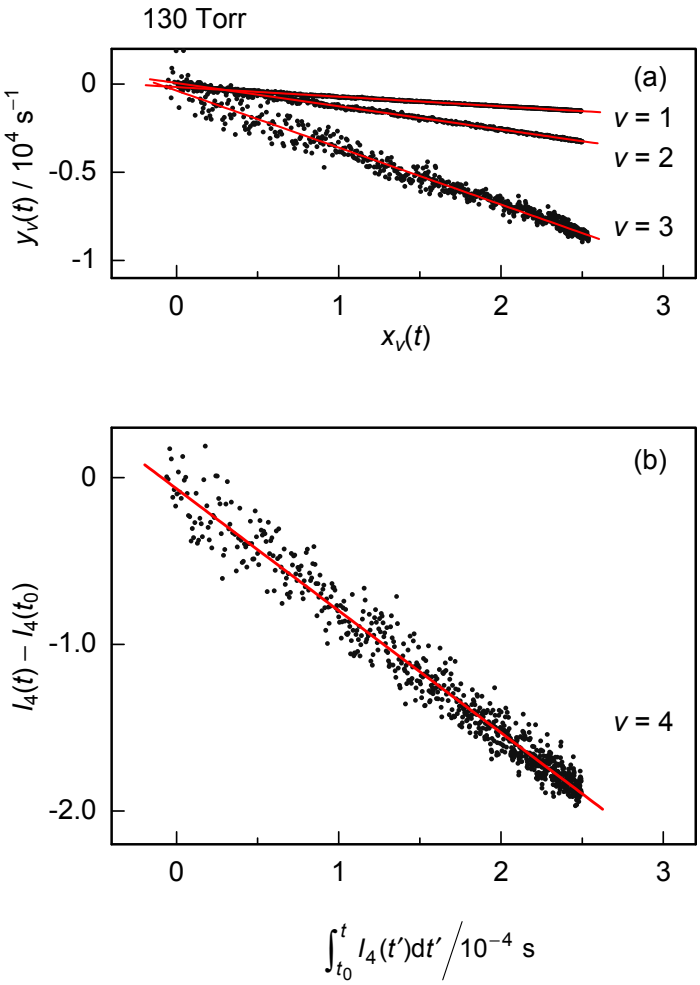

Figure 2.9. IPM plots made from the time profiles shown in Figure 2.6c at 130 Torr of He.

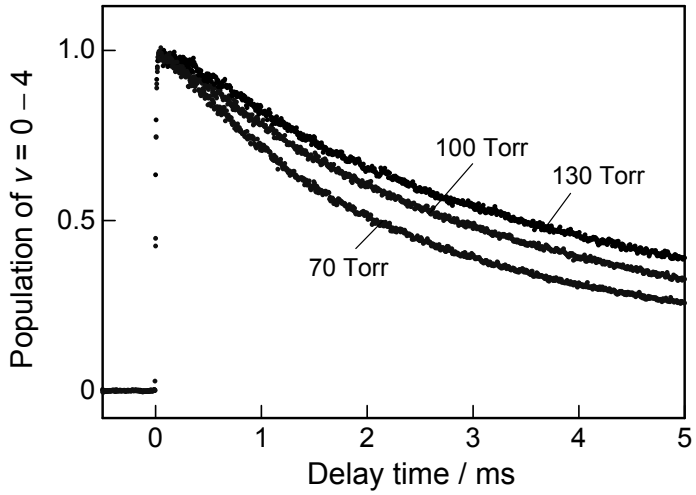

Figure 2.10. Time profiles of the total populations of $OH(v = 0-4)$ at different He pressures. The total populations are calculated from the observed time profiles shown in Figure 2.6 and the nascent vibrational energy distributions $v = 0/v = 1/v = 2/v = 3/v = 4 = 0.29/0.25/0.23/0.15/0.08$ reported in refs 31 and 32. The abscissa is the delay time between the photolysis and probe laser.

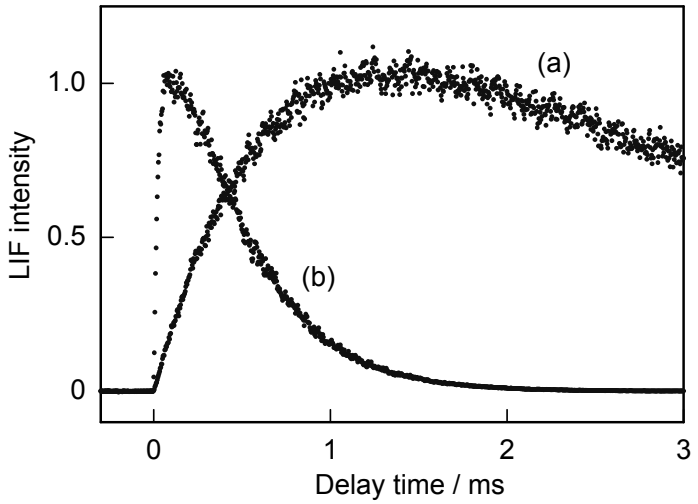

Figure 2.11. Time profiles of $OH(v=1)$ generated in the absence of H_2. The pressures of He buffer were 100 Torr. The partial pressures of the sample gases are (a) $p(O_3)$ = 0.01 mTorr and (b) $p(O_3)$ = 0.2 mTorr. Time profiles were independent of the pressure of O_3. The profile (a) was recorded after evacuation of the whole gas line for a day; the profile (b) was recorded under the condition that the gas line including the pressure regulator of gas cylinder was filled with He at 1000 Torr for a week without evacuation. Time profiles are so scaled as to make their maximum intensities the same.

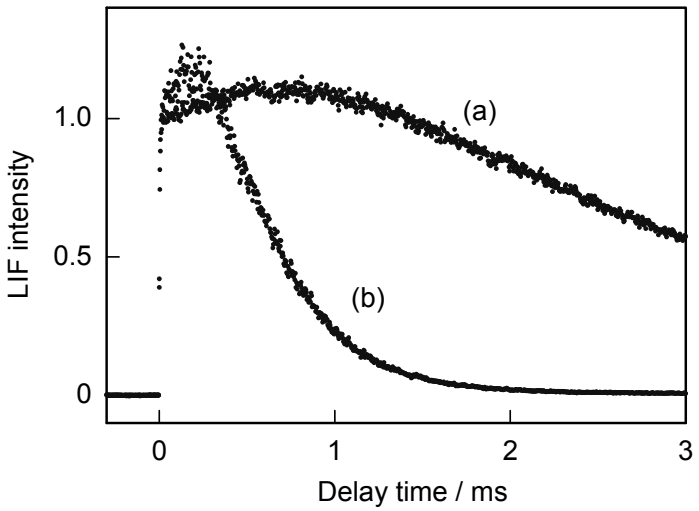

Figure 2.12. Time profiles of $OH(v=1)$ generated in the reaction $O(^1D) + H_2$. The pressures of He buffer were 100 Torr. The partial pressures of the sample gases are (a) $p(O_3)$ = 0.01 mTorr and (b) $p(O_3)$ = 0.2 mTorr; and $p(H_2)$ = 180 mTorr. Time profiles were independent of the pressure of O_3. The profiles (a) and (b) were recorded under the identical conditions with those of Figure 2.11a and b, respectively. Time profiles are so scaled as to make their initial intensities the same.

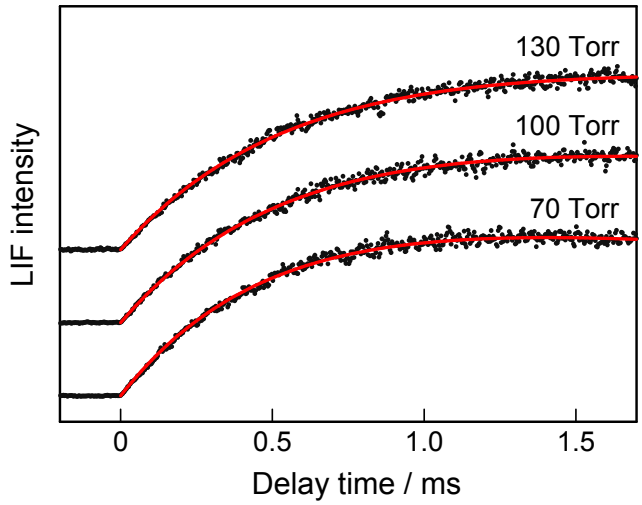

Figure 2.13. Time profiles of $OH(v = 0)$ generated in the absence of H_2 at different He pressures. The partial pressure of O_3 was 0.01 mTorr. The three profiles are depicted on the different baselines with the identical spacing. The black dots denote the observed data, and the red lines represent the fit by the exponential growth.

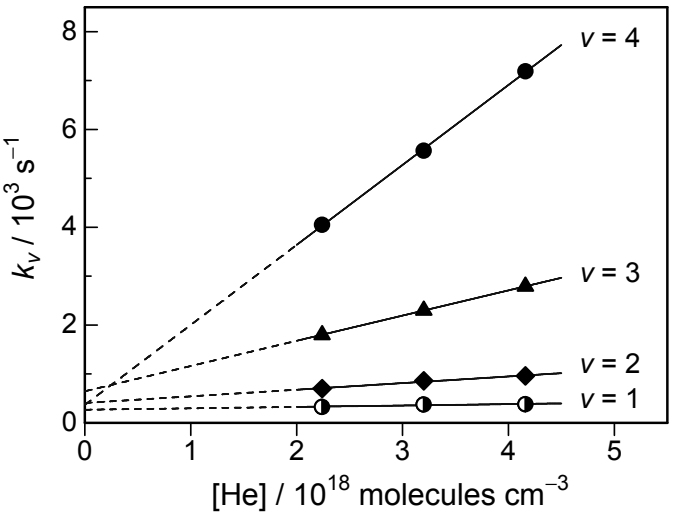

Figure 2.14. Plots of k_v versus [He] for $v = 1 - 4$. The definition of k_v is given in eq VIII in the text. The filled circles correspond to $v = 4$, the triangles to $v = 3$, the diamonds to $v = 2$, and the half-filled circles to $v = 1$. The slopes of the straight line fit from regression analysis give the bimolecular rate coefficients for relaxation by He k_v^{He}.

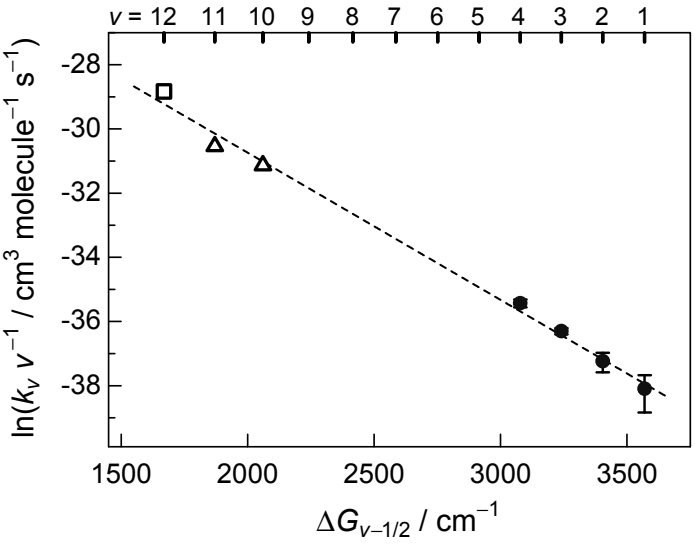

Figure 2.15. Correlation between semilogarithmic k_v^{He}/v and vibrational spacing $\Delta G_{v-1/2}$ of $\mathrm{OH}(\mathrm{X}^2\Pi)$. The numbers on the top abscissa are the vibrational quantum numbers of $\mathrm{OH}(\mathrm{X}^2\Pi)$. The open square corresponds to the data from ref 8, the open triangles from ref 12, and the solid circles to the present study with the confidence limits of 2σ. The broken line shows the result of linear regression.

CHAPTER 3 ACCELERATION OF THE REACTION OH + CO → H + CO_2 BY VIBRATIONAL EXCITATION OF OH

3.1 INTRODUCTION

The reaction of OH with CO has been attracting the researchers in the fields of the atmospheric and combustion chemistry. The reaction, OH + CO → H + CO_2, is one of the important processes as the removal of OH in the troposphere,[1] and a pivotal process to form CO_2 in combustion. The extensive kinetic studies on the reaction[2-6] have found that the reaction proceeds via an adduct OH–CO with a shallow minimum and HO–CO with a deep well on the way to the products H + CO_2 as shown in Figure 3.1.[7,8] Lester et al.[9] identified linear OH–CO in a supersonic expansion by infra-red spectrometry, and Jacox and co-workers[10,11] has detected both *trans*- and *cis*-HO–CO in matrices. There are two paths reaching the products H + CO_2 from the *trans*-HOCO: the one forms *cis*-HOCO via a low TS2 and dissociates H + CO_2 via a high TS3; the other proceeds with migration of H atom to O atom via a high TS4 and HCO_2 converts to H + CO_2 via a low TS5. Frost et al.[4] measured the temperature dependence (80 – 297 K) of the decay rates of OH, and made analysis based on the transition-state and RRKM theories, reporting the vibrationally adiabatic barrier at the entrance saddle point (TS1) to be within 120 – 210 cm^{-1}. They also determined the difference between the zero-point energies at TS1 and TS3, defined by $E_{TS3} - E_{TS1}$, to be about 640 cm^{-1} from the analysis including tunneling effect.

There have been numerous kinetic studies on the reaction,[12,13] for example, 140 rate coefficients are listed in NIST Chemical Kinetics Database.[14] The most recent recommended value of the rate coefficient for OH(v = 0) + CO → H + CO_2 is [1.5 ± 0.3(2σ)] × 10^{-13} cm^3 $molecule^{-1}$ s^{-1} at 298 K.[13] There, however, have been only few

reports on the effect of vibrational excitation of the reactants OH or CO. Chen and Macus[15] have recently reanalyzed the experimental data reported by Dreier and Wolfrum,[2] and evaluated the rate coefficients at the CO vibrational quantum number v_{CO}, showing that the rate coefficients decrease from $v_{CO} = 0$ to $v_{CO} = 1$: $k(v_{CO} = 1)/k(v_{CO} = 0) \approx 1/3$ and then increase with v_{CO} and recover at $v_{CO} = 4$: $k(v_{CO} = 4) \approx k(v_{CO} = 0)$.

Vibrational excitation of OH reactant has been performed by a few groups. Spencer et al.[16,17] generated OH($v \leq 2$) by discharge flow method and detected them by electron paramagnetic resonance, reporting that vibrational excitation of OH enhances the reaction with CO by about a factor of two: $k(v_{OH} = 2)/k(v_{OH} = 1)/k(v_{OH} = 0) \approx 2.2/1.7/1.0$. Unfortunately, the low sensitivity of their method and resultant large confidence limit (over 100 %) made it difficult to clarify the effect of vibrational excitation on the branching ratios between reaction and relaxation. Brunning et al.[3] generated OH and OD in $v = 0$ and 1 by the photolysis of HNO_3 (DNO_3) or H_2O (D_2O) with a flashlamp or laser, and detected the vibrational levels by the laser-induced fluorescence (LIF) technique, reporting the enhancement of the overall removal rate coefficients of OH and OD: $k(v_{OH} = 1)/k(v_{OH} = 0) \approx 7$ and $k(v_{OD} = 1)/k(v_{OD} = 0) \approx 17$. They have concluded that the rate coefficients for relaxation of the vibrationally excited levels correspond to that for the formation of adducts XOCO (X = H or D) based on the "proxy method."[18] The binding energy of XO–CO, about 103 kJ mol^{-1},[19,20] is large enough to relax the initially excited OX vibration in the adduct XO(v = 1)–CO, and consequently, the adduct does not decompose back to OX(v = 1) and CO but to OX(v = 0) and CO. The overall removal rates of vibrationally excited levels, therefore, give the association rates of OX and CO. Fulle et al.[6] measured the dependence of the reaction of OH with CO on a wide range of pressures and

temperatures based on the photolysis and probe technique, reporting the limiting high-pressure rate coefficient corresponding to association rate to be $k_\infty = 9.6 \times 10^{-13}$ cm^3 molecule^{-1} s^{-1} at 300 K. They also have measured the rate coefficient of vibrational relaxation from the overall decay of $\mathrm{OH}(v=1)$: $k(v_{\mathrm{OH}}=1) = 1.2 \times 10^{-12}$ cm^3 molecule^{-1} s^{-1} at 314 K which is nearly identical with k_∞, indicating that the proxy method is valid for OH + CO reaction.

There are two competing processes in the adduct HO(v)–CO formed from vibrationally excited OH(v) and CO: intramolecular vibrational relaxation HO(v)–CO $\rightarrow$ HO($v' < v$)–CO and chemical reaction to H + CO_2. To the best of our knowledge, there have been no experimental measurements on the vibrational level dependence of the branching ratios between intramolecular relaxation and chemical reaction. In the present study, we have performed the systematic measurements of the dependence of the contribution of reactive process, OH(v) + CO $\rightarrow$ H + CO_2, on the initial vibrational levels of OH. The results show that vibrational excitation of OH is more favorable for reactive process than intramolecular vibrational relaxation in the complex and that the stepwise intramolecular relaxation HO(v)–CO $\rightarrow$ HO(v–1)–CO is followed by re-dissociation to HO(v–1) + CO.

3.2 EXPERIMENT

3.2.1 Apparatus

Figure 3.2 shows the schematic diagram of the experimental apparatus. The details of the system have been described in Chapter 2 except the systems for detection of VUV fluorescence and dispersion with a monochromator (JEOL JSG-125S, f = 125 cm, $\Delta\lambda$(fwhm) = 3 nm). In this study, a VUV fluorescence detection system has been constructed to detect H atoms.

3.2.2 Generation of Vibrationally Excited OH(v)

A gaseous mixture $O_3/H_2/CO/He$ (typical conditions: p_{O_3} = 0.01 – 0.5 mTorr, p_{H_2} = 150 mTorr, p_{CO} = 0 – 400 mTorr, and $p_{total}(He)$ = 10 Torr) at 298 ± 2 K in a flow cell was irradiated with the fourth harmonic wave (266 nm) from a Nd^{3+}:YAG laser (Spectra Physics GCR-130). The UV light decomposes O_3 into $O(^1D)$ and $O_2(a^1\Delta_g)$ with a high quantum yields 0.9 ± 0.1,[1,12,13] and the fluence of photolysis laser was 5 mJ cm^{-2}. The reaction $O(^1D) + H_2 \rightarrow OH(v) + H$ generates vibrationally excited OH in the electronic ground state $X^2\Pi_i$. The highest vibrational level generated by the heat of reaction is $v = 4$.

The concentration of initially prepared $O(^1D)$ was estimated to be $(0.2 – 16) \times 10^{11}$ atoms cm^{-3} from the present experimental conditions: the partial pressure of O_3, 0.01 – 0.5 mTorr; the fluence of the photolysis laser, (5 – 9) mJ cm^{-2}; the photoabsorption cross section of O_3 at 266 nm, 9.68×10^{-18} cm^2; and the quantum yield of $O(^1D)$, 0.9 ± 0.1.[1,12,13] The pseudo-first-order reaction conditions $[H_2]/[O(^1D)]_0 > 900$ and thus $[CO]/[OH]_0 > 900$ were satisfied throughout the experiments.

3.2.3 Detection of Vibrationally Excited OH(v) by LIF Technique

The vibrational levels $v = 0 – 4$ of OH were excited via the $A^2\Sigma^+ – X^2\Pi$ transition with a Nd^{3+}:YAG laser (Spectra Physics GCR-130) pumped dye laser (Lambda Physik LPD3002) and the laser-induced fluorescence (LIF) was detected with a photomultiplier tube (PMT; Hamamatsu R1104) through two UV band-pass filters (Toshiba UV-D35 × 2). The typical pulse energies of the probe laser were 200 and 900 μJ $pulse^{-1}$ for $v = 0 – 2$ and $v = 3$ and 4, respectively. The vibrational sequence of $\Delta v = 0$ was excited for probing the levels $v = 0 – 2$ and $\Delta v = –3$ for $v = 3$ and 4, because fluorescence

quantum yields of the vibrational levels $v' \geq 3$ of $A^2\Sigma^+$ are very small as a result of predissociation. A frequency-doubled light from DCM dye was used for detecting $v = 0 - 2$, and a fundamental beam with C-440 dye for $v = 3$ and 4. Recorded LIF excitation spectra of OH($A^2\Sigma^+ - X^2\Pi$) of $v = 3$ and 4 are shown in Figure 3.3, and those of $v = 0 - 2$ have been shown in Chapter 2. All the peaks are assigned to the rotational lines at each vibrational level.

3.2.4 Detection of H Atoms by Two-photon LIF Technique

Figure 3.4 shows the scheme of the detection of H atoms by two-photon LIF technique. A light at 243.12 nm from the Nd^{3+}:YAG laser-pumped dye laser was focused with a quartz lens (f = 300 mm) and went through the flowing cell. H atoms were excited to $^2S(2s)$ state by two-photon absorption at 243.12 nm, and the $^2S(2s)$ state was efficiently converted to $^2P(2p)$ state by collisions with ambient gases. The Lyman-α emission $^2P(2p) \rightarrow {}^2S(2s)$ at 121.56 nm was collected with a MgF_2 lens (f = 45 mm) and detected with a solar-blind PMT (Hamamatsu R10454). An interference filter (Acton Research 122-N) was placed between the lens and PMT to block the stray light of the exciting laser. The light path from the observation window to the PMT was purged by the flow of dry N_2 to prevent residual O_2 from absorbing the VUV fluorescence. A frequency-doubled light from LD-489 dye (doubled with BBO I crystal delivered by Lambda Physik) was used for detecting H atoms. The system enables us to detect H atoms even at 200 μJ $pulse^{-1}$ of the laser pulse energy. In this study, the typical pulse energy, 900 μJ $pulse^{-1}$, was monitored with a joule meters (GENTEC ED-100A and Molectron J5-09). Figure 3.5 shows the LIF excitation spectra of H atoms.

3.2.5 Time Profiles of OH(v) and H Atoms

To record the time profiles of the LIF intensities, the wavelength of the probe laser was tuned to a rotational line of the vibrational level of OH or 243.12 nm for H atoms, after which the delay times between the photolysis and probe laser were automatically scanned with a pulse delay controller made in house. The buffer gas (He) at 10 Torr was sufficient for rapid rotational relaxation in about 5 μs, and consequently, LIF intensity excited via a single rotational line represents the time evolution of the population in a vibrational level. The transition probabilities of the sequence $\Delta v = -3$ are smaller than those of $\Delta v = 0$ by three to four orders of magnitude.[21] To observe the time profiles with nearly identical signal-to-noise ratio, 0.01 – 0.05 and 0.5 mTorr of O_3 were used for detecting the transitions with $\Delta v = 0$ and –3, respectively. Little difference in the relative populations or time profiles of all the vibrational levels was observed over the partial pressures 0.01 – 0.5 mTorr of O_3.

3.2.6 Removal of Impurity

A small part of CO was converted to $Ni(CO)_4$ at the surface of stainless steel, and the UV laser photolysis of the carbonyl at 266 nm gave unwanted intense emission from electronically excited Ni atoms. Figure 3.6 shows a dispersed emission collected with a lens (f = 80 mm) and focused on the entrance slit of a monochromator. The red bar in Figure 3.6 represents the transitions of the emission from electronically excited Ni atoms.[22] The emission from Ni, which appeared over the wavelengths of the fluorescence of OH, was not separated with optical filters. Pyrolysis, $Ni(CO)_4 \rightarrow Ni + 4CO$, at $T \gtrsim 450$ K was effective to remove $Ni(CO)_4$.[23] A U-shaped Pyrex glass was inserted in a flow line of CO (as shown in Figure 3.7) and warmed with a tape heater up to ~500 K. The temperature dependence of the intensity of emission from Ni was observed to find the optimum temperature. The most intense emission from Ni at 352

nm, indicated by the arrow in Figure 3.6, was recorded along with the temperature of the tape heater (Figure 3.8), indicating that unwanted emission disappeared completely at $T > 460$ K. Metallic Ni was coated on the inner wall of the glass tube, and Ni was not carried to the flowing cell.

3.2.7 Samples

O_3 was prepared by an electrical discharge in high-grade O_2 (Japan Fine Products, > 99.99995%) with a synthesizer made in house and stored in a 3 dm^3 glass bulb with He (0.3 – 7.8 % dilution). The total pressure of a sample gas was monitored with a capacitance manometer (Baratron 122A). The total pressure measurement together with the mole fractions as measured with calibrated flow controllers (Tylan FC-260KZ, STEC-410, and STEC SEC-400 mark3) gave the partial pressures of the reagents. High-grade O_2 (> 99.99995 %), H_2 (> 99.99999 %), CO (> 99.95 %), and He (> 99.99995 %), delivered by Japan Fine Products, were used without further purification.

3.3 RESULTS AND DISCUSSION

3.3.1 Analysis of the Time Profiles of OH(*v*) and H Atoms.

The rotational lines, $P_1(N = 2)$ of 0–0, 1–1, and 2–2, and $Q_1(N = 2)$ of 0–3 and 1–4 bands were excited to record the time-resolved LIF intensities of the vibrational levels of OH (red peaks in Figure 2.4 and Figure 3.3). The time profiles of OH($v = 0 - 4$) recorded at various CO pressures are shown in Figure 3.9. Several groups [24-32] have reported the nascent vibrational energy distributions of OH generated in the $O(^1D) + H_2 \rightarrow OH(v) + H$ reaction. Their sources of $O(^1D)$ were photolysis of O_3 at 248,[25,27,29] 266,[24,26,30], and 200–300 nm,[28] and O_2 at 157 nm.[31,32] The collision energies at the center of mass of $O(^1D)$ and H_2 are 661, 597, and 452 cm^{-1} for O_3/248, O_3/266, and

O_2/157 nm photolysis, respectively. The O_3/266 nm photolysis was employed in the present study, and O(^{1}D) was generated in a buffer gas at 10 Torr of He. The rate coefficient for velocity relaxation of hot O(^{1}D) by collisions with He is 9.9×10^{-11} cm^3 molecule^{-1} s^{-1},[33] and thermalization of the translational motion of O(^{1}D) is completed within 30 ns at 10 Torr of He. The thermal collision energy between O(^{1}D) and H_2 is $(3/2)RT$ = 311 cm^{-1} at 298 K and closest to the conditions of Yang's group.[31,32] All the profiles shown in Figure 3.9, therefore, are so scaled as to make their initial relative populations the identical with those reported by Yang's group:

$v = 0/v = 1/v = 2/v = 3/v = 4$ = 0.29/0.25/0.23/0.15/0.08

There are possible side reactions.

$$H + O_3 \rightarrow OH + O_2 \quad (1)$$

$$OH + O_3 \rightarrow HO_2 + O_2 \quad (2)$$

$$OH + H_2 \rightarrow H_2O + H \quad (3)$$

$$O(^3P) + OH \rightarrow O_2 + H \quad (4)$$

$$OH + OH \rightarrow H_2O + O \quad (5)$$

$$OH + CO + M \rightarrow HOCO + M \quad (6)$$

$$H + O_2 + M \rightarrow HO_2 + M \quad (7)$$

The rate coefficients for bimolecular reactions (1) – (5):[13] $k_1 = 2.9 \times 10^{-11}$; $k_2 = 7.3 \times 10^{-14}$; $k_3 = 6.7 \times 10^{-15}$; $k_4 = 3.3 \times 10^{-11}$; $k_5 = 1.8 \times 10^{-12}$ cm^3 molecule^{-1} s^{-1}, and corresponding pseudo-first-order reaction rate coefficients are estimated to be less than 400, 1, 30, 60, and 3 s^{-1}, respectively, under the present experimental conditions. The effective bimolecular rate coefficients for termolecular reactions (6) and (7):[13] $k_6 = 1.8 \times 10^{-15}$ and $k_7 = 1.4 \times 10^{-14}$ cm^3 molecule^{-1} s^{-1} give 23 and 0.03 s^{-1}. As shown in Figure 3.9, the time constants τ typical of the profiles of the vibrationally excited OH are less

than ~300 μs ($\tau^{-1} \gtrsim 3300\ s^{-1}$), and the side reactions are sufficiently slow not to affect the kinetics of OH(v). The decay of the relative populations of $OH(v = 1-4)$ was actually little dependent on the pressures of O_3 (0.01 – 0.5 mTorr), indicating that none of the possible side reactions disturbs the present measurements.

In Figure 3.9, the profiles of $v = 0$ show growth at high CO pressures, indicating the effect of vibrational relaxation from vibrationally excite levels to $v = 0$. The increase in the population of $v = 0$, however, is much smaller than expected from the nascent population ratio: $[v \geq 1]_0 / [v = 0]_0 = 2.4$ even at the highest CO pressure. All the excited vibrational levels $v \geq 1$ decay faster at higher CO pressures. These facts suggest that all the vibrational levels undergo both chemical reaction and vibrational relaxation. Reaction between vibrationally excited OH(v) and CO proceeds via the adduct HOCO, and the adduct may re-dissociation to the reactants OH(v) + CO, decompose to $OH(v' < v)$ + CO after intramolecular vibrational relaxation, or converts to the products H + CO_2.

$$\begin{array}{ccccc} OH(v) + CO & \underset{-a}{\overset{a}{\rightleftarrows}} & HOCO & \xrightarrow{b} & H + CO_2 \\ & & \downarrow c & & \\ & & OH(v') + CO & & \end{array} \qquad (8)$$

Previous studies[3,4,6] showed that the proxy method is valid for the present system, and consequently, the contribution of re-dissociation to OH(v) + CO, process –a, is negligibly slow compared to processes b and c for $v \neq 0$. The steady-state approximation to the concentration of HOCO gives

$$[HOCO] = \frac{k_a}{k_b + k_c}[OH(v)][CO] \qquad (I)$$

and the rate equations for OH in reaction (8) is

$$-\frac{\mathrm{d}[\mathrm{OH}(v)]}{\mathrm{d}t} = \left(k_\mathrm{a} \frac{k_\mathrm{b}}{k_\mathrm{b}+k_\mathrm{c}} + k_\mathrm{a} \frac{k_\mathrm{c}}{k_\mathrm{b}+k_\mathrm{c}} \right) [\mathrm{OH}(v)][\mathrm{CO}] \equiv [k_\mathrm{react}^\mathrm{CO}(v) + k_\mathrm{relax}^\mathrm{CO}(v)] \times [\mathrm{OH}(v)][\mathrm{CO}] \quad \text{(II)}$$

where $k_\mathrm{react}^\mathrm{CO}(v)$ and $k_\mathrm{relax}^\mathrm{CO}(v)$ are effective rate coefficients for chemical reaction and vibrational relaxation by CO. The resultant vibrational level v' ranges 0 to $v-1$. Smith[18] suggested that the energy of vibration that was initially excited is transferred in a step-wise manner ($v \rightarrow v-1$) in adduct, and that the adduct may dissociate rapidly after the energy of a single quantum of a high frequency vibration has been transferred to the other vibrational modes.

The validity of the single-quantum relaxation was confirmed by the analysis using the integrated profiles method (IPM).[34,35] The rate equation of the population of OH of a vibrational level v, $[v]$, is written in the following form.

$$\frac{\mathrm{d}[v]}{\mathrm{d}t} = -[k_\mathrm{remove}(v) + k_\mathrm{relax}(v)] \times [v] + k_\mathrm{relax}(v+1) \times [v+1] \quad \text{(IV)}$$

$$k_\mathrm{remove}(v) \equiv k_\mathrm{react}^\mathrm{CO}(v)[\mathrm{CO}] + k_\mathrm{diff}(v) \quad \text{(V)}$$

$$k_\mathrm{relax}(v) \equiv k_\mathrm{relax}^\mathrm{CO}(v) \times [\mathrm{CO}] + k_\mathrm{relax}^\mathrm{M}(v) \times [\mathrm{M}] \quad \text{(VI)}$$

where $k_\mathrm{react}^\mathrm{A}(i)$ is an effective rate coefficient for reactive removal of the of vibrational level i by species A, $k_\mathrm{relax}^\mathrm{A}(i)$ an effective rate coefficient for vibrational relaxation from the level i to $i-1$ by species A (the species M is mainly He), and $k_\mathrm{diff}(v)$ a first-order rate coefficient for diffusion loss from the observation volume. The first term of the right side of eq IV corresponds to the total loss of the level v, and the second term represents the formation of the level v by relaxation from the level $v+1$. Integration of eq IV from $t = t_0$ to an arbitrary time t gives

$$y_v(t) = -[k_{\text{remove}}(v) + k_{\text{relax}}(v)] \cdot x_v(t) + k_{\text{relax}}(v+1) \quad \text{(VII)}$$

$$y_v(t) = ([v] - [v]_0) \Big/ \int_{t_0}^{t} [v+1]\,dt' \quad \text{(VIII)}$$

$$x_v(t) \equiv \int_{t_0}^{t} [v]\,dt' \Big/ \int_{t_0}^{t} [v+1]\,dt' \quad \text{(IX)}$$

where t_0, the initial time of integration, was set to the time after completion of $O(^1D)$ + H_2 reaction, and $[v]_0$ is the population of OH(v) at t_0. Equation VII indicates that the slope of the plot $y_v(t)$ versus $x_v(t)$ gives the apparent first-order rate of the total loss $k_{\text{remove}}(v) + k_{\text{relax}}(v)$ of the level v. Figure 3.10, parts a and b, shows the plots $y_v(t)$ versus $x_v(t)$ for the vibrational levels v = 1 and 0, respectively. Both plots clearly show a good linear correlation, suggesting that relaxation process is governed mainly by single-quantum change $v \rightarrow v-1$. The IPM analysis including double-quantum relaxation ($v \rightarrow v-2$) indicated little contribution of the two quanta change of OH vibration in the adduct (OH(v)–CO → OH(v–2)–CO).

We also have performed numerical integration of the rate equations of the vibrational populations [OH(v)] by Runge–Kutta–Gill method, and evaluated the apparent first-order rate coefficients for reaction and relaxation with the single-quantum change ($v \rightarrow v-1$) in the complex HOCO. Calculated time-dependent populations of the levels using the effective rate coefficients for reaction and relaxation obtained by numerical integration, shown with the red lines in Figure 3.9, reproduce all the observed time profiles well.

Figure 3.11 shows the CO pressure dependence of the time-resolved LIF intensities of Lyman-α line of H atoms. H atoms were generated by two reactions $O(^1D) + H_2 \rightarrow OH + H$ and OH(v) + CO → H + CO_2. The cause of the small rise in the profiles recorded without CO is not known for certain. The time constant of the rise in the

profiles is about a few μs and no side reaction in (1) – (7) is a cause of the rise. A possible cause might be due to relaxation of translational motion of H atoms. The averaged fraction of relative translational energy between OH and H, $< f_v >$, has been reported to be 0.28 in collisions of O(^{1}D) with H_2 at 7.1 kJ mol^{-1} of relative translational energy.[36] The available energy of the reaction of O(^{1}D) and H_2 at 298 K is $\Delta_r H^\circ_{298} = -183$ kJ mol^{-1}, and the average relative translational energy between OH and H is 51 kJ mol^{-1}. The seventeen eighteenth parts (94 %) of this energy are deposited into the translational motion of H atoms. The average speed of H atoms, 9800 m s^{-1} leads to a wider Doppler width than that of OH with an average speed at 600 m s^{-1}, and relaxation of translational motion of H atoms by collisions with buffer gases may give the small rise in the profiles.

The apparent decay of H atoms is due mainly to diffusion loss from the observation volume of the probe laser. The time profiles recorded without CO subtracted from those with CO leave the profiles of the H atoms of the reaction OH(v) + CO → H + CO_2. The reaction of O(^{1}D) with H_2 generates the identical amounts of OH and H, and quantitative simulation of observed time profiles of H atoms can be made using the rate coefficients determined from the analysis of the profiles of OH(v) shown in Figure 3.9. As seen in Figure 3.11, the profiles of H atoms recorded at different pressures of CO are well reproduced by simulation, indicating that the effective rate coefficients for reaction and relaxation also are consistent with the profiles of H atoms.

3.3.2 Chemical Reaction and Intramolecular Vibrational Relaxation of HOCO.

Figure 3.12 shows the CO concentration dependences of the apparent first-order rates of removal $k_{\text{remove}}(v)$ and relaxation $k_{\text{relax}}(v)$ of OH(v) (both are defined by eqs V and VI). The slopes of the straight line fit from regression analysis give the

bimolecular rate coefficients, $k_{\text{react}}^{\text{CO}}(v)$ and $k_{\text{relax}}^{\text{CO}}(v)$, listed in Table 3.1. The nearly identical intercepts of Figure 3.12a show that the first-order rate coefficients of diffusion loss are independent of vibrational levels of OH. The intercepts in Figure 3.12b are relatively larger at higher vibrational levels, suggesting that relaxation by He is more efficient at vibrational higher levels. The rate coefficient for $v = 0$ agrees well with the recent recommended value: $(1.5 \pm 0.3) \times 10^{-13}$ cm^3 molecule^{-1} s^{-1}.[13] The overall rate coefficient $k_{\text{react}}^{\text{CO}}(v) + k_{\text{relax}}^{\text{CO}}(v)$ for $v = 1$ obtained in the present study, 1.1×10^{-12} cm^3 molecule^{-1} s^{-1}, is in excellent agreement with both 1.0×10^{-12} and 1.2×10^{-12} cm^3 molecule^{-1} s^{-1} measured by Brunning et al.[3] and Fulle et al.,[6] respectively. The overall rate coefficients for $v \geq 1$ are nearly identical within $(1.1 \pm 0.2) \times 10^{-12}$ cm^3 molecule^{-1} s^{-1}, indicating that the proxy method is eligible to the present system.

Based on the proxy method, Brunning et al.[3] have reported that about 20 % of $\text{OH}(v = 0) - \text{CO}$ complex formed from OH(v = 0) and CO converts to H + CO_2 and the remainder re-dissociates to OH(v = 0) + CO at 300 K. The limiting high- and low-pressure rate coefficients measured by Fulle et al. ($k_{1a,\infty}$ and $k_{1b,0}$ in ref 6) give the fraction of the adduct HO(v = 0)–CO converting to H + CO_2 about 14 % which is in reasonable agreement with that reported by Brunning et al.[3] Figure 3.13 shows vibrational level dependence of the effective bimolecular rate coefficients for chemical reaction $k_{\text{react}}^{\text{CO}}(v)$ and relaxation $k_{\text{relax}}^{\text{CO}}(v)$ of OH(v). Clearly seen in Figure 3.13, two processes have the opposite dependence on the vibrational quantum number of OH: reaction is accelerated and relaxation is decelerated by vibrational excitation of OH, although the overall rate coefficients are nearly identical for $v \geq 1$. The branching fraction of reaction, $k_{\text{react}}^{\text{CO}} / (k_{\text{react}}^{\text{CO}} + k_{\text{relax}}^{\text{CO}}) = k_{\text{b}} / (k_{\text{b}} + k_{\text{c}})$, increases with the vibrational energy of OH: 31 % (v = 1), 53 % (v = 2), 86 % (v = 3), and 90 % (v = 4). The countertrend of the rate coefficients for reaction and relaxation can be elucidated by

the competition between the two processes. All the vibrational levels of OH(v) form the transient adduct HOCO with the nearly identical overall rate coefficients: $\sim 1 \times 10^{-12}$ cm^3 $molecule^{-1}$ s^{-1}, after which the adduct converts to the products H + CO_2 or decomposes to OH(v–1) + CO (as shown in Figure 3.14).

Some theoretical studies of the reaction dynamics for the reaction OH + CO have been reported motivated by the present study. Lakin et al.[7] performed quasiclassical trajectory calculation on the full-dimensional potential energy surface, reporting that excitation of OH vibration by one quantum is much more effective in promoting reactivity than excitation of CO vibration by two quanta. Zhang and co-warkers[37-39] also carried out full-dimensional state-to-state quantum dynamics and time-dependent wave packet calculations on the Lakin-Troya-Schatz-Harding (LTSH) potential energy surface[7] and concluded that vibrational excitation of OH up to v = 1 considerably enhances the reactivity because it enhances the probability for complex, HOCO, going to products, while excitation of CO up to v = 1 has less the reactivity. Guo and co-workers[40-43] performed quasi-classical trajectory and full-dimensional quantum dynamics calculation on the global potential energy surface for OH + CO reaction and reported that vibrational excitation of OH enhances reactivity, due to its promoting effect over the transition state between the HOCO intermediate. The conclusion drawn by Li et al.[41] is also in agreement with our experimental results and discussion. They reported that the vibrational energy of OH is sufficiently preserved in the O–H bond of HOCO and enhances the reactivity, and that the energy randomization in HOCO is not complete because of its short lifetime. In addition, our analysis shows that chemical reaction of OH(v = 1) is faster than that of OH(v = 0) by a factor of 2.6, which agrees well with 2.4 obtained by Lakin et al.[7] by quasiclassical trajectory calculation at relative translational energy of 0.08 eV (645 cm^{-1}).

3.4 SUMMARY

We have measured the branching ratios between chemical reaction and vibrational relaxation of adduct HO(v)–CO formed from vibrationally excited OH(v = 0 – 4) and CO. The efficiency of chemical reactions, HO(v)–CO → H + CO_2 grows with the vibrational quantum number v from 31 % of v = 1 to 90 % of v = 4. The overall rate coefficients of OH(v = 1 – 4) + CO are nearly identical, indicating that the proxy method is valid for the present system. However, vibrational energies initially stored in OH are not completely randomized before the adduct HOCO re-dissociates to OH and CO. A kinetic analysis made by integrated profiles method shows that vibrational relaxation proceeds via single-quantum relaxation in the adduct, HO(v)–CO → OH(v–1)–CO, followed by decomposition to OH(v–1) + CO. As a result of competition with chemical reaction, vibrational relaxation is less effective at higher vibrational levels of OH.

References

(1) Warneck, P. *Chemistry of the Natural Atmosphere,* 2nd ed.; Academic Press: London, 2000.

(2) Dreier, T.; Wolfrum, J. *18th International Symposium on Combustion*; Waterloo, Canada, Aug 17–22, 1980; The Combustion Institute: Pittsburgh, PA, 1981; pp 801–809.

(3) Brunning, J.; Derbyshire, D. W.; Smith, I. W. M.; Williams, M. D. Kinetics of OH(v = 0, 1) and OD(v = 0, 1) with CO and the Mechanism of the OH + CO Reaction. *J. Chem. Soc., Faraday Trans. 2* **1988**, *84*, 105–119.

(4) Frost, M. J.; Sharkey, P.; Smith, I. W. M. Reaction between hydroxyl (deuteroxyl) radicals and carbon monoxide at temperatures down to 80 K: experiment and theory. *J. Phys. Chem.* **1993**, *97*, 12254–12259.

(5) Petty, J. T.; Moore, C. B. Transient infrared absorption spectrum of the ν1 fundamental of trans-DOCO. *J. Chem. Phys.* **1993**, *99*, 47–55.

(6) Fulle, D.; Hamann, H. F.; Hippler, H.; Troe, J. High pressure range of addition reactions of HO. II. Temperature and pressure dependence of the reaction HO + CO ⇔ HOCO → H + CO_2. *J. Chem. Phys.* **1996**, *105*, 983–1000.

(7) Lakin, M. J.; Troya, D.; Schatz, G. C.; Harding, L. B. A quasiclassical trajectory study of the reaction OH + CO → H + CO_2. *J. Chem. Phys.* **2003**, *119*, 5848–5859.

(8) Yu, H.-G.; Muckerman, J. T.; Sears, T. A theoretical study of the potential energy surface for the reaction H + CO → H + CO_2. *Chem. Phys. Lett.* **2001**, *349*, 547–554.

(9) Lester, M. I.; Pond, B. V.; Anderson, D. T.; Harding, L. B.; Wagner, A. F. Exploring the OH + CO reaction coordinate via infrared spectroscopy of the OH–CO reactant complex. *J. Chem. Phys.* **2000**, *113*, 9889–9892.

(10) Milligan, D. E.; Jacox, M. E. Infrared Spectrum and Structure of Intermediates in the Reaction of OH with CO. *J. Chem. Phys.* **1971**, *54*, 927–942.

(11) Jacox, M. E. The vibrational spectrum of the *t*–HOCO free radical trapped in solid argon. *J. Chem. Phys.* **1988**, *88*, 4598–4607.

(12) Atkinson, R.; Baulch, D. L.; Cox, R. A.; Crowley, J. N.; Hampson, R. F., Jr.; Hynes, R. G.; Jenkin, M. E.; Kerr, J. A.; Rossi, M. J.; Troe, J. *Summary of Evaluated Kinetic and Photochemical Data for Atmospheric Chemistry*; 2006; http://www.iupac-kinetic.ch.cam.ac.uk/.

(13) Friedl, R. R.; Golden, D. M.; Kurylo, M. J.; Moortgat, G. K.; Rudek, K.-H.; Wine, P. H.; Ravishankara, A. R.; Kolb, C. E.; Molina, M. J.; Pitts, F.-B. J.; Huie, R. E.; Orkin, V. L.; F.-Pitts, B. J. *Chemical Kinetics and Photochemical Data for Use in Atmospheric Studies,* Evaluation No. 15; Jet Propulsion Laboratory, California Institute of Technology: Pasadena, CA, 2006.

(14) Manion, J. A.; Huie, R. E.; Levin, R. D.; Burgess, D. R., Jr.; Orkin, V. L.; Tsang, W.; McGivern, W. S.; Hudgens, J. W.; Knyazev, V. D.; Atkinson, D. B.; Chai, E.; Tereza, A. M.; Lin, C.-Y.; Allison, T. C.; Mallard, W. G.; Westley, F.; Herron, J. T.; Hampson, R. F.; Frizzell, D. H. *NIST Chemical Kinetics Database, NIST Standard Reference Database 17*; Version 7.0 (Web Version), Release 1.4.3, Data version 2008.12, National Institute of Standards and Technology: Gaithersburg, Maryland; http://kinetics.nist.gov/.

(15) Chen, W.-C.; Marcus, R. A. On the theory of the reaction rate of vibrationally excited CO molecules with OH radicals. *J. Chem. Phys.* **2006**, *124*, 024306.

(16) Spencer, J. E.; Endo, H.; Glass, G. P. *16th International Symposium on Combustion*; Cambridge, USA, Aug 15-20, 1976; The Combustion Institute: Pittsburgh, PA, 1977; pp 829–839.

(17) Spencer, J. E.; Glass, G. P. Some Reactions of OH(v = 1). *Int. J. Chem. Kinet.* **1977**, *9*, 111–122.

(18) Smith, I. W. M. Collisional energy transfer, intramolecular vibrational relaxation and unimolecular reactions. *J. Chem. Soc., Faraday Trans.* **1997**, *93*, 3741–3750.

(19) Ruscic, B.; Litorja, M. Photoionization of HOCO revisited: a new upper limit to the adiabatic ionization energy and lower limit to the enthalpy of formation. *Chem. Phys. Lett.* **2000**, *316*, 45–50.

(20) Duncan, T. V.; Miller, C. E. The HCO_2 potential energy surface: Stationary point energetics and the HOCO heat of formation. *J. Chem. Phys.* **2000**, *113*, 5138–5140.

(21) Luque, J.; Crosley, D. R. *LIFBASE: Database and Spectral Simulation Program,* version 1.5; SRI international Report MP 99-009: Menlo Park, CA,1999.

(22) Kramida, A.; Ralchenko, Y.; Reader, J.; Saloman, E. B.; Sansonetti, J. E.; Fuhr, J. R.; Podobedova, L. I.; Wiese, W. L.; Olsen, K.; Carpentier, E.; Carpentier, T.; Zimmerman, A.; Hamins-Puertolas, A.; Hamins-Puertolas, M.; Sharova, A.; Curry, J. J.; Dalton, G. R.; Dragoset, R.; Jou, F.-C. (J.); Martin, W. C.; Mohr, P. J.; Musgrove, A.; Sansonetti, C. J.; Wiersma, G. *NIST Atomic Spectra Database*; Version 5, National Institute of Standards and Technology, http://www.nist.gov/pml/data/asd.cfm#.

(23) Winter, M. *WebElements: the periodic table on the WWW*; The University of Sheffield and WebElements Ltd.; U.K.; http://www.webelements.com (accessed December 2010).

(24) Smith, G. K.; Butler, J. E. OH ($X^2\Pi_i$) product internal energy distribution formed in the reaction of O($^1D_2$) with H_2. *J. Chem. Phys.* **1980**, *73*, 2243–2253.

(25) Butler, J. E.; MacDonald, R. G.; Donaldson, D. J.; Sloan, J. J. Vibrational

excitation of OH($X^2\Pi$) produced in the reaction of O(^{1}D) with H_2. *Chem. Phys. Lett.* **1983**, *95*, 183−188.

(26) Butler, J. E.; Jursich, G. M.; Watson, I. A.; Wiesenfeld, J. R. Reaction dynamics of O($^1D_2$) + H_2, HD, D_2: OH, OD($X^2\Pi_i$) product internal energy distributions. *J. Chem. Phys.* **1986**, *84*, 5365−5377.

(27) Aker, P. M.; Sloan, J. J. The initial product vibrational energy distribution in the reaction between O($^1D_2$) and H_2. *J. Chem. Phys.* **1986**, *85*, 1412−1417.

(28) Huang, Y.; Gu, Y.; Liu, C.; Yang, X.; Tao, Y. The nascent product vibrational energy distribution of the reaction O(^{1}D) + H_2 by the grating selection chemical laser technique. *Chem. Phys. Lett.* **1986**, *127*, 432−437.

(29) Cleveland, C. B.; Jursich, G. M.; Trolier, M.; Wiesenfeld, J. R. Dynamics of the reaction O($^1D_2$) + $H_2 \rightarrow$ OH($X^2\Pi$, $v'' = 2, 3$) + H: Full characterization of product energetics. *J. Chem. Phys.* **1987**, *86*, 3253−3264.

(30) Mikulecky, K.; Gericke, K.-H. The influence of vibrational and translational motion on the reaction dynamics of O(^{1}D) + H_2($^1\Sigma_g^+$, *v*). *J. Chem. Phys.* **1992**, *96*, 7490−7499.

(31) Liu, X.; Lin, J. J.; Harich, S.; Schatz, G. C.; Yang, X. A Quantum State-Resolved Insertion Reaction: O(^{1}D) + H_2(*J* = 0) → OH($^2\Pi$, *v*, *N*) + H(^{2}S). *Science* **2000**, *289*, 1536−1538.

(32) Aoiz, F. J.; Bañares, L.; Castillo, J. F.; Herrero,V. J.; M.-Haya, B.; Honvault, P.; Launay, J. M.; Liu, X.; Lin, J. J.; Harich, S. A.; Wang, C. C.; Yang, X. The O(^{1}D) + H_2 reaction at 56 meV collision energy: A comparison between quantum mechanical, quasiclassical trajectory, and crossed beam results. *J. Chem. Phys.* **2002**, *116*, 10692−10703.

(33) Matsumi, Y.; Shamsuddin, S. M.; Sato, Y.; Kawasaki, M. Velocity relaxation

of hot O(^{1}D) atoms by collisions with rare gases, N_2, and O_2. *J. Chem. Phys.* **1994**, *101*, 9610–9618.

(34) Yamasaki, K.; Watanabe, A. A New Method of Determining the Rate Constants for State-to-State Vibrational Relaxation: An Integrated Profiles Method. *Bull. Chem. Soc. Jpn.* **1997**, *70*, 89–95.

(35) Yamasaki, K.; Watanabe, A.; Kakuda, T.; Tokue, I. Application of a New Method to the Determination of Rate Constants: Examination of the Effect of Noise on the Data. *Int. J. Chem. Kinet.* **1998**, *30*, 47–54.

(36) Hernando, J.; Sayós, R.; González, M. A QCT study of the microscopic mechanisms proceeding via the ground PES of the O(^{1}D) + H_2 ($X^1\Sigma_g^+$) → OH($X^2\Pi$) + H(^{2}S) reaction. *Chem. Phys. Lett.* **2003**, *380*, 123–134.

(37) Liu, S.; Xu, X.; Zhang, D. H. Communication: State-to-state quantum dynamics study of the OH + CO → H + CO_2 reaction in full dimensions (J = 0). *J. Chem. Phys.* **2011**, *135*, 141108.

(38) Liu, S.; Xu, X.; Zhang, D. H. A full-dimensional time-dependent wave packet study of the OH + CO → H + CO_2 reaction. *Theor Chem Acc* **2012**, *131*, 1068.

(39) Wang, C.; Liu, S.; Zhang, D. H. Effects of reagent vibrational excitation on the state-tostate quantum dynamics of the OH + CO → H + CO_2 reaction in six dimensions (J = 0). *Chem. Phys. Lett.* **2012**, *537*, 16–20.

(40) Li, J.; Wang, Y.; Jiang, B.; Ma, J.; Dawes, R.; Xie, D.; Bowman, J. M.; Guo, H. Communication: A chemically accurate global potential energy surface for the HO + CO → H + CO_2 reaction. *J. Chem. Phys.* **2012**, *136*, 041103.

(41) Li, J.; Xie, C.; Ma, J.; Wang, Y.; Dawes, R.; Xie, D.; Bowman, J. M.; Guo, H. Quasi-Classical Trajectory Study of the HO + CO → H + CO_2 Reaction on a New ab Initio Based Potential Energy Surface. *J. Phys. Chem. A* **2012**, *116*, 5057–5067.

(42) Ma, J.; Li, J.; Guo, H. Quantum Dynamics of the HO + CO → H + CO_2 Reaction on an Accurate Potential Energy Surface. *J. Phys. Chem. Lett.* **2012**, *3*, 2482−2486.

(43) Xie, C.; Li, J.; Xie, D.; Guo, H. Quasi-classical trajectory study of the H + CO_2 → HO + CO reaction on a new ab initio based potential energy surface. *J. Chem. Phys.* **2012**, *137*, 024308.

Table 3.1. Effective Rate Coefficients for Chemical Reaction $k_{\text{react}}^{\text{CO}}$ and Vibrational Relaxation $k_{\text{relax}}^{\text{CO}}$ of OH(v = 0 – 4) by CO. Rate coefficients are in units of 10^{-13} cm^3 molecule^{-1} s^{-1} and the stated confidence limits are ±2σ.

v	0	1	2	3	4
chemical reaction	1.3 ± 0.2 [a]	3.4 ± 0.4	4.9 ± 0.9	9.3 ± 1.3	12 ± 1.5
vibrational relaxation		7.4 ± 0.4	4.3 ± 0.9	1.5 ± 1.5	1.3 ± 1.3

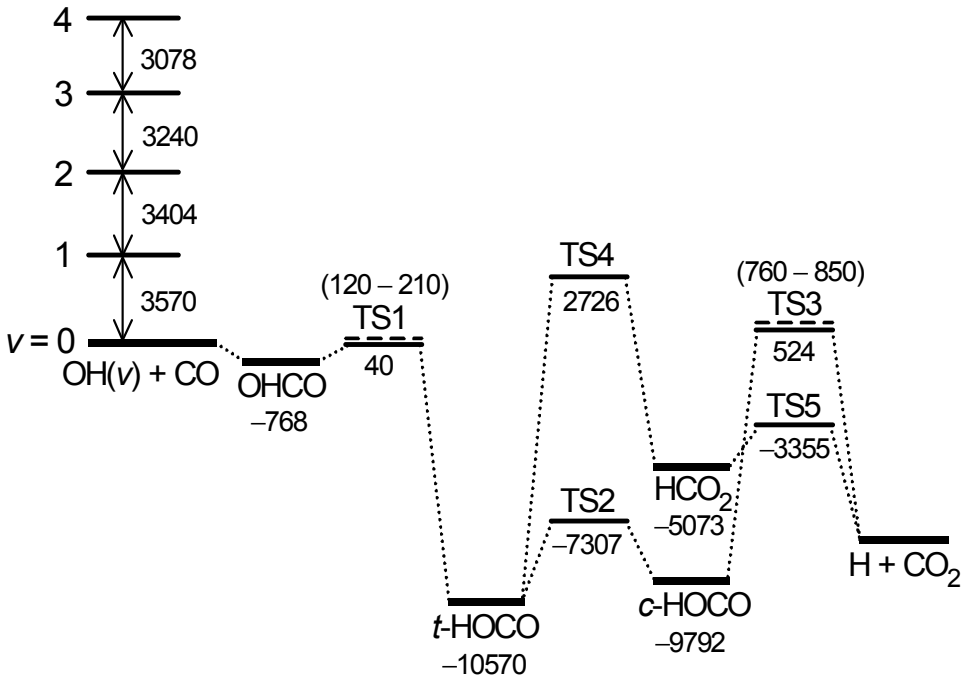

Figure 3.1. Energy diagram of the reaction system of $OH(X^2\Pi_i, v) + CO$. All the numbers are energies in units of cm^{-1}. The energies of the intermediates and transition states are relative values to that of reactants $OH(v = 0) + CO$. The numbers without parentheses are cited from LTSH potential calculated in refs 7 and 8 (solid lines); those in parentheses are experimental values reported in ref 3 (broken lines). The vibrational levels up to $v = 4$ of OH are shown over the reactants, and the numbers between vibrational levels are the energy differences between the vibrational levels of OH.

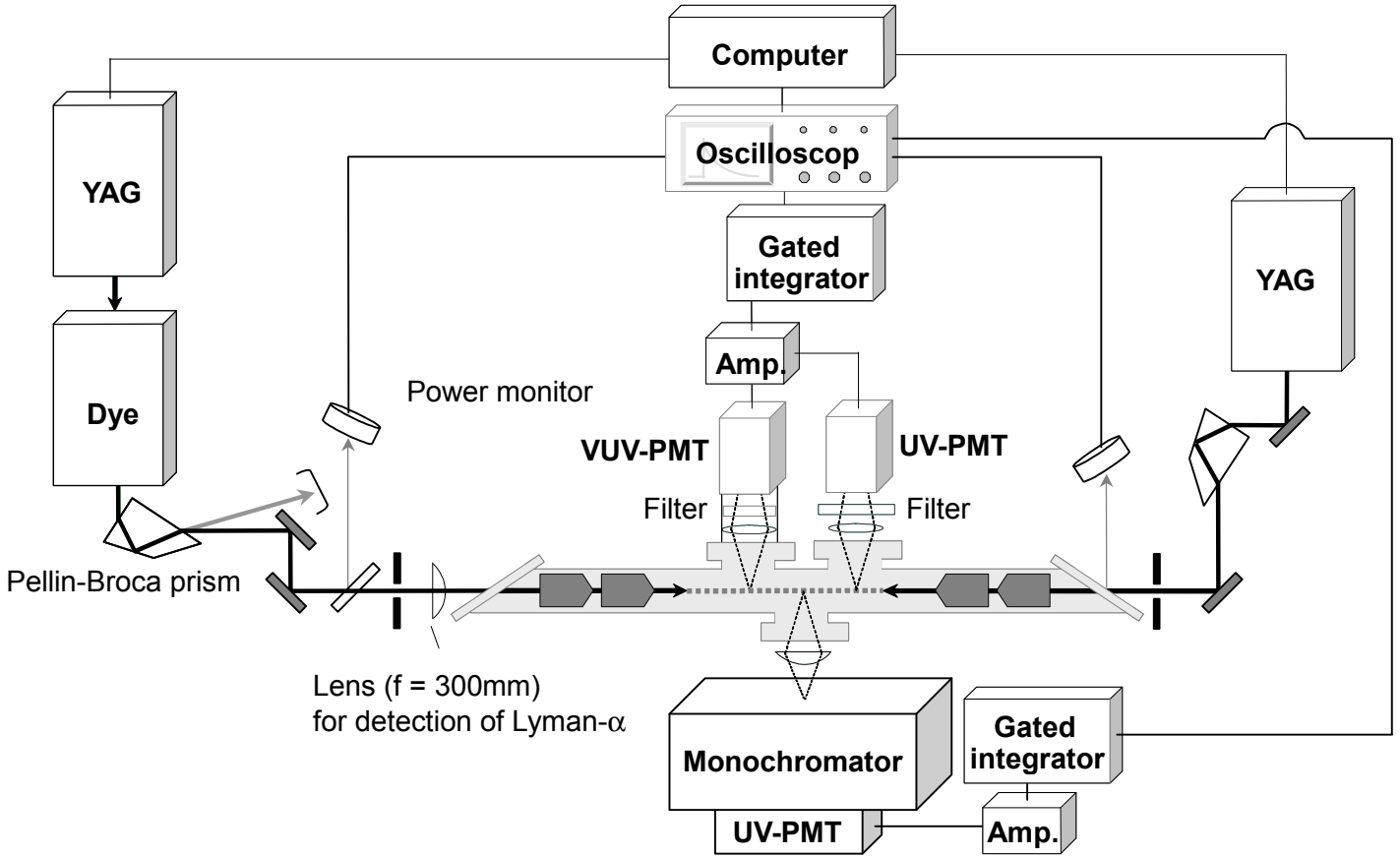

Figure 3.2. A schematic diagram of experimental apparatus. Amp. : preamplifier made with Op-amp LF356, PMT : photomultiplier.

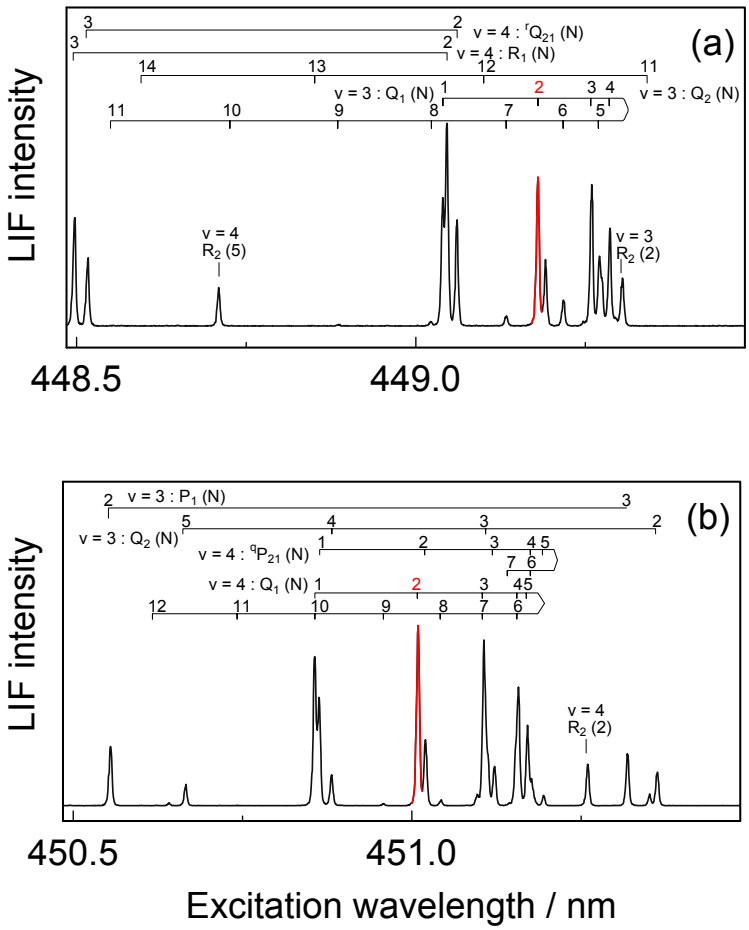

Figure 3.3. Laser-induced fluorescence excitation spectra of OH($X^2\Pi$, v = 3 and 4) generated in the O(^{1}D) + H_2 reaction. The fluorescence was excited via the $\Delta v = -3$ sequence: (a) 0–3; (b) 1–4. Delay times between the photolysis and probe lasers were 10 μs in both spectra.

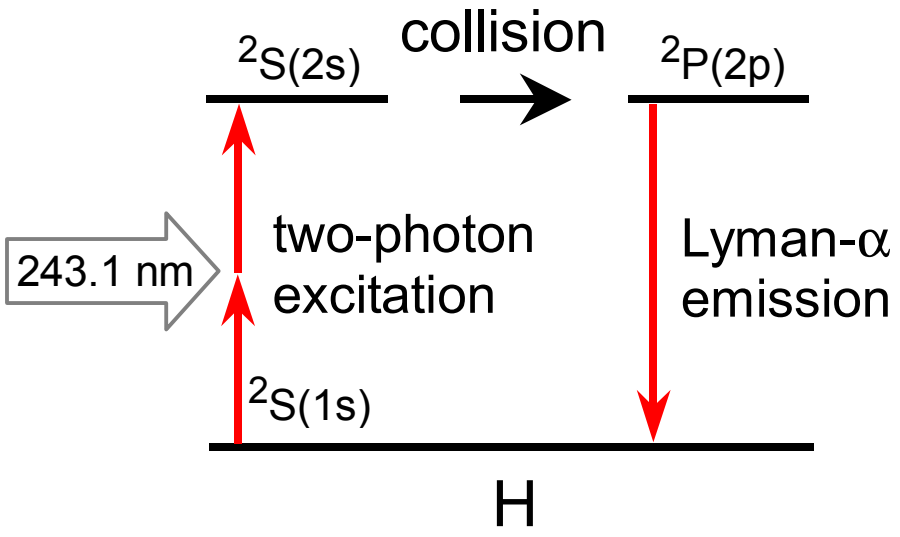

Figure 3.4. The scheme of the detection of H atoms by two-photon LIF technique.

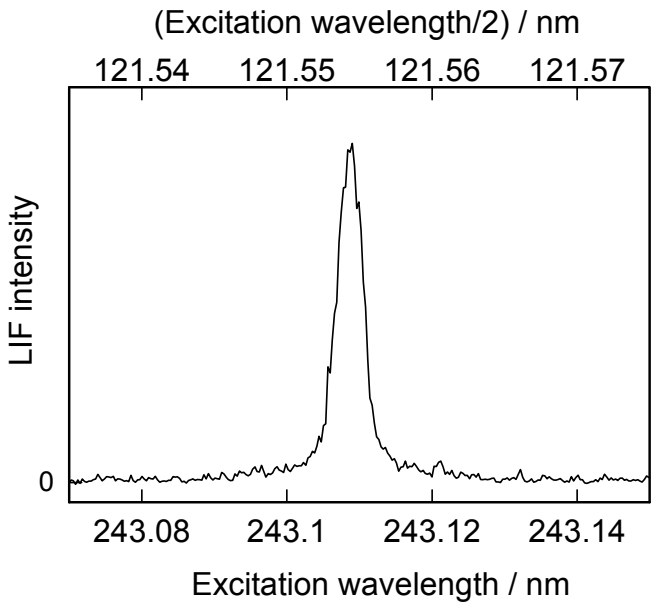

Figure 3.5. Laser-induced fluorescence excitation spectra of H atoms produced in the $O(^1D) + H_2$ reaction. The fluorescence was excited via the $^2S(2s) \neg\ ^2S(1s)$ by two-photon absorption. The lower abscissa corresponds to the wavelength of the probe laser, and upper abscissa shows the wavelength of the fluorescence.

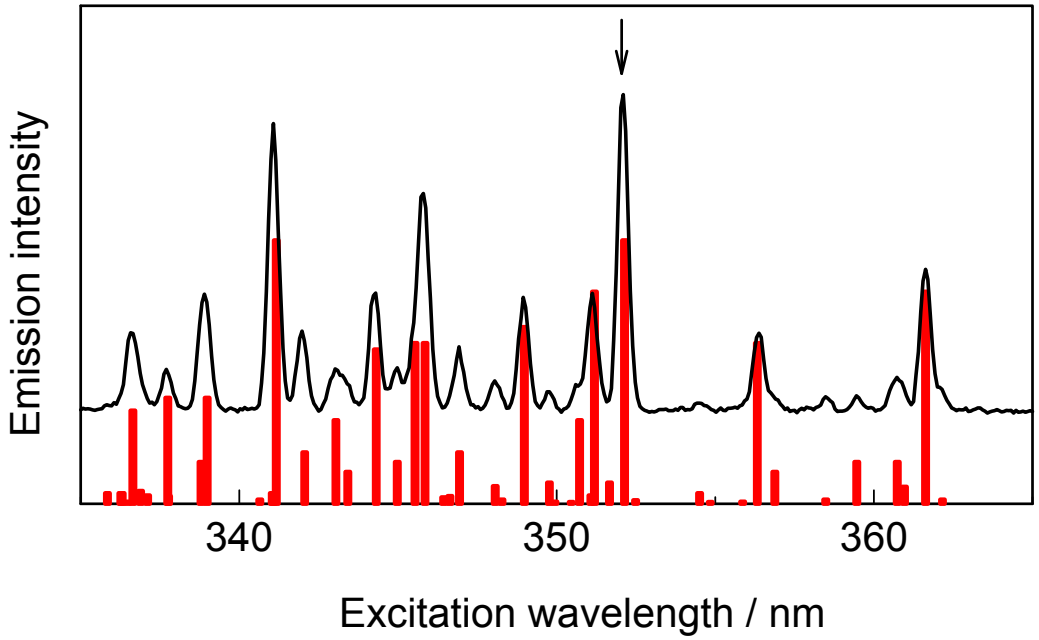

Figure 3.6. Dispersed emission spectra recorded with a monochromator (f = 125 cm, $\Delta\lambda$(fwhm) = 3 nm). The red bar represents the transitions of the emission from electronically excited Ni atoms. The pressure of He buffer was 10 Torr. The partial pressure of CO was 200 mTorr.

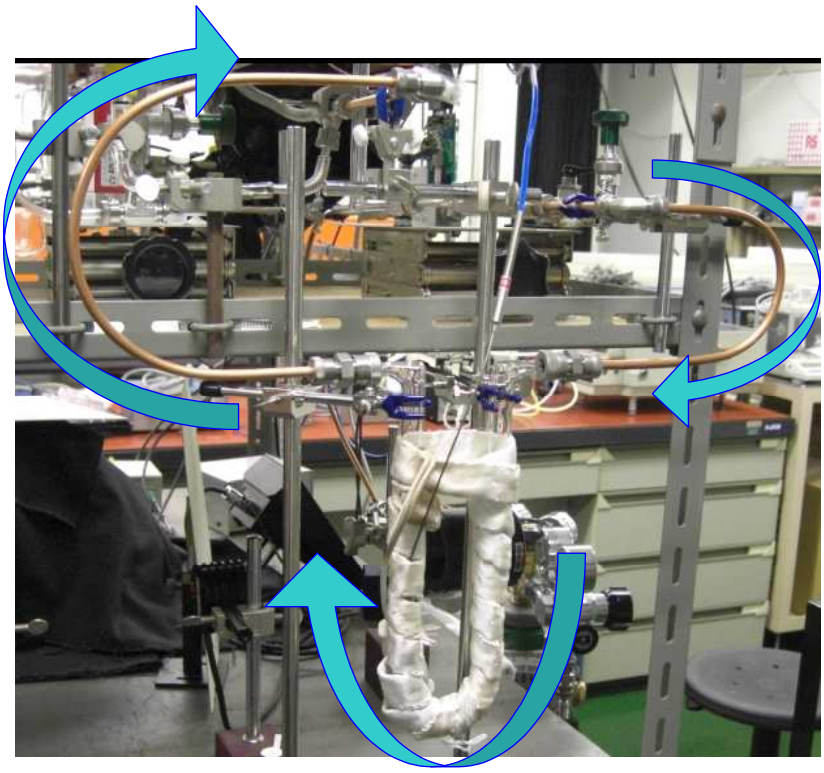

Figure 3.7. The photo of the U-shaped Pyrex glass coiled with a tape heater. The blue arrows show the direction of flow of CO.

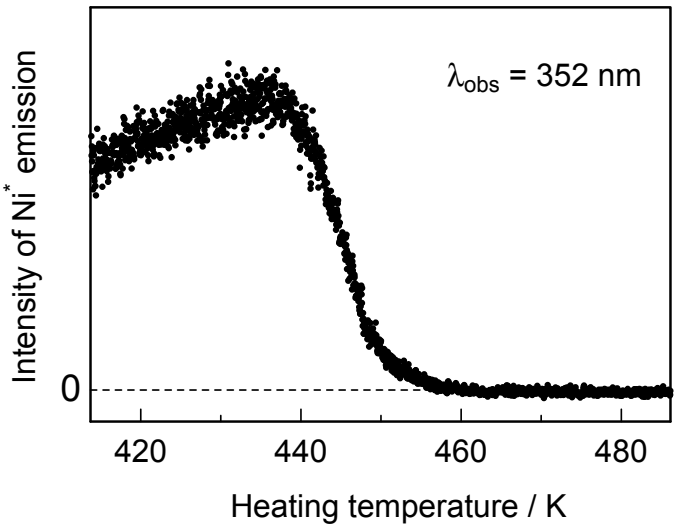

Figure 3.8. Temperature dependence of the intensity of emission from Ni. The emission was observed at 352 nm (Figure 3.6). The pressure of He buffer was 10 Torr. The partial pressure of CO was 200 mTorr.

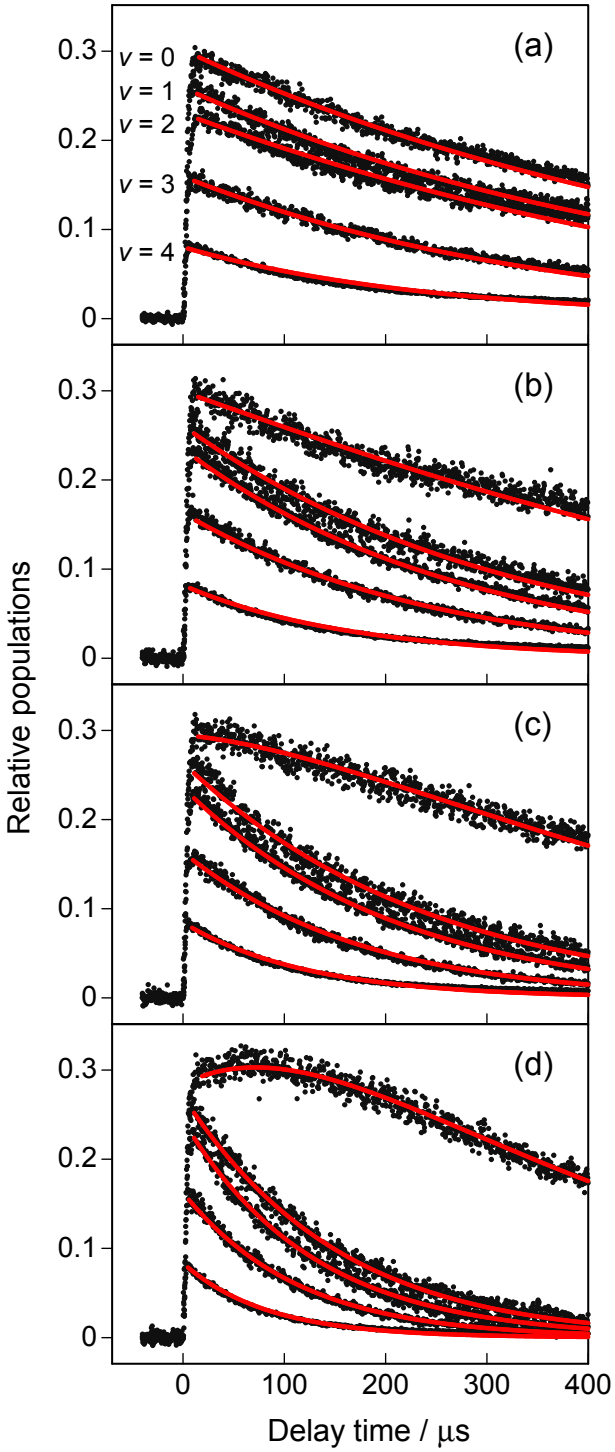
(a)
(b)
(c)
(d)
v = 0
v = 1
v = 2
v = 3
v = 4
Relative populations
Delay time / μs
0
0.1
0.2
0.3
0
100
200
300
400

Figure 3.9.

Figure 3.9. Time-resolved relative populations of vibrational levels of OH(v = 0 – 4). The abscissa is the delay times between the photolysis and probe laser. The black dots denotes observed data, and the red lines represent the calculated time profiles using rate coefficients determined by numerical integration of rate equations. The profiles are so scaled as to make the sum of initial populations unity. The pressures of CO: 0, (a); 50, (b); 100 (c); 200 mTorr, (d); O_3: 0.01, v = 0 and 1; 0.05, v = 2; 0.5 m Torr, v = 3 and 4; H_2: 150 mTorr; buffer gas (He): 10 Torr. The step sizes of time scans were 440 ns. Each data point is the averaged signals from ten laser shots, and a single time profile is the average of three scans.

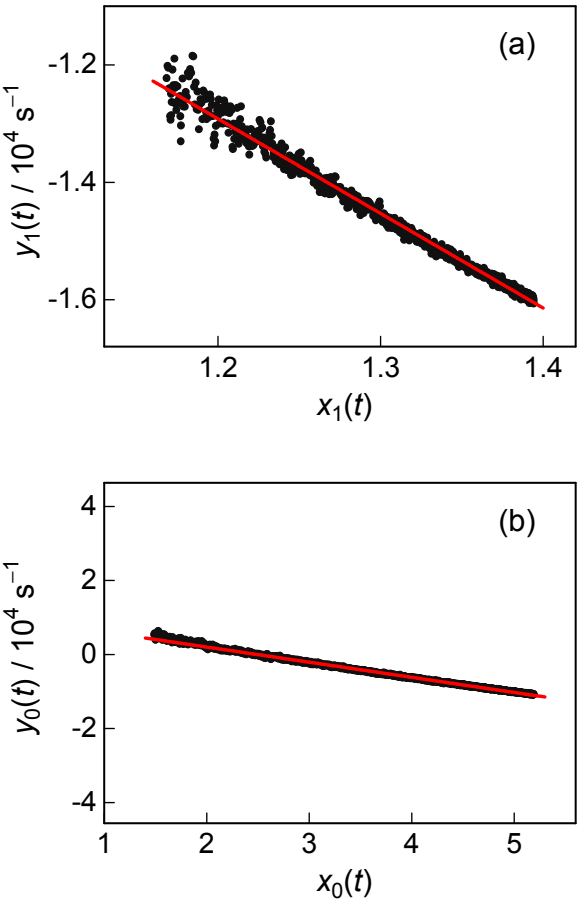

Figure 3.10. Plots of $y_v(t)$ vs $x_v(t)$ made by IPM for (a) $v = 1$ and (b) $v = 0$. $y_v(t)$ and $x_v(t)$ are defined by eqs (VIII) and (IX) in the text, respectively. The ratios of the scales of the ordinates and abscissas are 2 for both plots. The slopes given by a linear regression (red lines) correspond to the apparent first-order rates of the total loss of the vibrational levels.

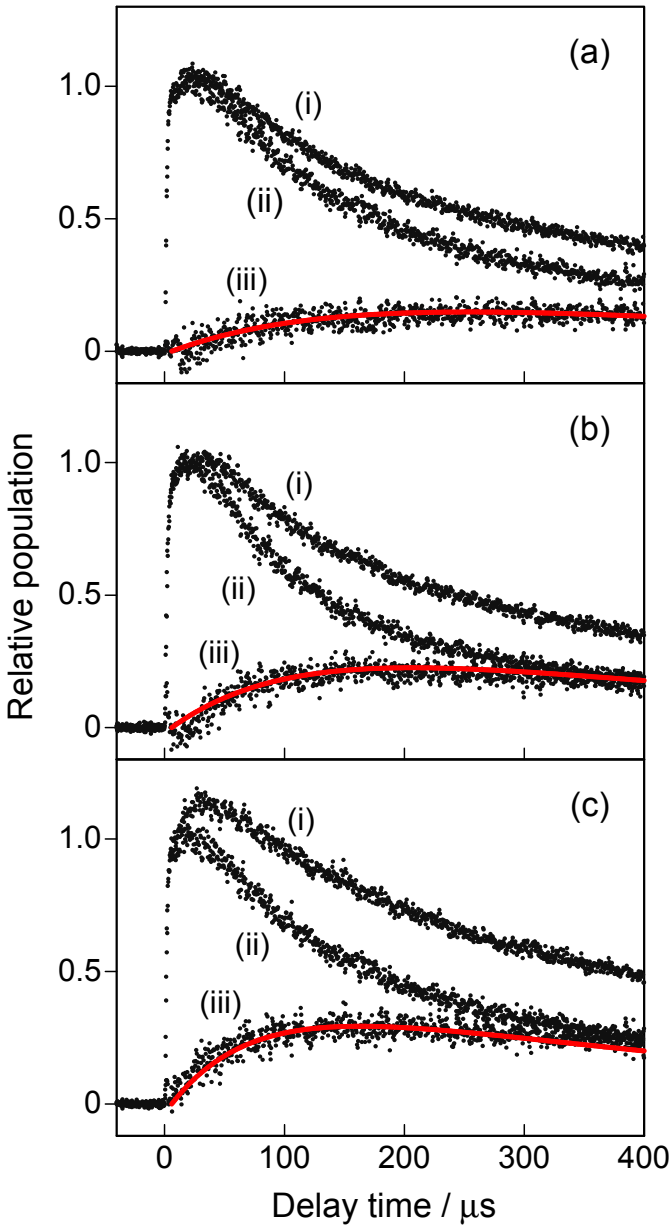
(a)
(b)
(c)
(i)
(ii)
(iii)
1.0
0.5
0
Relative population
0
100
200
300
400
Delay time / μs

Figure 3.11.

Figure 3.11. Time profiles of the H atoms generated in the reaction system. The profiles (i) and (ii) were recorded in the presence and absence of CO, respectively. The profiles (ii) subtracted from (i) leave the profiles (iii). The black dots denotes observed data, and the red lines denote the results of simulation using the rate coefficients obtained from the analysis of the profiles of OH(v = 0 – 4). The unity on the ordinate corresponds to the total amount of OH generated in reaction $O(^1D) + H_2 \rightarrow OH + H$. The pressures of CO: 100, (a); 200, (b); 400 mTorr, (c); O_3: 0.2, (a) and (c); 0.5 mTorr, (b); H_2: 150 mTorr; buffer gas (He): 10 Torr. The step sizes of time scans were 440 ns. Each data point is the averaged signals from ten laser shots, and a single time profile is the average of at least ten scans.

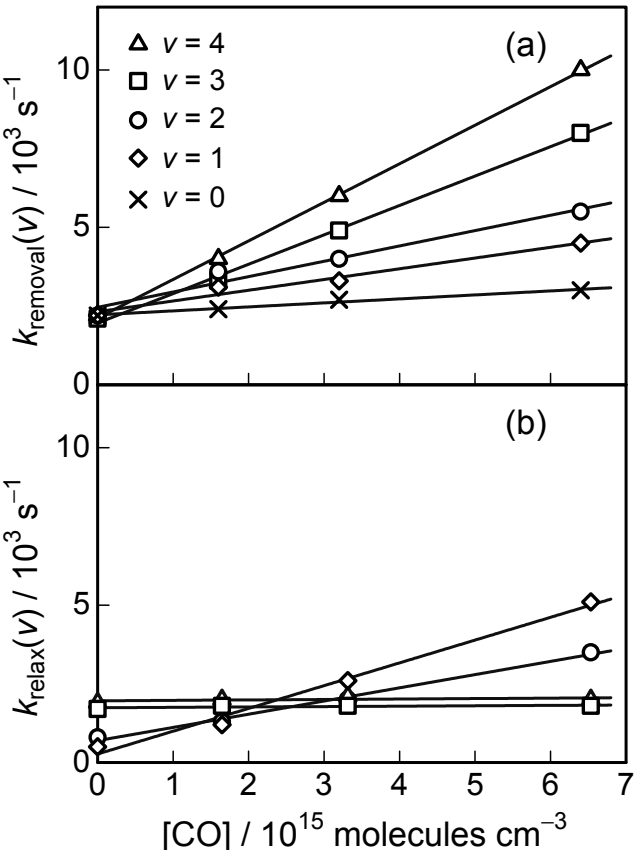

Figure 3.12. CO concentration dependences of the first-order rate coefficients for (a) removal $k_{\mathrm{remove}}(v)$ and (b) relaxation $k_{\mathrm{relax}}(v)$ of the vibrational levels of OH(v = 0 – 4). $k_{\mathrm{remove}}(v)$ and $k_{\mathrm{relax}}(v)$ are defined by eqs (V) and (VI) in the text, respectively. The slopes of the straight line fit of (a) and (b) give the effective bimolecular rate coefficients for chemical reaction $k_{\mathrm{react}}^{\mathrm{CO}}$ and vibrational relaxation $k_{\mathrm{relax}}^{\mathrm{CO}}$, respectively.

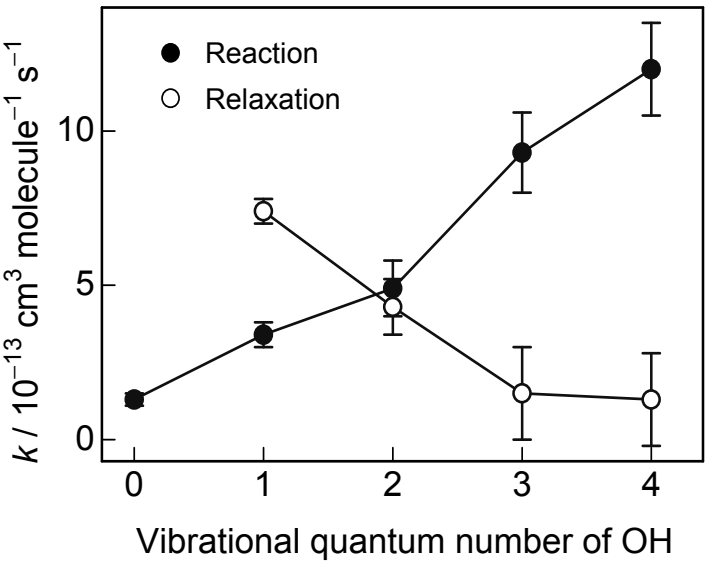

Figure 3.13. Vibrational level dependence of effective bimolecular rate coefficients for chemical reaction $k_{\text{react}}^{\text{CO}}$ and vibrational relaxation $k_{\text{relax}}^{\text{CO}}$ of OH(v) by CO.

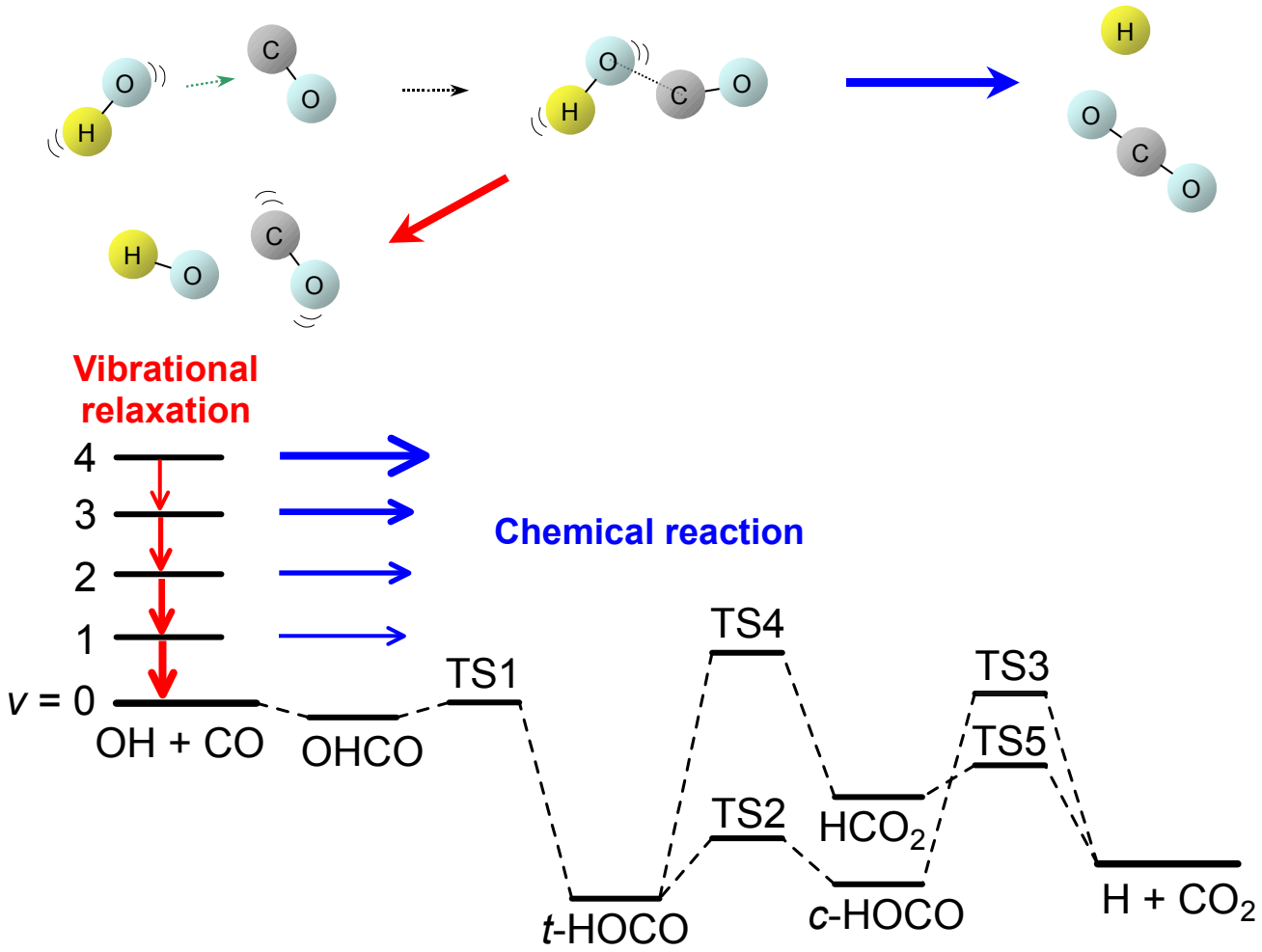

Figure 3.14. Schematic diagram of the chemical reaction and vibrational relaxation of OH(v) by collision with CO.

CHAPTER 4 ENHANCEMENT OF THE $NH_2 + NO \rightarrow OH + H + N_2$ REACTION BY VIBRATIONAL EXCITATION OF NH_2

4.1 INTRODUCTION

The reaction of amidogen (NH_2) with nitrogen monoxide (NO) has attracted the attention of many researchers engaged in atmospheric[1,2] and combustion chemistry.[3,4] Oxidation of ammonia in the atmosphere is initiated by the reaction $OH + NH_3 \rightarrow NH_2 + H_2O$. Because the reactivity of NH_2 with O_2 is very low,[5] the loss of NH_2 is governed by the trace species NO, particularly in the urban areas. Noncatalytic reduction of NO_x by ammonia, called thermal $DeNO_x$ process,[3,6] has been widely used in practical combustion systems, e.g., power plant. The reactions of NH_2 with NO at room temperature proceeds through the following exothermic channels via an adduct such as H_2NNO:

$$NH_2 + NO \rightarrow N_2H + OH \rightarrow N_2 + H + OH \qquad \Delta H^\circ = -23.8 \text{ kJ mol}^{-1} \qquad (1a)$$

$$\rightarrow H_2 + N_2O \qquad \Delta H^\circ = -198.7 \text{ kJ mol}^{-1} \qquad (1b)$$

$$\rightarrow N_2 + H_2O \qquad \Delta H^\circ = -522.6 \text{ kJ mol}^{-1} \qquad (1c)$$

Energy diagram of above channels are shown in Figure 4.1.[7,8] Channel 1a is nearly thermo neutral. There is no experimental report on the detection of N_2H because of its short lifetime (theoretical studies predicted the lifetime to be $\sim 10^{-11}$ s at room temperature[9,10]). Channel 1b has a single high barrier, and channel 1c with large exothermicity generates two stable products. There have been extensive studies on the rate constants and branching ratios among the channels.[7,11-50] Previous reports have shown the negative temperature dependence of reaction 1. No production of N_2O was observed by Andresen et al.[19] in the end product analysis, and Silver and Kolb[20] have

estimated the upper limit of the branching ratio of 1b to be 0.9 % at 300 K. Branching ratios for the processes producing radicals (1a) and stable molecules (1c) have studied over a wide range of temperature.[7,25-30,32,33,35,36,38-43,47-49] Most of the studies have reported that the fraction of OH production, $(k_{1a} + k_{1b})/k_1$, is about 0.1 at 298 K and increases with temperature up to 0.4 at 1500 K.

Vibrational motion of reactants may accelerate reactions or open new channels. Translation and rotation are thermalized at the rate of gas kinetic collisions; vibrationally excited states, on the other hand, have long lifetimes because of large energy level spacing. In the present study, the effect of the internal degrees of freedom of reactant, particularly vibration of NH_2, on the rate coefficients and the branching ratios between reaction paths have been investigated. The author's group[44] have studied the vibrational level dependence of the rate coefficients for removal of $NH_2(0_0$ and $2_1)$ by NO using NH_3/193 nm photolysis coupled with laser-induced fluorescence (LIF) technique for detecting of NH_2. Here, the label $NH_2(X_n)$ indicates the vibrational mode, X, with *n* quanta in the ground state of NH_2. The previous study has shown that the overall removal rate of vibrational excited $NH_2(2_1)$ by collisions with NO is 30 % faster than that of vibration less state. Marcy et al.[51] have studied the effects of vibrationally and electronically excited NH_2 on the collisions between NH_2 and NO, reporting that channel 1b does not proceed without vibrational excitation of NH_2 because of the high barrier and that water is generated after NH_2 completely relaxes to vibration-less state. They, however, did not refer to channel 1a. To the best of our knowledge, there is no experimental report on the effect of vibrational excitation of the reactant on channel 1a. In the present study, we have performed the experimental study on the effect of vibrational excitation of NH_2 on channel 1a.

4.2 EXPERIMENT

4.2.1 Apparatus

Figure 4.2 shows the schematic diagram of the experimental apparatus. The details of the system have been described in the previous chapters (Chapters 2 and 3). An ArF excimer laser (Lambda Physik LEXtra50) was employed for photolysis of NH_3.

4.2.2 Generation of Vibrationally Excited $NH_2(v)$

A gaseous mixture NH_3/NO/CF_4/He (typical conditions: p_{NH_3} = 0.5 mTorr, p_{NO} = 5 – 100 mTorr, p_{CF_4} = 0 – 200 mTorr, and p_{total}(He) = 5 Torr) at 298 ± 2 K in a flow cell was irradiated with the UV light (193 nm) from an ArF excimer laser. The fluence of photolysis laser was E = 200–400 μJ cm^{-2}, and NH_3 was photolyzed into vibrational excited NH_2 and H atoms. The NH_3/193 nm photolysis generates highly vibrationally excited NH_2 owing to a large available energy, 185 kJ mol^{-1} (the bond dissociation energy of N–H in NH_3 is 435 kJ mol^{-1}[52]). Not only electronic ground state, $\tilde{X}^2B_1$, but also excited state, $\tilde{A}^2A_1$ is generated by the photolysis.[53-55] $NH_2(\tilde{A}^2A_1)$ does not disturb the observation of the reaction between $NH_2(\tilde{X}^2B_1)$ and NO under the present experimental conditions. Most of the studies have reported that ground state of NH_2 is a dominant product. Donnelly et al. reported the branching fraction of NH_3/193 nm photolysis: $\phi(\tilde{X}) = 0.965$ and $\phi(\tilde{A}) = 0.024$.[54] Additionally, the excited state $NH_2(\tilde{A}^2A_1)$ is completely quenched by collisions with buffer He in about 1 μs in the present study, because $NH_2(\tilde{A}^2A_1)$ is efficiently quenched even by rare gases, $k^{He}_{quench} = 2\times10^{-11} \sim 1.45\times10^{-10}$ cm^3 molecule^{-1} s^{-1}.[56,57]

The initial number density of $NH_2(\tilde{X}^2B_1)$ generated in the photolysis of NH_3 was estimated to be $[NH_2(\tilde{X}^2B_1)]_0 = (4.5-9.0)\times10^9$ molecules cm^{-3} from the following equation:

$$[NH_2(\tilde{X}^2B_1)]_0 = \phi[NH_3](1 - e^{-\sigma\rho}) \quad \text{(I)}$$

and the experimental conditions: the photoabsorption cross section of NH_3 at 193 nm, $\sigma = 1.5 \times 10^{-18}$ cm^2;[58] the typical fluence of laser light, E = 200–400 μJ cm^{-2}; the energy of a single photon $\varepsilon = 1.03 \times 10^{-18}$ J; the quantum yields of photolysis, $\phi = 0.965$;[54] the number density of NH_3, $[NH_3] = 1.6 \times 10^{13}$ molecules cm^{-3} (p_{NH_3} = 0.5 mTorr).

4.2.3 Detection of Vibrationally Excited $NH_2(v)$

The vibrational levels of the bending mode, v_2 = 0 and 1, of $NH_2(\tilde{X}^2B_1)$ were excited via the $\tilde{A}^2A_1 - \tilde{X}^2B_1$ transition with a Nd^{3+}:YAG laser (Spectra Physics GCR-130) pumped dye laser (Lambda Physik LPD3002). The rovibronic transitions of NH_2 are congested because of the properties of polyatomic molecules, and two or more vibrational states are liable to be excited simultaneously. A monochromator instead of optical filters was used for detection of the LIF from a specific rovibrational level of NH_2. The LIF was collected with a quartz lens (f = 80 mm) and focused on the entrance slit of a monochromator (JEOL JSG-125S, f = 125 cm, Δλ(fwhm) = 3 nm)), and detected with a photomultiplier tube (PMT, Hamamatsu R928). A fundamental light from a laser dye DCM was used and typical pulse energy of the dye laser was 600 μJ pulse^{-1}. Recorded LIF excitation spectra of $NH_2(\tilde{A}^2A_1 - \tilde{X}^2B_1)$ of 2_0^3 and 2_1^4 are shown in Figure 4.3. Here, the label X_n^m indicates a transition between the vibrational mode X with m quanta in the electronically excited state and n quanta in the electronic ground state.[59-64]

4.2.4 Detection of Vibrationally Excited $OH(v)$

The vibrational levels $v = 0$ and 1 of OH generated by reaction 1a were detected by LIF technique via the $A^2\Sigma^+ - X^2\Pi$ transition with a Nd^{3+}:YAG laser pumped dye laser, and the LIF was detected with a photomultiplier tube (PMT; Hamamatsu R1104) through a band-pass filter.

A small part of NO was excited to the electronically excited state, $B^2\Pi(v = 7)$, from the ground state, $X^2\Pi(v = 0, N = 27)$, at 193 nm, and the $B^2\Pi$ state was converted to $A^2\Sigma^+(v = 3)$ state by collisions with the ambient gases. The emission from the $A^2\Sigma^+$ to the $X^2\Pi$ state (γ-band) was quite intense because of the large transition probability. Figure 4.4 shows a dispersed emission spectrum. The blue line represents the simulated spectrum of the emission from the $A^2\Sigma^+$ to the $X^2\Pi$ state of NO.[65] The vibrational populations of the $A^2\Sigma^+$ state in simulations: $p(v'=0) = 0 : p(v'=1) = 0.09 : P(v'=2) = 0.15 : P(v'=3) = 0.76$. In order to separate the emission of NO, the band-pass filters (Melles Griot, 3039 (custom-made filter) and 3071) were used for detection of $OH(v = 0$ and 1), respectively. The transmittance curves of filters are shown in Figure 2.3. The typical pulse energies of the probe laser were 200 and 500 μJ $pulse^{-1}$ for $v = 0$ and 1, respectively. The vibrational sequence of $\Delta v = 0$ was excited, and a frequency-doubled light from DCM dye (doubled with BBO III crystal (Lambda Physik)) was employed. Recorded LIF excitation spectra of OH($A^2\Sigma^+ - X^2\Pi$) are shown in Figure 2.4 in Chapter 2.

4.2.5 Detection of H Atoms

The H atoms were detected by two-photon LIF technique with a Nd^{3+}:YAG laser pumped dye laser, and the Lyman-α emission was collected with a MgF_2 lens ($f = 45$ mm) and focused on the photocathode of a solar-blind PMT (Hamamatsu R10454). A frequency-doubled light from LD-489 dye (doubled with BBO I (Lambda Physik)) was

used, and the typical pulse energy was 300 μJ pulse^{-1}. The details of the detection of H atoms and the LIF excitation spectra are described in Chapter 3.

4.2.6 Samples

The total pressure of a sample gas was monitored with a capacitance manometer (Baratron 122A). The total pressure measurement together with the mole fractions as measured with calibrated flow controllers (Tylan FC-260KZ, STEC-410, and STEC SEC-400 mark3) gave the partial pressures of the reagents. Highly pure grade NH_3 (Nihon-Sanso, 99.999 %), NO (Takachiho Kagaku Cogyo, 99.9%, $NO_2 < 10$ ppm), CF_4 (Showa-Denko, 99.99%), and He (Japan Fine Products, > 99.99995 %) were used without further purification.

4.3 RESULTS AND DISCUSSION

4.3.1 Vibrational Relaxation of $NH_2(v)$ by Collisions with CF_4

The rotational lines, $^rR_{0,2}$ and $^rQ_{0,4}$ of 2_0^3 and 2_1^4 bands, respectively, were excited to record the time-resolved LIF intensities of the vibrational levels of NH_2 (red peaks in Figure 4.3). The buffer gas (He) at 5 Torr was high enough for rotational relaxation to terminate within about 10 μs, and consequently, LIF intensity excited via a single rotational line represents the time evolution of the population in a vibrational level.

The time profiles of $NH_2(0_0)$ recorded at various CF_4 pressures are shown in Figure 4.5. The yields and growing rates of $NH_2(0_0)$ increases with the pressure of CF_4. The decay is mainly governed by the reaction with NO, and the rate is independent of CF_4. The time profiles of $NH_2(2_1)$ were also recorded at various CF_4 pressure, as shown in Figure 4.6. Both the rates of growth and decay of $NH_2(2_1)$ increase with the pressure of CF_4. The fact indicates that vibrationally excited NH_2 is efficiently relaxed to the

vibration less state by collisions with CF_4. The apparent 1st-order decay rates, $k(NH_2(2_1))$, obtained by a single-exponential analysis were in proportion to the concentration of CF_4 (Figure 4.7). The rate coefficient for vibrational relaxation of $NH_2(2_1)$ by CF_4 has been obtained from the slope of the straight line fit of regression analysis, $(2.4 \pm 0.6) \times 10^{-11}$ cm^3 molecule^{-1} s^{-1} (the stated confidence limits are 2σ). This rate coefficient is a little smaller than $(3.2 \pm 0.5) \times 10^{-11}$ cm^3 molecule^{-1} s^{-1} previously measured by the author's lab.[44] This discrepancy might be due to the tentative single-exponential analysis and low signal-to-noise (S/N) ratios in the present study. The intercept in Figure 4.7 corresponds to the sum of the rates for the reaction with NO, vibrational relaxation by NO, NH_3 and He, and diffusion loss.

4.3.2 The Effect of Vibrational Excitation of NH_2 on the Production of OH.

The rotational lines, $P_1(N = 2)$ of 0–0, 1–1 bands of OH were excited to record the time-resolved LIF intensities of the vibrational levels v = 0 and 1 (red peaks in Figure 2.4). Rotational motion was completely thermalized within about 10 μs in the present experiment (buffer gas He at 5 Torr), and consequently, LIF intensity excited via a single rotational line represents the time evolution of the population in a vibrational level. The population on v = 1 generated by reaction 1a was much smaller than 3 % of $v = 0$ estimated from the LIF intensity.

Figure 4.8 shows the time profiles of OH(v = 0) recorded at different CF_4 pressures. As clearly seen in Figure 4.8a, the relative concentration of OH decreased by the addition of CF_4 to the system. This result indicates that the yield of OH is high under the condition of higher vibrational energy of NH_2 at lower CF_4 pressure, and that vibrational excitation of NH_2 enhances reaction 1a. Figure 4.9 shows the time profiles of OH(v = 3) generated in the $O(^1D) + H_2$ reaction at 0–200 mTorr of CF_4, indicating

that CF_4 has no effect on vibrational relaxation or chemical reaction of OH under the present conditions. The decay of time profiles in Figure 4.8a corresponds to diffusion loss and the chemical reaction with NO. Under the present experimental conditions, the decay is mainly governed by diffusion loss, because the pseudo-first-order rate coefficient for chemical reaction with NO is estimated to be less than 20 s^{-1}.[66] Figure 4.8b shows the detail view of growth, and the rate is faster at high pressure of CF_4, suggesting that the species generating OH is removed faster at high pressure of CF_4. In addition, the time constants of the growth of OH(v = 0) are nearly identical with those of the decay of the vibrationally excited $NH_2(2_1)$ (as shown in Figure 4.8 and Figure 4.6, respectively).

The time profiles of OH(v = 1) were also recorded at different CF_4 pressures, as shown in Figure 4.10. The trend is same as that of v = 0. The fast decay is due to the vibrational relaxation by NO. The time constant is smaller than that of the decay of $NH_2(2_1)$, indicating that OH(v = 1) is generated by vibrationally excited NH_2 higher than v_2 = 1.

The LIF intensity of OH increased with an increase in NO, because reaction 1a competes with vibrational relaxation of $NH_2(v)$ by NH_3 and He. The simple scheme for the production of OH is shown in Figure 4.11. Under the high NO pressure condition, all the processes, chemical reaction and vibrational relaxation, are governed by NO. At high pressure of NO, the contribution of vibrational relaxation by CF_4 is small, and then the reduction of OH by CF_4 is small as shown in Figure 4.12.

4.3.3 Branching Ratio of Reaction Channel 1a

In order to determine the absolute yield of channel 1a, the time-resolved LIF intensities of H atoms were observed. Figure 4.13 shows the schematic time profile of

H atoms. First, H atoms generated by the photolysis of NH_3, NH_3 + 193 nm → NH_2 + H, and the concentration is identical with that of NH_2 (the red arrow in Figure 4.13). Second, the increase after the photolysis is due to the H atoms generated by the reaction, NH_2 + NO → N_2 + H + OH (the blue arrow in Figure 4.13). The ratio between the sizes of the red and blue arrows is the yield of channel 1a. Figure 4.14a and b show the time profiles of H atoms in the presence and absence of NO, respectively. The fast decay of the profiles a and b is due mainly to diffusion. The profile b subtracted from the profile a leaves the profile c, which represents the profile of H atoms generated by channel 1a. The number densities of H atoms generated by channel 1a are estimated by the following equation:

$$[\mathrm{H}] = \frac{k_1[\mathrm{NH_2}]_0}{k_1 + k_{\mathrm{d,NH_2}} - k_{\mathrm{d,H}}} \left\{ \exp(-k_{\mathrm{d,H}}\, t) - \exp[-(k_1 + k_{\mathrm{d,NH_2}})t] \right\} \qquad \text{(II)}$$

where k_1 is the first-order rate coefficient for chemical reaction of NH_2 with NO, and $k_{\mathrm{d,NH_2}}$ and $k_{\mathrm{d,H}}$ are the first-order rate coefficients for diffusion loss of NH_2 and H atoms, respectively. The increase of H atoms in the absence of the diffusion loss of H atoms (the blue arrows in Figure 4.13) have been expected from the double-exponential analysis based on eq II (the red line in Figure 4.14). The production yield of H atoms from the analysis is 23 %. The previous studies performed over a wide range of temperature, indicate that reaction channel 1a is effectively accelerated by temperature rise.[7,20,25-30,32,33,35,36,38-43,47-49,67,68] Most of the studies reported that the yield of OH at room temperature was about 10 %[20,25,28,29,33,35,38,39,43,48,49,67,68]. The discrepancy is not surprising because NH_2 produced in this study is vibrationally excited. To elucidate the dependence of the production yield on vibrational energy of NH_2, the time profiles of H atoms were recorded at various CF_4 pressure. The dependence on CF_4, however, was not observed. This is because, H atoms generated by the reaction were detected at

higher pressure of NO: the relative vibrational relaxation rate by CF_4 was slow (as shown in Figure 4.12). At lower pressure of NO, the diffusion rate of H atoms was too fast to observe the increasing of the amount of H atoms generated by the reaction. With a view to uncovering the effect of vibrational excitation of NH_2 to this chemical reaction more quantitatively, the observation of H atoms at higher total pressure, which gives slower diffusion rates, must be made.

References

(1) McConnell, J. C. Atmospheric ammonia. *J. Geophys. Res.* **1973**, *78*, 7812−7821.

(2) Logan, J. A.; Prather, M. J.; Wofsy, S. C.; McElroy, M. B. Tropospheric chemistry: A global perspective. *J. Geophys. Res.* **1981**, *86*, 7210−7254.

(3) Lyon, R. K. The NH_3-NO-O_2 reaction. *Int. J. Chem. Kinet.* **1976**, *8*, 315−318.

(4) Miller, J. A.; Branch, M. C.; Kee, R. J. A chemical kinetic model for the selective reduction of nitric oxide by ammonia. *Combust. Flame* **1981**, *43*, 81−98.

(5) DeMore, W. B.; Sander, S. P.; Golden, D. M.; Hampson, R. F.; Kurylo, M. J.; Howard, C. J.; Ravishankara, A. R.; Kolb, C. E.; Molina, M. J. Chemical Kinetics and Photochemical Data for Use in Stratospheric Modeling. NASA JPL Publication 97-4; Jet Propulsion Laboratory: California Institute of Technology: Pasadena, 1997.

(6) Lyon, R. K. Method for the reduction of the concentration of NO in combustion effluents usin NH3. U. S. Patent 3900554, 1975.

(7) Wolf, M.; Yang, D. L.; Durant, J. L. A Comprehensive Study of the Reaction NH_2 + NO → Products: Reaction Rate Coefficients, Product Branching Fractions, and ab Initio Calculations. *J. Phys. Chem. A* **1997**, *101*, 6243−6251.

(8) Baker, L. A.; Su, S. An ab initio molecular orbital study of the reaction NH_2 + NO → H_2 + N_2O. *Chemical Physics* **1998**, *228*, 9−16.

(9) Phillips, L. F. A priori rate constant for the reaction NH_2 + NO → N_2 + H_2O. *Chem. Phys. Lett.* **1987**, *135*, 269−274.

(10) Bozkaya, U.; Turney, J. M.; Yamaguchi, Y.; Schaefer III, H. F. The barrier height, unimolecular rate constant, and lifetime for the dissociation of HN_2. *J. Chem. Phys.* **2010**, *132*, 064308

(11) Gordon, S.; Mulac, W.; Nangia, P. Pulse radiolysis of ammonia gas. II. Rate of

disappearance of the $NH_2(\tilde{X}^2B_1)$ radical. *J. Phys. Chem.* **1971**, *75*, 2087–2093.

(12) Gehring, M.; Hoyermann, K.; Schacke, H.; Wolfrum, J. Direct studies of some elementary steps for the formationand destruction of nitric oxide in the H-N-O system. *Symp. Int. Combust. Proc.* **1973**, *14*, 99–105.

(13) Hancock, G.; Lange, W.; Lenzi, M.; Welge, K. H. Laser fluorescence of NH_2 and rate constant measurement of NH_2 + NO. *Chem. Phys. Lett.* **1975**, *33*, 168–172.

(14) Lesclaux, R.; Khe, P. V.; Dezauzier, P.; Soulignac, J. C. Flash photolysis studies of the reaction of NH_2 radicals with NO. *Chem. Phys. Lett.* **1975**, *35*, 493–497.

(15) Sarkisov, O. M.; Cheskis, S. G.; Sviridenkov, E. A. Study of NH_2 + NO reaction employing intraresonator laser spectroscopy. *Bull. Russ. Acad. Sci. USSR, Div. Chem. Sci.* **1978**, *27*, 2336–2338.

(16) Roose, T. R.; Hanson, R. K.; Kruger, C. H. Decomposition of NO in the Presence of NH_3. *Symp. Int. Shock Tubes Waves Proc.* **1978**, *11*, 245

(17) Kurasawa, H.; Lesclaux, R. Kinetics of the reaction of NH_2 with NO_2. *Chem. Phys. Lett.* **1979**, *66*, 602–607.

(18) Hack, W.; Schacke, H.; Schroter, M.; Wagner, H. G. Reaction rates of NH_2-radicals with NO, NO_2, C_2H_2, C_2H_4 and other hydrocarbons. *Symp. Int. Combust. Proc.* **1979**, *17*, 505–513.

(19) Andresen, P.; Jacobs, A.; Kleinermanns, C.; Wolfrum, J. Direct investigations of the NH_2 + NO reaction by laser photolysis at different temperatures. *Symp. Int. Combust. Proc.* **1982**, *19*, 11–22.

(20) Silver, J. A., Kolb, C. E. Kinetic measurements for the reaction of amidogen + nitric oxide over the temperature range 294–1215 K. *J. Phys. Chem.* **1982**, *86*, 3240–3246.

(21) Stief, L. J.; Brobst, W. D.; Nava, D. F.; Borkowski, R. P.; Michael, J. V. Rate

constant for the reaction NH_2 + NO from 216 to 480 K. *J. Chem. Soc., Faraday Trans. 2* **1982**, *78*, 1391–1401.

(22) Whyte, A. R.; Phillips, L. F. Rates of reaction of NH_2 with N, NO AND NO_2. *Chem. Phys. Lett.* **1983**, *102*, 451–454.

(23) Jeffries, J. B.; McCaulley, J. A.; Kaufman, F. Kinetics of polyatomic radical reactions using a versatile flow reactor apparatus. *Chem. Phys. Lett.* **1984**, *106*, 111–116.

(24) Gericke, K.-H.; Torres, L. M.; Guillory, W. A. State selected removal of vibrationally excited $NH_2[\widetilde{X}^2B_1(0,\nu_2,0)]$ radicals. *J. Chem. Phys.* **1984**, *80*, 6134–6140.

(25) Hall, J. L.; Zeitz, D.; Stephens, J. W.; Kasper, J. V. V.; Glass, G. P.; Curl, R. F.; Tittel, F. K. Studies of the amidogen-nitric oxide reaction by infrared kinetic spectroscopy. *J. Phys. Chem.* **1986**, *90*, 2501–2505.

(26) Dolson, D. A. Experimental determination of the hydroxyl product yield from amidogen + nitric oxide at 300 K. *J. Phys. Chem.* **1986**, *90*, 6714–6718.

(27) Silver, J. A.; Kolb, C. E. A reevaluation of the branching ratio for the reaction of amidogen with nitric oxide. *J. Phys. Chem.* **1987**, *91*, 3713–3714.

(28) Atakan, B.; Jacobs, A.; Wahl, M.; Weller, R.; Wolfrum, J. Kinetic measurements and product branching ratio for the reaction NH_2 + NO at 294–1027 K. *Chem. Phys. Lett.* **1989**, *155*, 609–613.

(29) Bulatov, V. P.; Ioffe, A. A.; Lozovsky, V. A.; Sarkisov, O. M. On the reaction of the NH_2 radical with NO at 295–620 K. *Chem. Phys. Lett.* **1989**, *161*, 141–146.

(30) Atakan, B.; Wolfrum, J.; Weller, R. Kinetik der gasphasenreaktion NH_2 + NO im temperaturbereich 294–1025K. *Ber. Bunsen-Ges. Phys. Chem.* **1990**, *94*, 1372–1375.

(31) Unfried, K. G.; Glass, G. P.; Curl, R. F. Thermal deNOx: no HNO at room temperature. *Chem. Phys. Lett.* **1990**, *173*, 337–342.

(32) Pagsberg, P.; Sztuba, B.; Ratajczak, E.; Sillesen, A. Spectrokinetic Studies of

the Gas Phase Reactions NH_2 + NO_x Initiated by Pulse Radiolysis. *Acta Chem. Scand.* **1991**, *45*, 329

(33) Stephens, J. W.; Morter, C. L.; Farhat, S. K.; Glass, G. P.; Curl, R. F. Branching ratio of the reaction amidogen + nitric oxide at elevated temperatures. *J. Phys. Chem.* **1993**, *97*, 8944–8951.

(34) Yu, T., Lin, M. C. Kinetics of the C_6H_5 + NO Association Reaction. *J. Phys. Chem.* **1994**, *98*, 2105–2109.

(35) Diau, E. W.; Yu, T.; Wagner, M. A. G.; Lin, M. C. Kinetics of the NH_2 + NO Reaction: Effects of Temperature on the Total Rate Constant and the OH/H_2O Branching Ratio. *J. Phys. Chem.* **1994**, *98*, 4034–4042.

(36) Wolf, M.; Yang, D. L.; Durant, J. L. Kinetic studies of NH_x radical reactions. *J. Photochem. Photobiol. A: Chem.* **1994**, *80*, 85–93.

(37) Imamura, T.; Washida, N. Measurements of Rate Constants for HO_2 + NO and NH_2 + NO Reactions by Time-Resolved Photoionization Mass Spectrometry. *Laser Chem.* **1995**, *16*, 43–51.

(38) Park, J.; Lin, M. C. Direct Determination of Product Branching for the NH_2 + NO Reaction at Temperatures between 302 and 1060 K. *J. Phys. Chem.* **1996**, *100*, 3317–3319.

(39) Park, J.; Lin, M. C. Laser-Initiated NO Reduction by NH_3: Total Rate Constant and Product Branching Ratio Measurements for the NH_2 + NO Reaction. *J. Phys. Chem. A* **1997**, *101*, 5–13.

(40) Glarborg, P.; Kristensen, P. G.; D.-Johansen, K.; Miller, J. A. Branching Fraction of the NH_2 + NO Reaction between 1210 and 1370 K. *J. Phys. Chem. A* **1997**, *101*, 3741–3745.

(41) Deppe, J.; Friedrichs, G.; Romming, H.-J.; Wagner, H. G. A kinetic study of

the reaction of NH_2 with NO in the temperature range 1400–2800 K. *Phys. Chem. Chem. Phys.* **1999**, *1*, 427–435.

(42) Votsmeier, M.; Song, S.; Hanson, R. K.; Bowman, C. T. A Shock Tube Study of the Product Branching Ratio for the Reaction NH_2 + NO Using Frequency-Modulation Detection of NH_2. *J. Phys. Chem. A* **1999**, *103*, 1566–1571.

(43) Park, J.; Lin, M. C. Product Branching Ratios in the NH_2 + NO Reaction: A Re-Evaluation. *J. Phys. Chem. A* **1999**, *103*, 8906–8907.

(44) Yamasaki, K.; Watanabe, A.; Tanaka, A.; Sato, M.; Tokue, I. Kinetics of the Reaction $NH_2(\tilde{X}^2B_1, v_2 = 0$ and 1) + NO. *J. Phys. Chem. A* **2002**, *106*, 6563–6569.

(45) SONG, S.; HANSON, R. K.; BOWMAN, C. T.; GOLDEN, D. M. Shock Tube Determination of the Overall Rate of NH_2 + NO → Products at High Temperatures. *Proceedings of the Combustion Institute* **2000**, *28*, 2403–2409.

(46) SONG, S.; HANSON, R. K.; BOWMAN, C. T.; GOLDEN, D. M. Shock Tube Determination of the Overall Rate of NH_2 + NO → Products in the Thermal De-NO_x Temperature Window. *Int. J. Chem. Kinet.* **2001**, *33*, 715–721.

(47) SONG, S.; HANSON, R. K.; BOWMAN, C. T.; GOLDEN, D. M. A Shock Tube Study of the Product Branching Ratio of the NH_2 + NO Reaction at High Temperatures. *J. Phys. Chem. A* **2002**, *106*, 9233–9235.

(48) Miller, J. A.; Klippenstein, S. J. Theoretical Considerations in the NH_2 + NO Reaction. *J. Phys. Chem. A* **2000**, *104*, 2061–2069.

(49) Fang, D.-C.; Harding, L. B.; Klippenstein, S. J.; Miller, J. A. A direct transition state theory based analysis of the branching in NH_2+ NO. *Faraday Discuss.* **2001**, *119*, 207–222.

(50) Friedrichs, G.; Colberg, M.; Fikri, M.; Huang, Z.; Neumann, J.; Temps, F. Validation of the Extended Simultaneous Kinetics and Ringdown Model by

Measurements of the Reaction NH_2 + NO. *J. Phys. Chem. A* **2005**, *109*, 4785–4795.

(51) Marcy, T. P.; Heard, D. E.; Leone, S. R. Product Studies of Inelastic and Reactive Collisions of NH_2 + NO: Effects of Vibrationally and Electronically Excited NH_2. *J. Phys. Chem. A* **2002**, *106*, 8249–8255.

(52) Darwent, B. deB. Bond Dissociation Energies in Simple Molecules. *Nat. Stand. Ref. Data Ser.* **1970**, *31*, 48

(53) Donnelly, V. M.; Baronavski, A. P.; McDonald, J. R. Excited state dynamics and bimolecular quenching processes for $NH_2(\tilde{A}^2A_1)$. *Chem. Phys.* **1979**, *43*, 283–293.

(54) Donnelly, V. M.; Baronavski, A. P.; McDonald, J. R. ArF laser photodissociation of NH_3 at 193 nm: internal energy distributions in NH_2 $\tilde{X}^2B_1$ and $\tilde{A}^2A_1$, and two-photon generatin of NH $A^3\Pi$ and $b^1\Sigma^+$. *Chem. Phys.* **1979**, *43*, 271–281.

(55) Biesner, J.; Schnieder, L.; Ahlers, G.; Xie, X.; Welge, K. H.; Ashfold, M. N. R.; Dixon, R. N. State selective photodissociation dynamics of $\tilde{A}$ state ammonia. II. *J. Chem. Phys.* **1989**, *91*, 2901–2911.

(56) Halpern, J. B.; Hancock, G.; Lenzi, M.; Welge, K. H. Laser induced fluorescence from $NH_2(^2A_1)$. State selected radiative lifetimes and collisional de-excitation rates. *J. Chem. Phys.* **1975**, *63*, 4808–4816.

(57) Wysong, I. J.; Jeffries, J. B.; Crosley, D. R. Rotational level dependence of the electronic quenching of NH_2 A by helium. *J. Chem. Phys.* **1990**, *93*, 237–241.

(58) Cheng, B.-M.; Lu, H.-C.; Chen, H.-K.; Bahou, M.; Lee, Y.-P.; Mebel, A. M.; Lee, L. C.; Liang, M.-C.; Yung, Y. L. ABSORPTION CROSS SECTIONS OF NH_3, NH_2D, NHD_2, AND ND_3 IN THE SPECTRAL RANGE 140–220 nm AND IMPLICATIONS FOR PLANETARY ISOTOPIC FRACTIONATION. *APJ* **2006**, *647*, 1535–1542.

(59) Dressler, K.; Ramsay, D. A. The Electronic Absorption Spectra of NH_2 and

ND_2. *Philos. Trans. R. Soc. A* **1959**, *251*, 553–602.

(60) Johns, J. W. C.; Ramsay, D. A.; Ross, S. C. The $\tilde{A}^2A_1 - \tilde{X}^2B_1$ absorption spectrum of NH_2 between 6250 and 9500 Å. *Can. J. Phys.* **1976**, *54*, 1804–1814.

(61) Vervloet, M.; M.-Lafore, M. F.; Ramsay, D. A. Molecular constants for the 010 level of the $\tilde{X}^2B_1$ ground state of NH_2. *Chem. Phys. Lett.* **1978**, *57*, 5–7.

(62) Kawaguchi, K.; Yamada, C.; Hirota, E.; Brown, J. M.; Buttenshaw, J.; Parent, C. R.; Sears, T. The laser magnetic resonance spectrum of the ν_2 band of NH_2. *J. Mol. Spectrosc.* **1980**, *81*, 60–72.

(63) Burkholder, J. B.; Howard, C. J.; McKellar, A. R. W. Fourier transform infrared spectrum of the ν_2 band of the NH_2 radical. *J. Mol. Spectrosc.* **1988**, *127*, 415–424.

(64) Ross, S. C.; Birss, F. W.; Vervloet, M.; Ramsay, D. A. The absorption spectrum of NH_2 in the region 5300 to 6800 Å. *J. Mol. Spectrosc.* **1988**, *129*, 436–470.

(65) Luque, J.; Crosley, D. R. LIFBASE: Database and Spectral Simulation Program, Version 1.5. SRI international Report MP 99-009: Menlo Park, CA,1999.

(66) Sander, S. P.; Friedl, R. R.; Abbatt, J. P. D.; Barker, J. R.; Burkholder, J. B.; Golden, D. M.; Kolb, C. E.; Kurylo, M. J.; Moortgat, G. K.; Wine, P. H.; Huie, R. E.; Orkin, V. L. Chemical Kinetics and Photochemical Data for Use in Atmospheric Studies, Evaluation No. 17. Jet Propulsion Laboratory, California Institute of Technology: Pasadena, CA, 2011.

(67) Diau, E. W.-G.; Smith, S. C. Temperature Dependence of Rate Coefficients and Branching Ratios for the NH_2 + NO Reaction via Microcanonical Variational Transition State Theory. *J. Phys. Chem.* **1996**, *100*, 12349–12354.

(68) Miller, J. A., Glarborg, P. Modeling the thermal De-NO_x process: Closing in on a final solution. *Int. J. Chem. Kinet.* **1999**, *31*, 757–765.

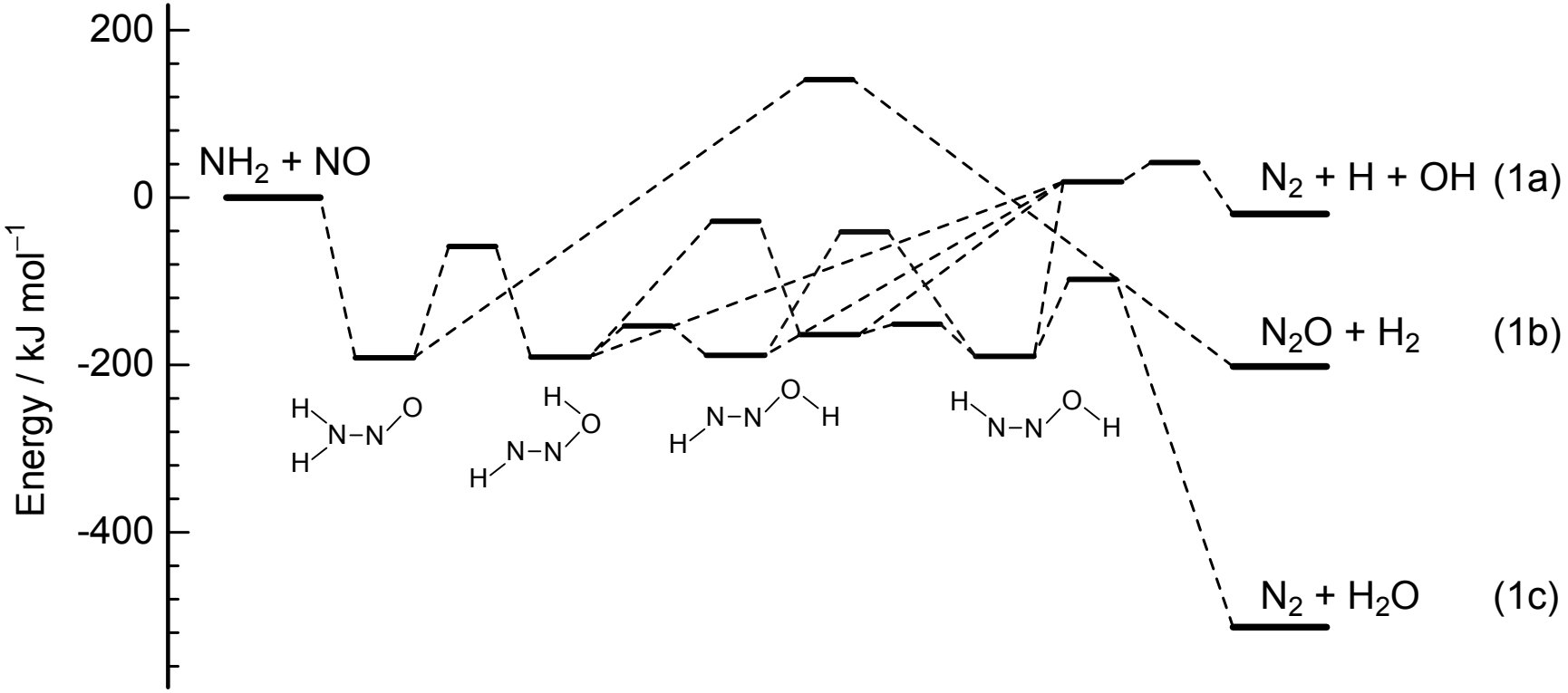

Figure 4.1. Energy diagram of the reaction system of $NH_2(\tilde{X}^2B_1)$ + NO.[7,8]

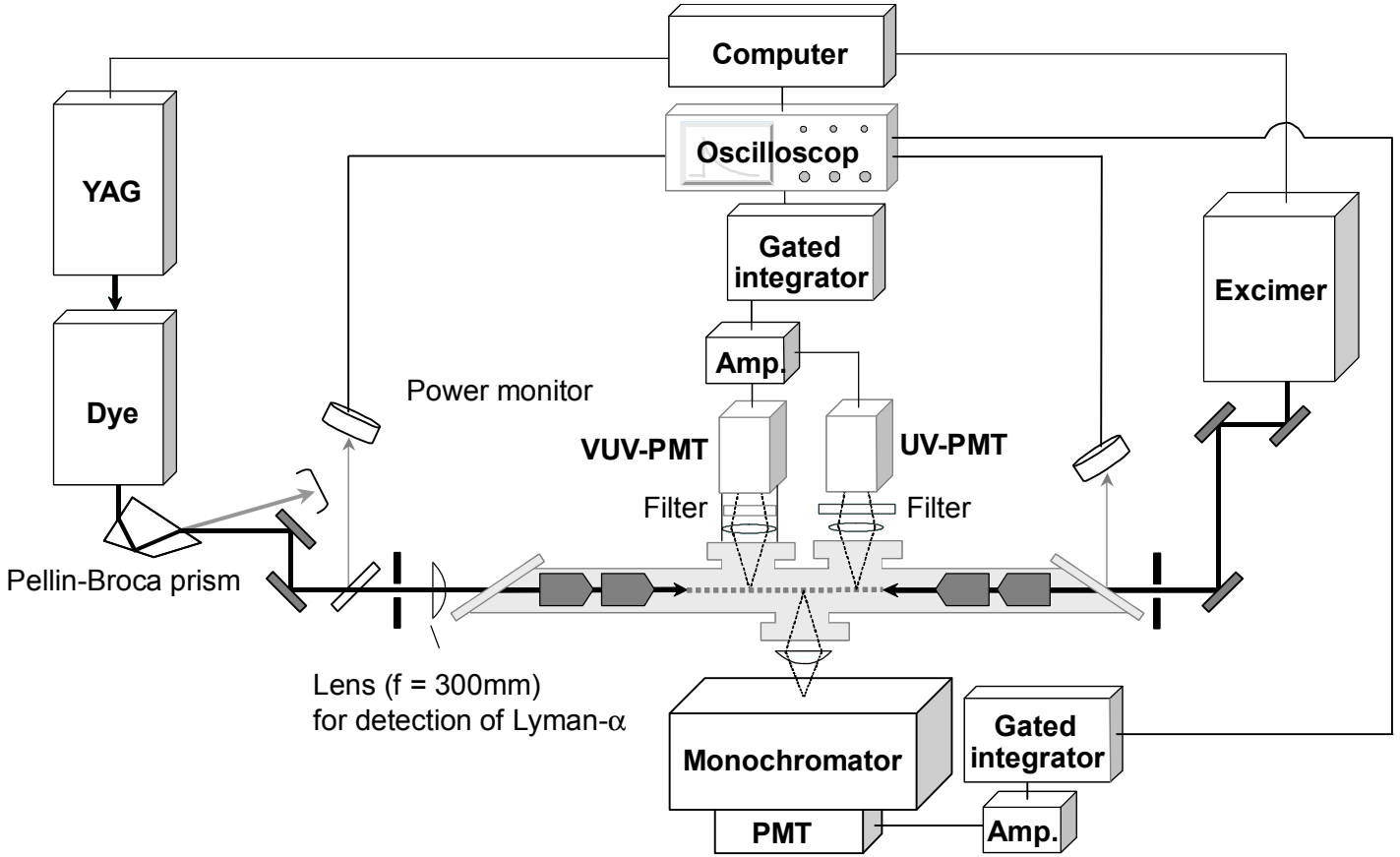

Figure 4.2. A schematic diagram of experimental apparatus. Amp. : preamplifier made with Op-amp LF356, PMT : photomultiplier.

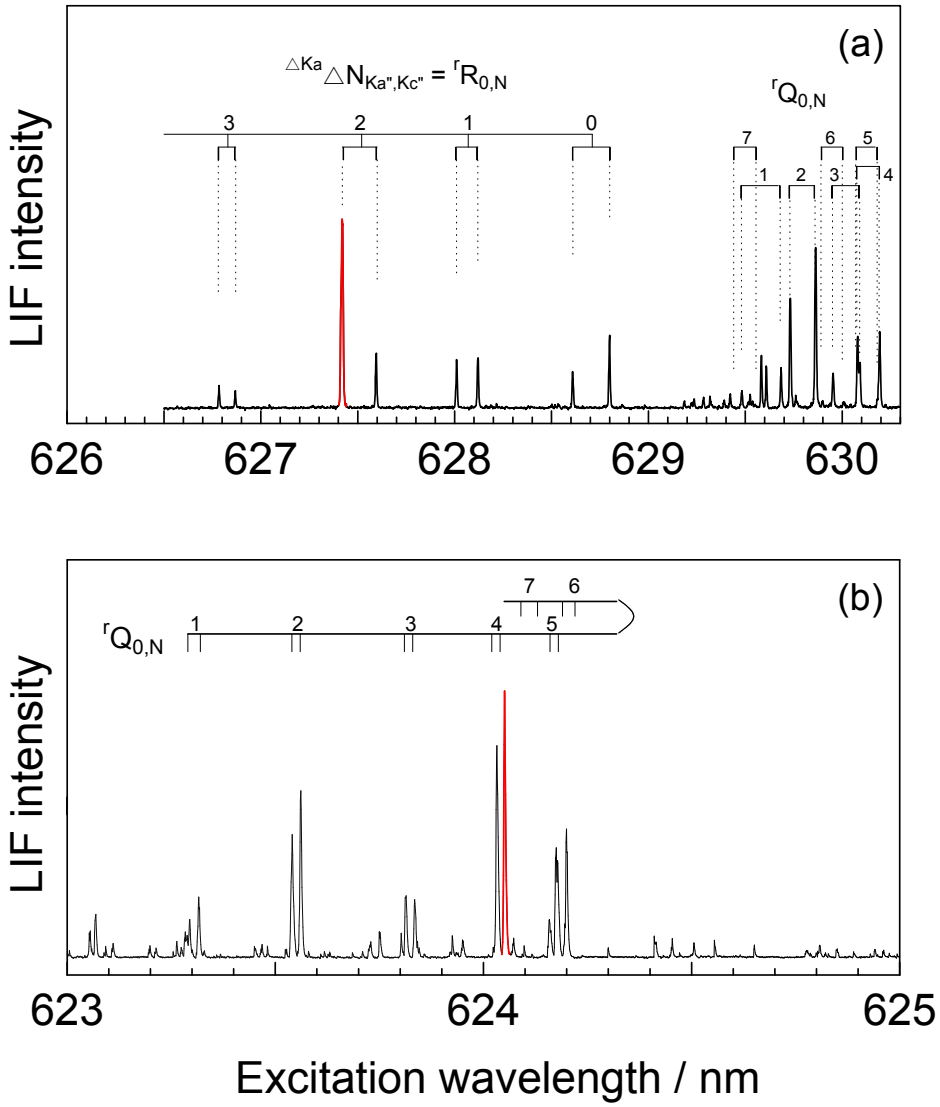

Figure 4.3. Laser-induced fluorescence excitation spectra of $NH_2(\tilde{X}^2B_1, v = 0$ and $v_2 = 1)$ generated in the photolysis of NH_3. The fluorescence was excited via the $\tilde{A}^2A_1 - \tilde{X}^2B_1$ transition: (a) 2_0^3; (b) 2_1^4. The pressure of He buffer was 1 Torr and the partial pressure of NH_3 was 10 mTorr in both spectra. Delay times between the photolysis and probe lasers were 150 and 75 μs as for (a) and (b), respectively.

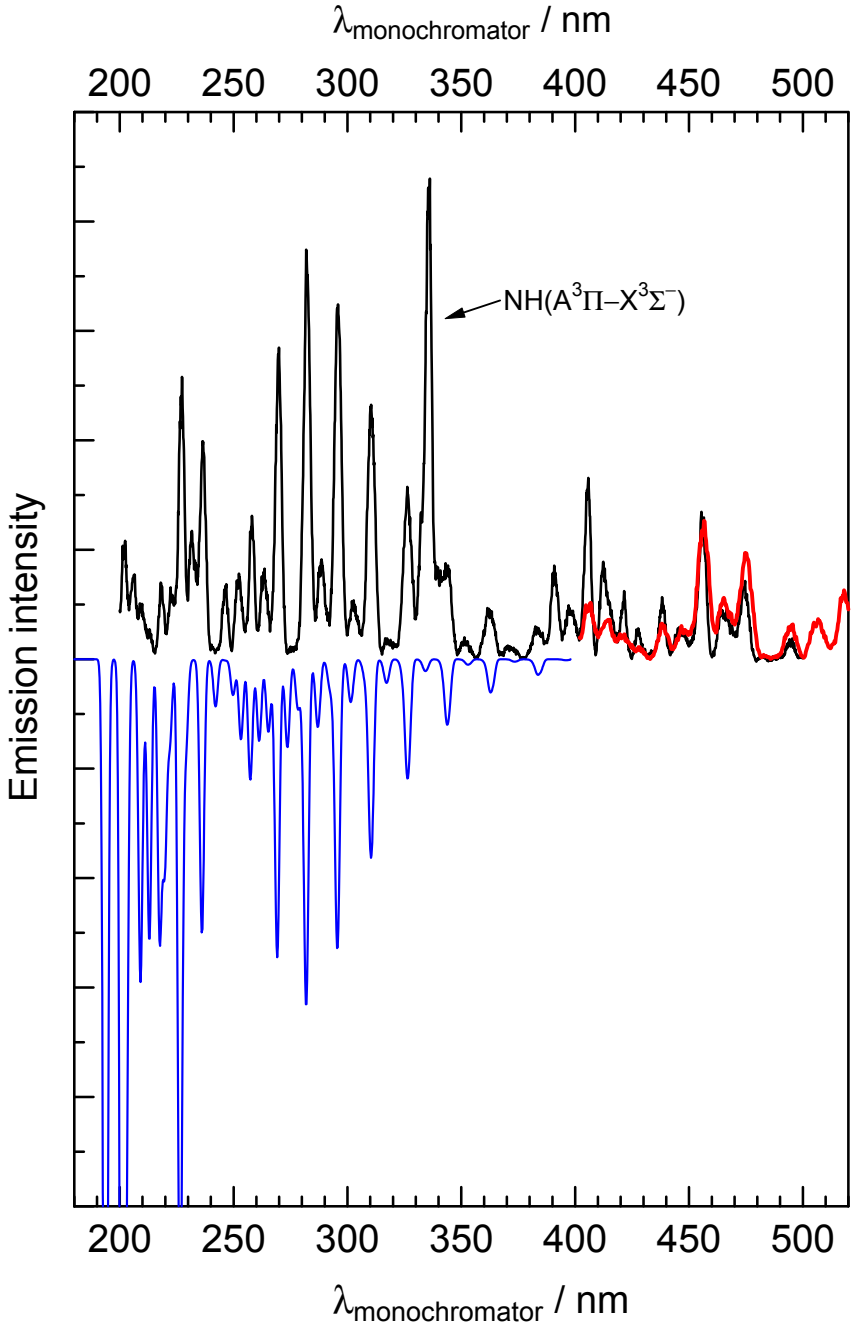
λmonochromator / nm
200
250
300
350
400
450
500
NH(A3Π–X3Σ−)
Emission intensity
200
250
300
350
400
450
500
λmonochromator / nm

Figure 4.4.

Figure 4.4. Dispersed emission spectra recorded with monochromator (f = 125 cm, $\Delta\lambda$(fwhm) = 3 nm). The blue line represents the simulation spectrum of the emission from the $A^2\Sigma^+$ to the $X^2\Pi$ state of NO^{65}. The red line denotes the second-order spectrum made of the emission appeared over the wavelength of 200 – 250 nm. The pressure of He buffer was 5 Torr. The partial pressure of NH_3 was 0.5 mTorr and that of NO was 50 mTorr.

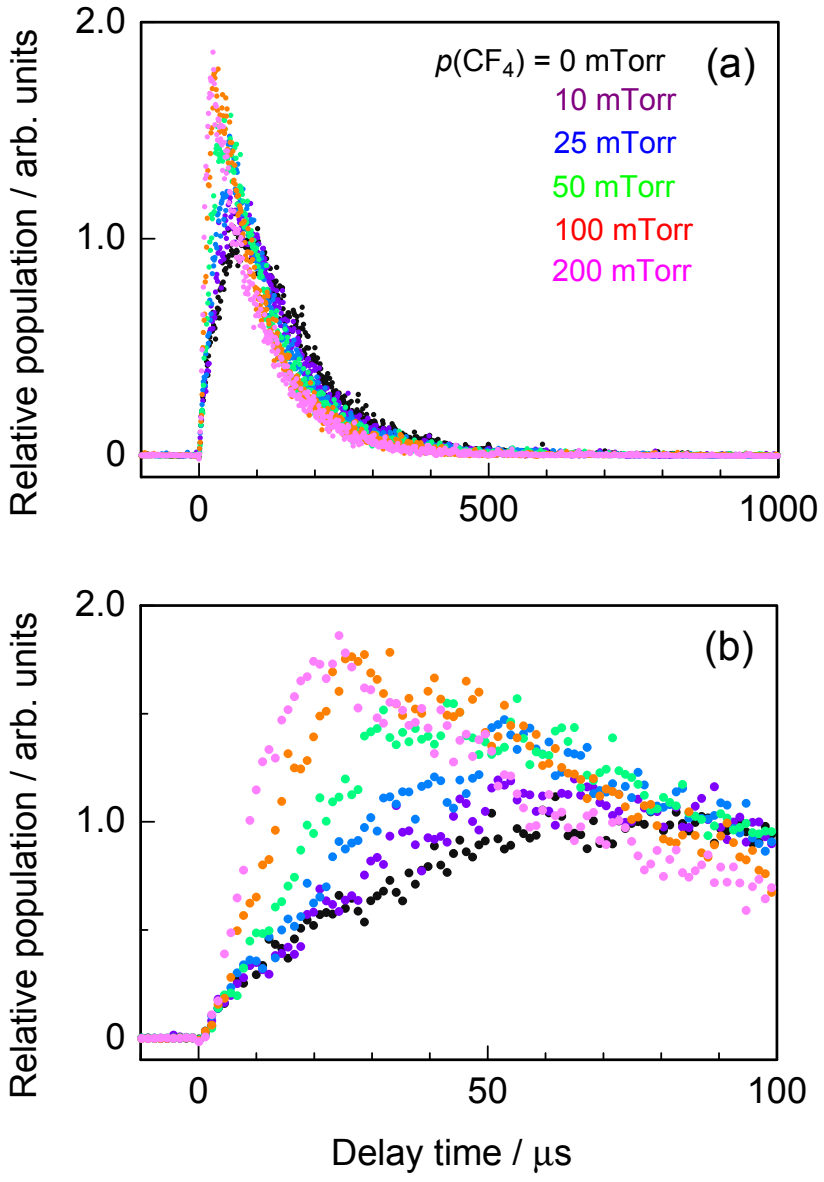

Figure 4.5. CF_4 pressure dependence of the time-resolved LIF intensities of $NH_2(0_0)$ generated in the NH_3/193 nm photolysis. Part b is the expanded figure of the initial 100 μs of part a. The pressures of NO: 5 mTorr; NH_3: 0.5 mTorr; CF_4: 0–200 mTorr; buffer gas (He): 5 Torr.

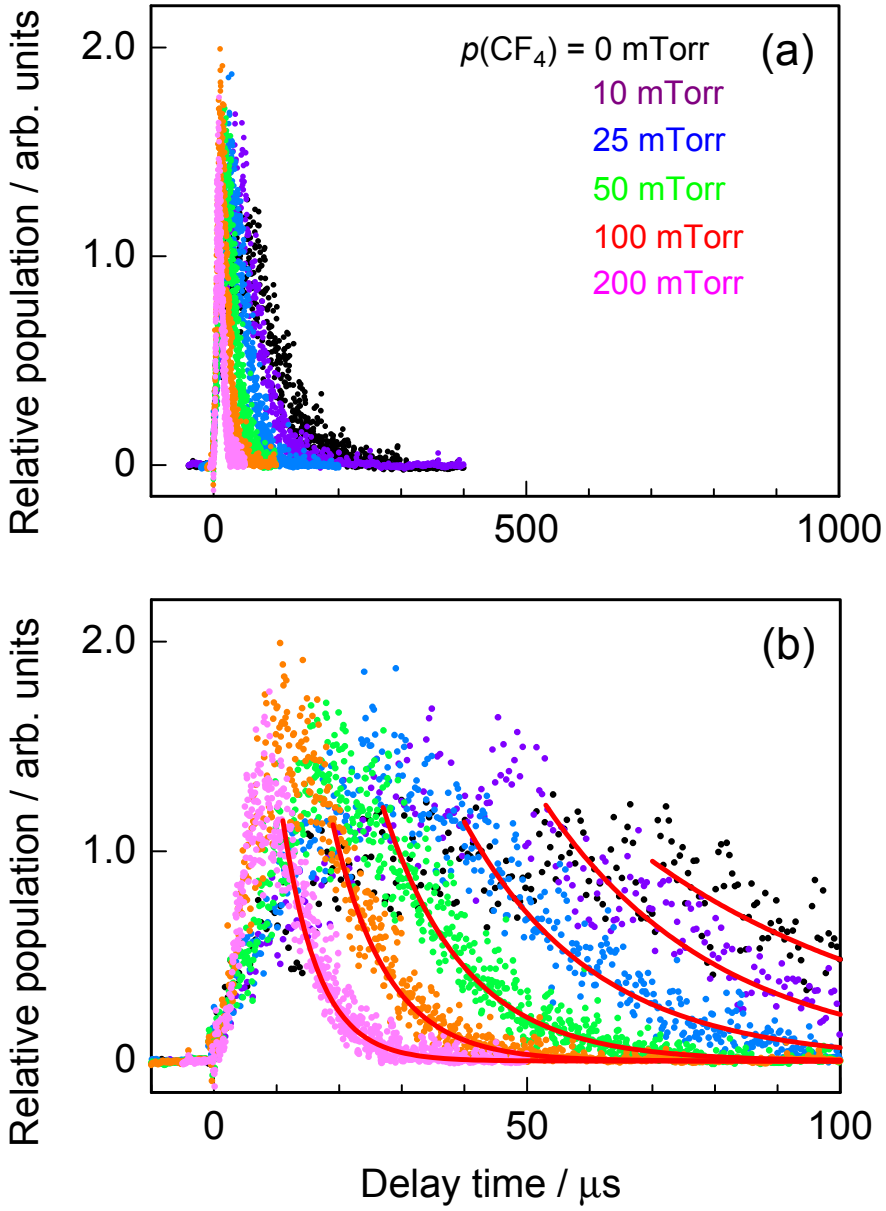

Figure 4.6. CF_4 pressure dependence of the time-resolved LIF intensities of $NH_2(2_1)$ generated in the NH_3/193 nm photolysis. Part b is the expanded figure of the initial 100 μs of part a. The red lines represent the fit by a single-exponential analysis. The pressures of NO: 5 mTorr; NH_3: 0.5 mTorr; CF_4: 0–200 mTorr; buffer gas (He): 5 Torr.

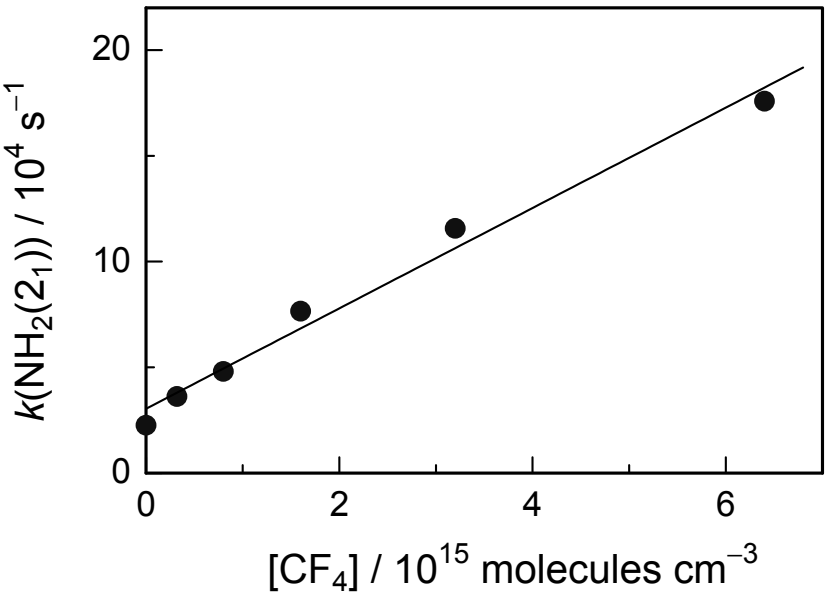

Figure 4.7. Plots of $k(NH_2(2_1))$ versus $[CF_4]$ for $NH_2(2_1)$. The slop of the straight line fit from regression analysis gives the bimolecular rate coefficient for relaxation by CF_4.

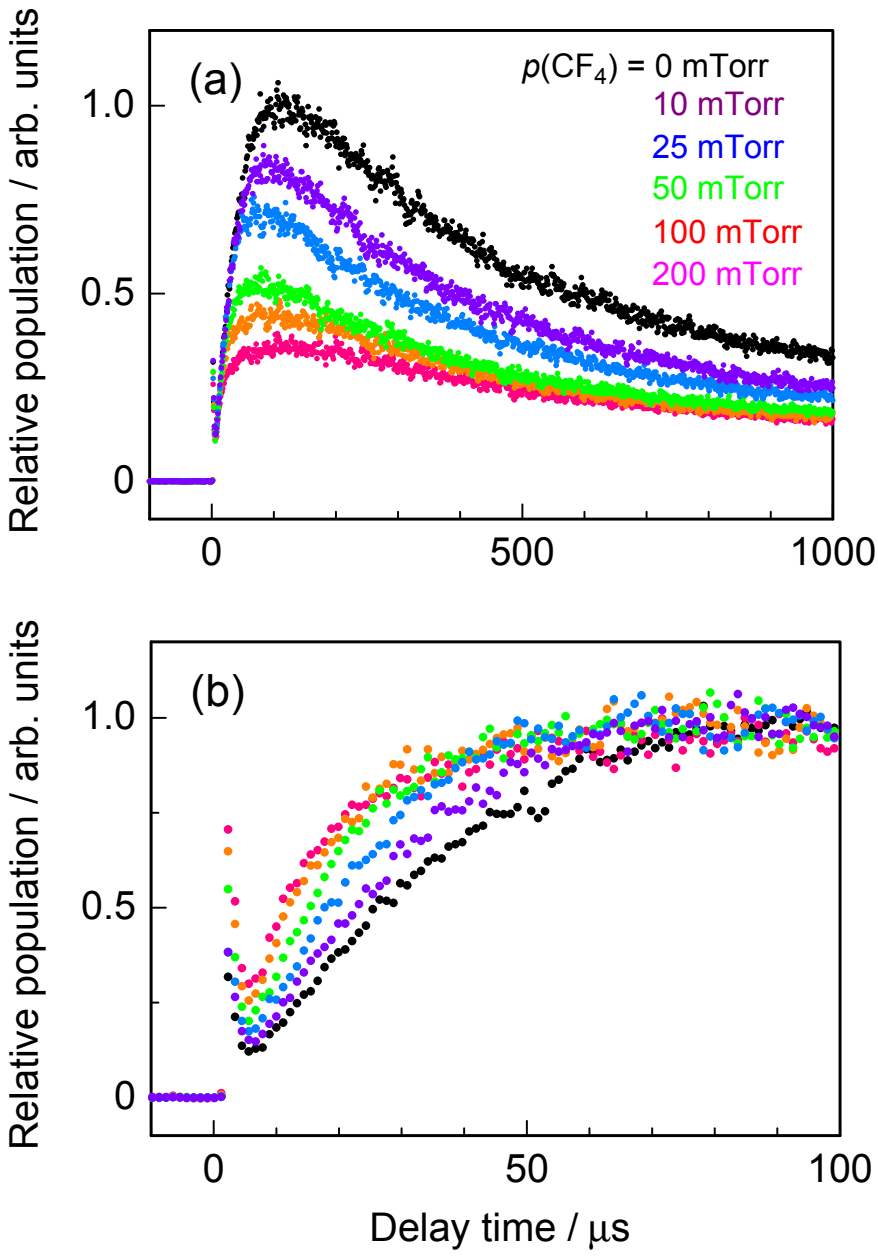

Figure 4.8. CF_4 pressure dependence of the time-resolved LIF intensities of OH(v = 0) generated in the reaction system. Part b is the expanded figure of the initial 100 μs of part a. Time profiles in part b are so scaled as to make their maximum intensities the same. The pressures of NO: 5 mTorr; NH_3: 0.5 mTorr; CF_4: 0–200 mTorr; buffer gas (He): 5 Torr.

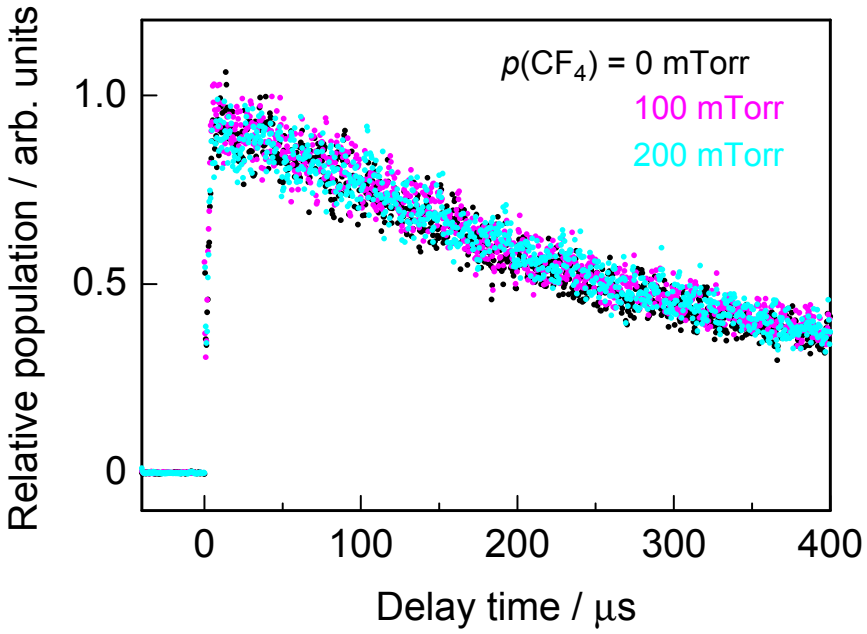

Figure 4.9. CF_4 pressure dependence of the time-resolved LIF intensities of OH($v = 3$) generated in the $O(^1D) + H_2$ reaction. The pressures of O_3: 0.5 mTorr; H_2: 150 mTorr; CF_4: 0–200 mTorr; buffer gas (He): 10 Torr.

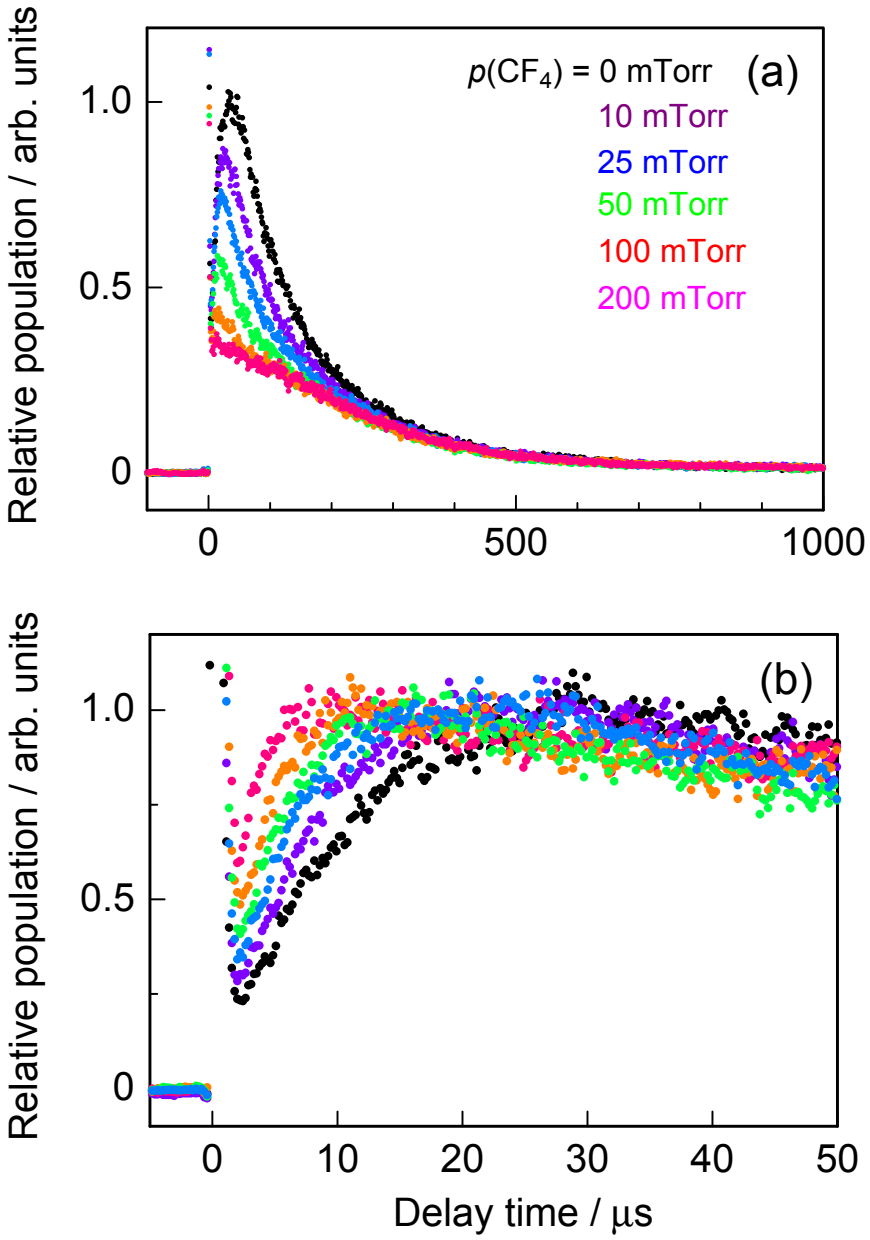

Figure 4.10. CF_4 pressure dependence of the time-resolved LIF intensities of OH(v = 1) generated in the reaction system. Part b is the expanded figure of the initial 100 μs of part a. Time profiles in part b are so scaled as to make their maximum intensities the same. The pressures of NO: 5 mTorr; NH_3: 0.5 mTorr; CF_4: 0–200 mTorr; buffer gas (He): 5 Torr.

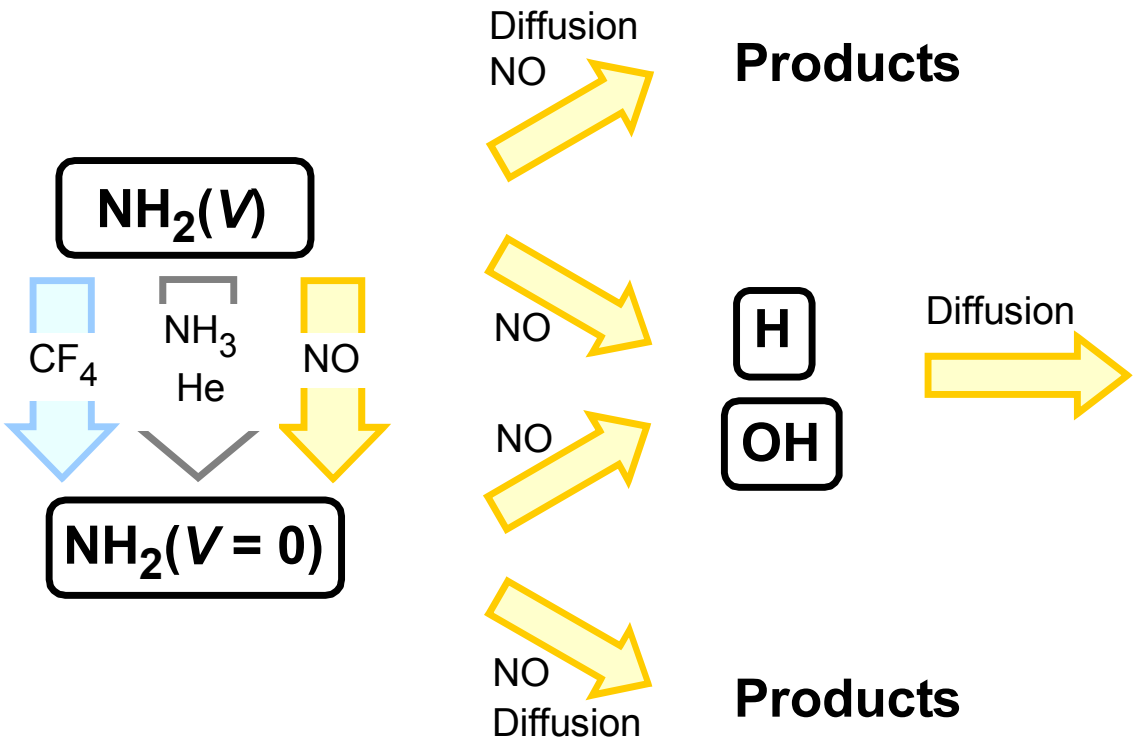

Figure 4.11. The scheme for production of OH by chemical reaction of NH_2 with NO.

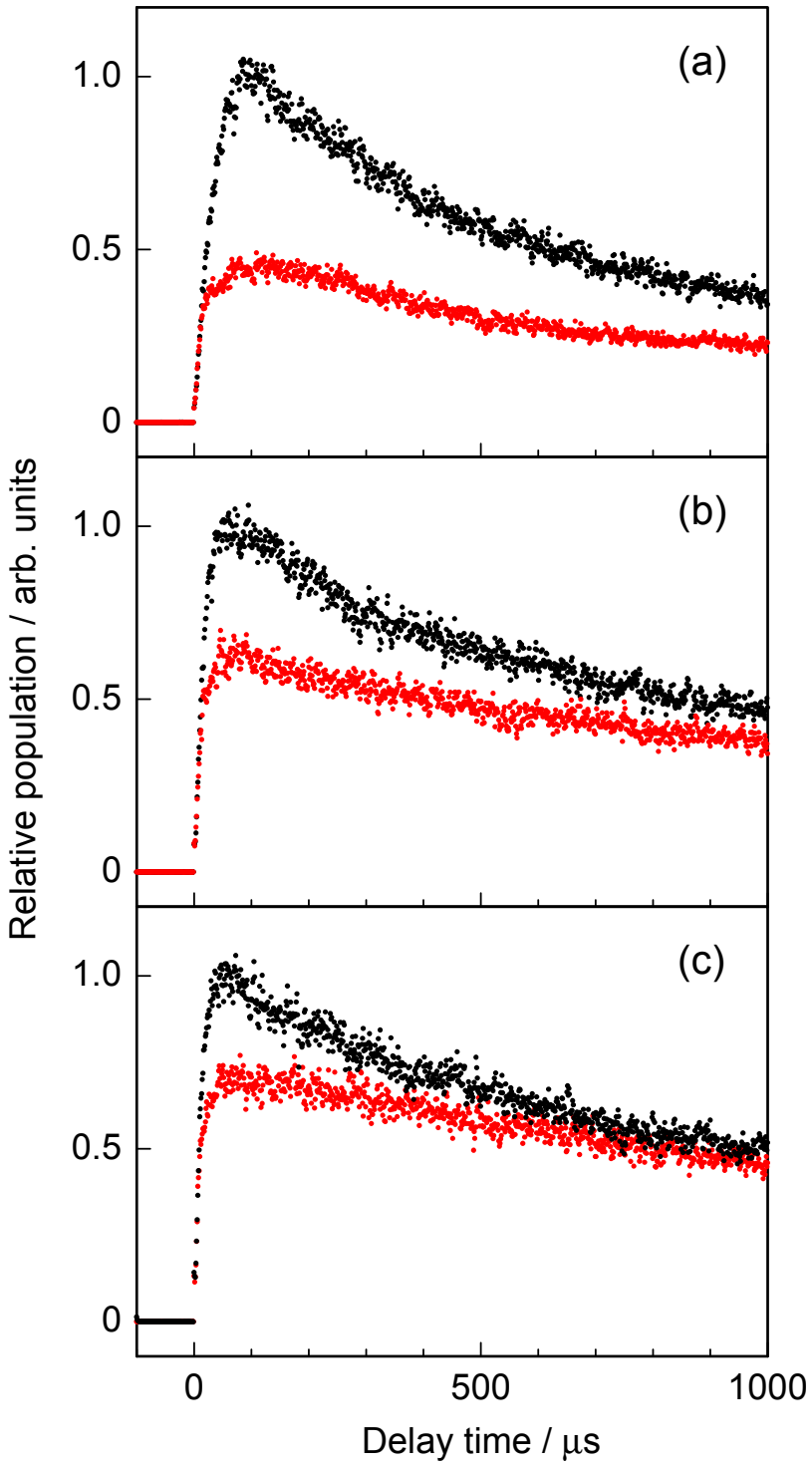
(a)
(b)
(c)
1.0
0.5
0
Relative population / arb. units
0
500
1000
Delay time / μs

Figure 4.12.

Figure 4.12. NO pressure dependence of the time-resolved LIF intensities of OH(v = 0) generated in the reaction system. The black dots denote the time profiles of OH(v = 0) in the absence of CF_4, and the red dots are the time profiles at 200 mTorr of CF_4. The pressures of NO: (a) 5, (b) 50, (c) 100 mTorr ; NH_3: 0.5 mTorr; CF_4: 0–200 mTorr; buffer gas (He): 5 Torr.

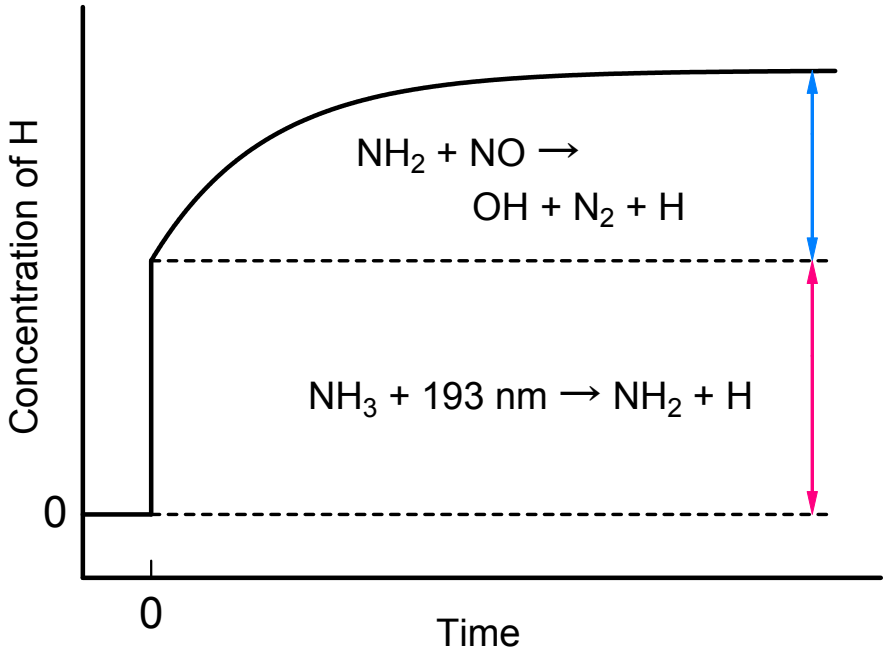

Figure 4.13. The schematic time profile of H atoms. The red arrow denotes the yield of H atoms and NH_2 generated by the photolysis of NH_3, and the blue arrow is the yield of H atoms generated in the reaction, $NH_2 + NO \rightarrow N_2 + H + OH$.

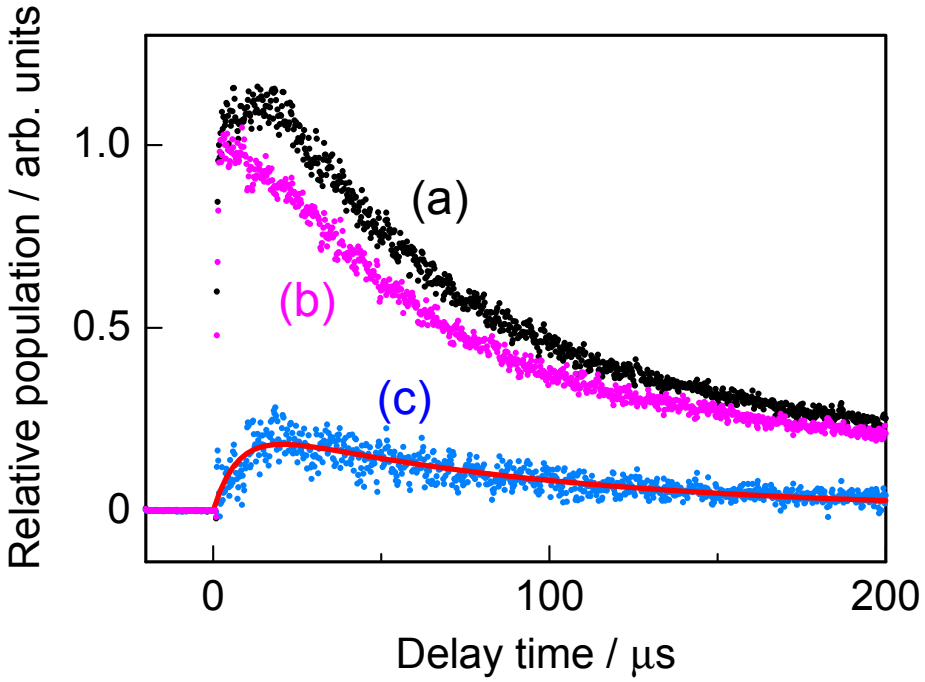

Figure 4.14. The time-resolved LIF intensities of H atoms. The profiles (a) and (b) were recorded in the presence and absence of NO, respectively. The profile (b) subtracted from (a) leaves the profile (c). The black dots denote the observed data, and the red line represents the fit by the double-exponential analysis. The pressure of NO: 100 mTorr, (a); NH_3: 0.5 mTorr; buffer gas (He): 5 Torr.